TORQUE GENERATION DURING THE UNSTEADY EXPANSION PROCESS IN CURVED CHANNELS OF A WAVE DISC ENGINE

By

Raul Quispe-Abad

A DISSERTATION

Submitted to
Michigan State University
In partial fulfillment of the requirements
for the degree of

Mechanical Engineering – Doctor of Philosophy

2017

ABSTRACT

TORQUE GENERATION DURING THE UNSTEADY EXPANSION PROCESS IN CURVED CHANNELS OF A WAVE DISC ENGINE

By

Raul Quispe-Abad

Worldwide demand for power has been growing exponentially, but its production is causing undeniably negative effects; environmental regulations are changing and becoming stricter. The desire for economical but environmentally friendly engines is focusing on toward alternative methods to produce power. “The Wave Disc Engine” (WDE) is a proposed technology to surpass these requirements. The reduction of mechanical parts in the drive train compared with an IC engine and the use of CNG or any other renewable fuel gas make this WDE an attractive technology to generate power. This new engine concept is a radial rotor in which the typical processes of an Internal Combustion Engine (Compression, Combustion, and Expansion) are realized. Several prototypes were built between 2011 and 2013. For torque production, the unsteady expansion process of outflowing combusted gases is harnessed. This is a new engine concept with incipient research, investigating the mechanism to generate power under unsteady-state conditions. This research work focuses on determining factors that contribute to produce torque in radial rotor channels under unsteady-state conditions. Computational fluid dynamic numerical simulations and analytical method were employed in this investigation.

The study initially focuses on the influence of channel parameters (width, height and length); and concludes that channel length and pressure side area all influence torque generation. Both length and pressure side area combine to raise the efficiency and power generated.

Because of the unsteady expansion of the gas, an alternative approach was used to evaluate the performance. The Exergetic efficiency produced results for the channel geometry and conditions tested in the range of 31 to 67%. In addition to that, the approach revealed between 82 to 89% of the exergy, initially contained in the channel, still has the potential to be converted into torque in subsequent stages.

In addition, a zero dimensional macroscopic approximate balance equation was derived based on the first law of thermodynamics to calculate the unsteady generated work from the unsteady expansion process. Results show prolonging the duration of unsteady expansion process enhances the isentropic extracted work toward the maximum value. In addition to that, the gas expands more efficiently at lower pressure ratios.

The impact on the tangential force by the parameters: beta angle, area of influence, and static pressure on pressure and suction sides of a constant cross-section channel, are investigated. The first two parameters change inversely but when combined show similar values at each pressure and suction wall location. Also, most of the generated torque was found in zones near the channel outlet.

Furthermore, the torque generation composed of the action of two effects: the change of the angular momentum of the fluid within channel and the outflow rate of the angular momentum at the channel outlet is investigated. These two components are referred as unsteady and steady effects respectively based on the mechanism to produce torque. Results show the torque production benefits when the channel opens quickly. The increase of rotational velocity approximates the quick opening. Unsteady effects produce a significant part of the generated torque and the steady effect can be small at high speed.

Dedicated to my wife
Thank you for your support all these years during the PhD program

TABLE OF CONTENTS

LIST OF TABLES

LIST OF FIGURES

KEY TO ABBREVIATIONS

A	area
A_{ref}	Reference area value
A_{out}	Outlet area of the channel
AoI	Area of influence
cm	Torque coefficient
CNG	Compressed natural gas
CV	Control volume
e	specific total energy of the system
e_{fe}	Specific flow exergy at the exit
$\vec{e}_k$	Unit vector in the k direction
$\vec{e}_\theta$	Unit vector in the azimuthal (tangential) direction
$\vec{e}_r$	Unit vector in the radial direction
E_{system}	Total Energy contained in the system
E	Exergy
E_{cv}	Exergy of the control volume considered
$\dot{E}_d$	Exergy destruction rate
$\dot{E}_{in}$	Total Energy rate that is coming in the system
$\dot{E}_{out}$	Total Energy rate that is coming out the system
$\vec{F}_p$	Vector force component due to pressure on the wall
EWTT	Expansion wave travel-time
$\vec{F}_s$	Vector surface forces over the control volume

$\vec{F}_v$	Vector force component due to viscous effects
F_θ	Scalar value of tangential component of force
fv	Finite value
g	Gravity
h	Specific enthalpy
h_0	Specific enthalpy at the dead state
IR	Inner radius
ke	Specific kinetic energy
KE	Kinetic energy
LHS	Left hand side
L_{ref}	Reference length value
m_{syst}	Mass contained in the system
$\dot{m}_e$	Mass flow rate at the exit
n	Number of finite stages, normal direction
OR	Outer radius
p	Absolute static pressure
p_0	Pressure at the dead state
pe	Specific potential energy
P_{in_i}	Area-weighted average value of static pressure at inlet for time “i”
P_{in_i-1}	Area-weighted average value of static pressure at inlet for previous time respect to “i”
P_{PS}	Pressure on pressure side
P_{SS}	Pressure on suction side
PS	Pressure side

$\widehat{P}_0$	Mass-weighted average pressure at the beginning of the expansion process
r	Particle's radial position at r-θ plane
r_{out}	Radius at the channel outlet position
R	Radius of curvature
R_{cg}	Radio of the center of gravity of the channel
R_{out}	Radius at the channel outlet position
PR	Static Pressure ratio
RHS	Right hand side
SLT	Second Law of Thermodynamic
s	Specific entropy
S	Entropy
SS	Suction side
s_0	Specific entropy at the dead state
S_0	Entropy at the dead state
S_{gen}'''	Entropy generation rate per unit volume
t	Time
t_x	Time when density's inflection (undulation) point occurs during the expansion process
t_{2s}	Total duration time of the isentropic expansion process
T	Torque magnitude
T_j	Temperature on the boundary "j" where the heat transfer occurs
$\vec{T}_{shaft}$	Vector torque on the shaft
T_0	Temperature at the dead state
$\widehat{T}_0$	Mass-weighted average temperature at the beginning of the expansion process

u	Specific internal energy
U	Internal energy, tip speed
U_0	Internal energy at the dead state
Ꝟ	Volume of the channel or element
$Ꝟ_0$	Volume of the channel at the dead state
V_{cg}	Velocity magnitude at the center of gravity of the channel
V_{out}	Outlet velocity magnitude with respect to inertial reference frame
V	Velocity Magnitude with respect to inertial reference frame
V_{ref}	Reference velocity value
V_r	Radial velocity component with respect to inertial reference frame
V_θ	Tangential velocity component with respect to inertial reference frame
W_a	Actual work
$\dot{W}_{cv}$	Time rate of energy transfer by work
W_{isent}	Isentropic work
WDE	Wave Disc Engine
W_{xyz}	Relative velocity in xyz coordinates
W_r	Relative velocity component in r- direction
W_θ	Relative velocity component in θ- direction
×	Cross product

Greek Symbols

β_{out}	Channel outlet angle
ρ	Density

ρ_{ref}	Reference density value
ω	Rotational velocity
ω_i	Rotational velocity of the channel in the stage “i” [rps]
$\dot{\theta}$	Rotational velocity
Θ	Specific total energy for a flowing fluid
Φ	Viscous dissipation

Subscripts

in	In
out	Out
cg	Center of gravity
i	“i” represents an element
cv	Control volume
cs	Control surface
θ	Azimuthal direction (tangential direction)
r	Radial direction (cylindrical coordinates)

Superscripts

→	Vector quantity
·	Partial derivative with respect to time

CHAPTER 1. INTRODUCTION

1.1. Motivation

“The Wave Disc Engine” has been considered an attractive technology to produce power. Several reasons could point out to make this a very promising technology. The use of this new Wave Disc Generator Technology was predicted to be as 74 million low-cost WDG hybrid vehicles on American roads, using CNG or any other renewable fuel gas, and the impact of this would save 3.5 million barrels of imported oil per day [1]. Another reason was the reduction of mechanical parts in the drive train of this new technology compared with an IC engine. Additionally, the supremacy of unsteady over steady flow as a mechanism of mechanical energy transfer in fluid flows where there is not combustion and body forces [2].

Since this is a new engine concept with little knowledge of the mechanism to generate power under unsteady-state conditions, based on the knowledge of the author, this research work focuses on the investigation of the unsteady expansion process to produce torque in radial rotor channels.

1.2. Structure of the Dissertation

This dissertation is a compilation of several investigations to determine factors that contribute to produce torque in radial rotor channels under unsteady state conditions. It starts reviewing previous work investigating the mechanism to generate power under unsteady conditions. As an extension of this, some previous work on re-utilization of burned gases is presented. Chapter 2 discusses the influence on torque generation by varying channel geometric parameters. Chapter 3 proposes exergetic approach to evaluate the performance of an unsteady expansion process generating torque and characterizes losses and remaining useful exergy. Chapter 4 analyzes the unsteady expansion process based on the first law of thermodynamics using an approximate derived equation. Chapter 5 investigates pressure distribution on channel walls as a result of instant and gradual opening conditions. In addition, force distribution as the result of geometric parameter (beta angle distribution at pressure and suction sides) and channel outlet opening method, is included in the investigation. Also, the combination of line-contour orientation (expansion wave) with channel length increase (θ angle), is discussed. Chapter 6 discusses the torque generation composed of two terms: rate of change and outflow rate of the angular momentum to give understanding of the working mechanisms in torque generation. Chapter 7 provides conclusions and recommendation for future work.

1.3. Methods

This research was accomplished with data generated from two sources: numerical simulations and an approximate derived equation. Numerical simulations were performed using the commercial software, fluent with 2- and 3-dimensional cad models. Chapter 2 results are based on a 2-dimensional cad model in which boundary layer effects on top and bottom are not taken into account, only those from pressure and suction sides of the channel. Results in Chapters 3, 5 and 6 are based on a 3-dimensional cad model. Details of numerical simulation set up are given in Appendix D. The working fluid used throughout the entire dissertation was air that follows the ideal gas law.

1.4. The Inspiration for the Wave Disc Engine idea

The idea for the WDE came to be through a series of well-developed modifications. The axial wave rotor has been used widely in its four-port version: straight channels with the flow going in and out through the rotor in axial direction; one of the applications was as a topping device for gas turbine cycles (Figure 1-1(a)). This design presented a disadvantage during the scavenging process due to the flow leaving in axial direction, causing recirculation of one-burned gases [3]. A substitute configuration was proposed by Jenny and Bulaty, where the rotor had a conical shape with oblique channels and the flow entering and leaving the channels at the front and rear, respectively, and the axial effect still highly interferes with the scavenging process [3]. A breakthrough in new configurations, locating the combustion process inside the channels of the wave rotor, was later proposed to simplify the porting (Figure 1-1 (b)) [3]. According to literature, NASA's wave rotor research was focused on the concept of combustion inside of wave rotor channels [3], [4], [5] . Further modification was proposed in 2004 [3]; this was the introduction of the Wave Disc Engine (WDE) concept (Figure 1-1 (c)). The WDE is a radial-flow rotor concept which addresses the uncorrected imperfection in the second modification of the wave rotor (Figure 1-1(b)). Thus, this new design will improve both the scavenging process through centrifugal forces, and the self-aspirating advantage. Initially the idea of radial rotor with straight channel was suggested, then, curved radial channels were proposed, due to their advantages over straight channels. One benefit is the greater length which might be allocated with the same disc diameter. Curved channels allow the adjustment of the inlet and outlet channel angles to improve the work extraction [3]. The compression process is accomplished within the channel by compression waves, and so this process can be done without a compressor. Another idea was the WDE attached to an external turbine, a proposal configured to enhance the work extraction of the exhaust gases (Figure 1-1 (d)).

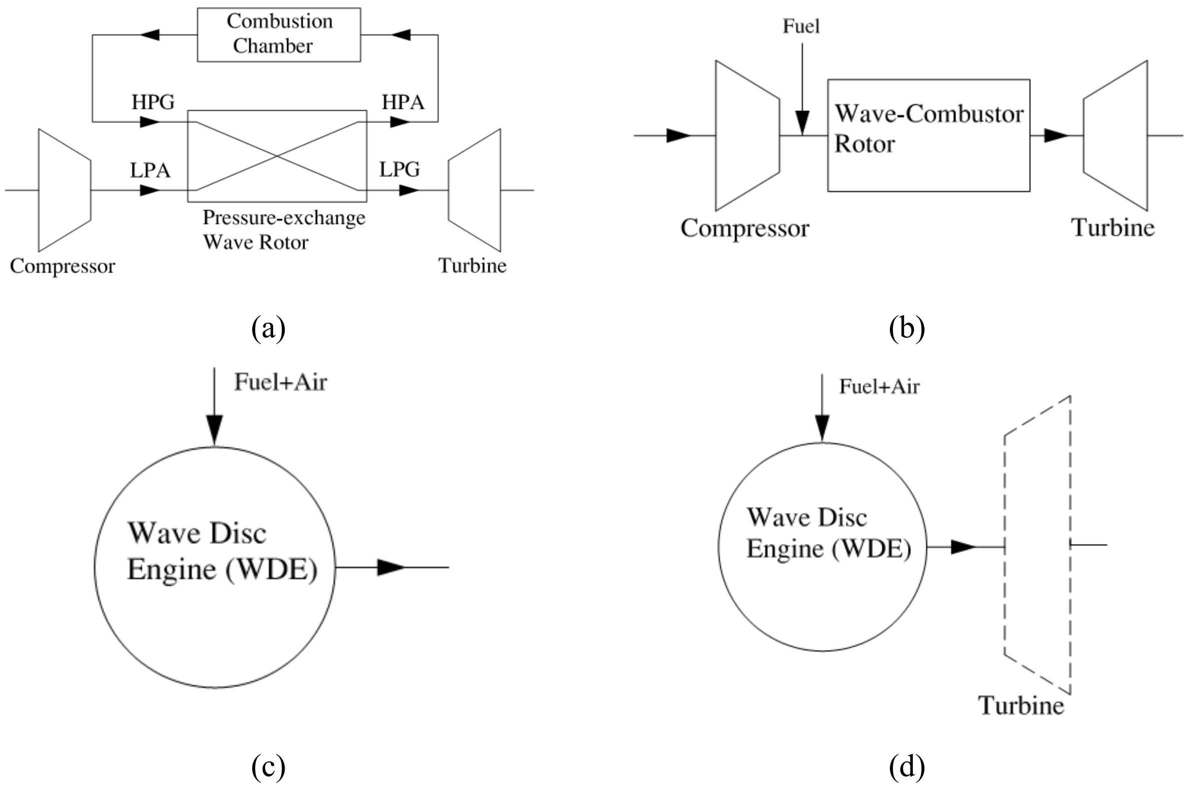

(a) (b) (c) (d)

Figure 1-1: Steps toward the WDE

Another configuration envisioned is a compact WDE with two turbochargers (Figure 1-2).

This research project at the MSU turbomachinery Lab, to build a prototype, was funded by ARPA-E from January 2010 to January 2012, and then extended to May 2013 with $2.5 and $0.5 million, respectively, and since inception investigation have been dedicated to the research of this proposed engine concept.

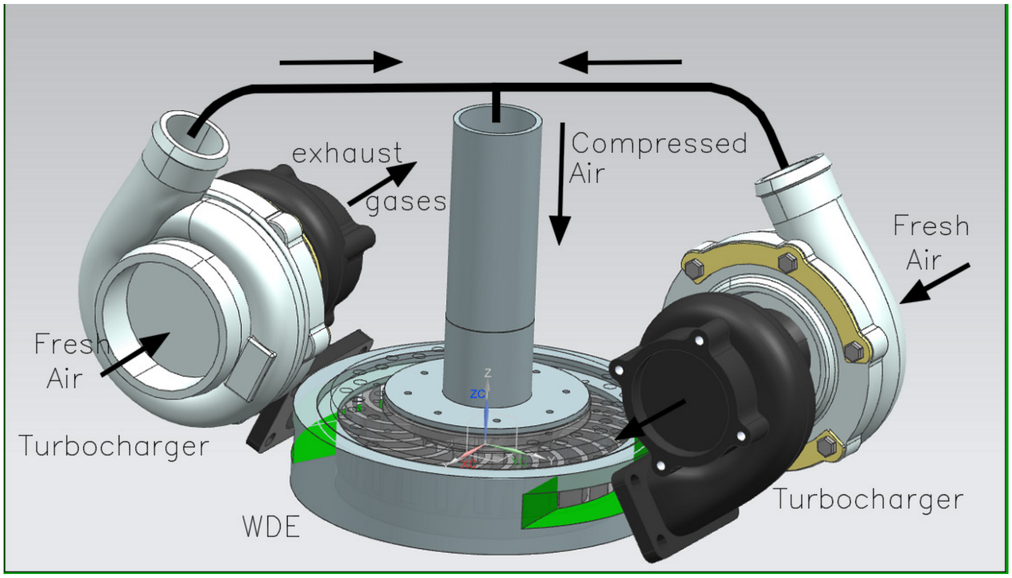

Figure 1-2: Future compact configuration of the WDE connected to two turbochargers

1.5. Working Principles of the WDE

This new engine concept is a radial rotor in which the typical processes of an Internal Combustion Engine (Intake, Compression, Combustion, and Expansion) are executed. The intake process delivers the fresh air-fuel mixture and fills the channel while creating turbulence to augment the mixing process before ignition of the mixture. The onset of this process overlaps the scavenging period and the mass flow rate of the incoming fresh mixture is intensified due to the suction effect produced by the exhaust gases (Figure 1-3 (a)). The outlet of the channel then begins to close and at that time the fresh mixture is ready to fully fill the channel (Figure 1-3(b)). The later stage of this process also overlaps the compression stage when the outlet port of the channel is fully closed (Figure 1-4(a)). Fresh mixture still enters the channel until it is fully closed.

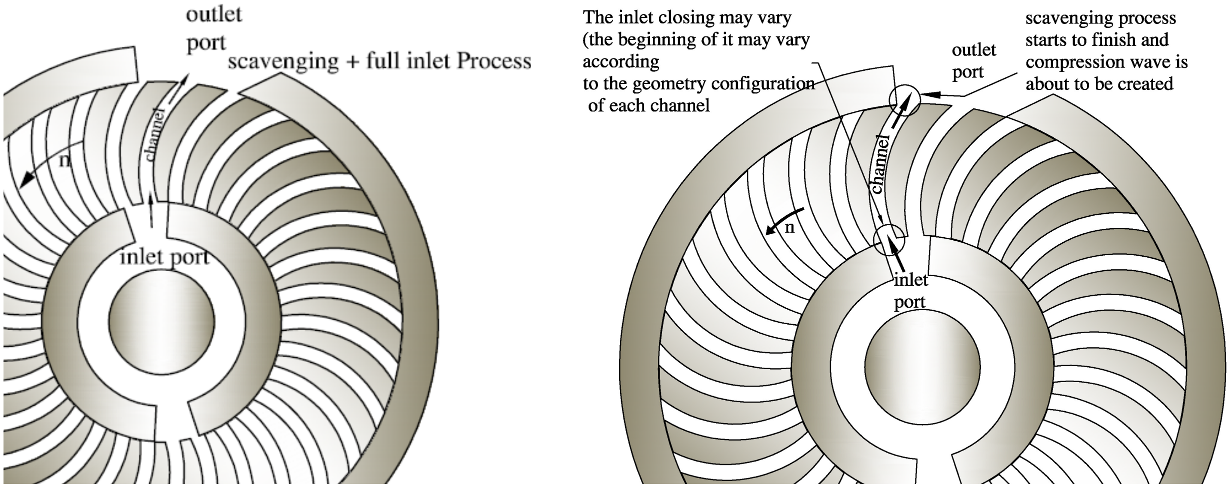

(a) (b)

Figure 1-3: Overlap period for early Intake with Scavenging period

The Compression process starts when the outlet port quickly closes. A compression wave or shock wave is created that travels back toward the inlet port and compresses unsteadily the fresh mixture entering the channel (Figure 1-4(b)). The degree of compression by the wave depends on the velocity of the incoming flow into the channel.

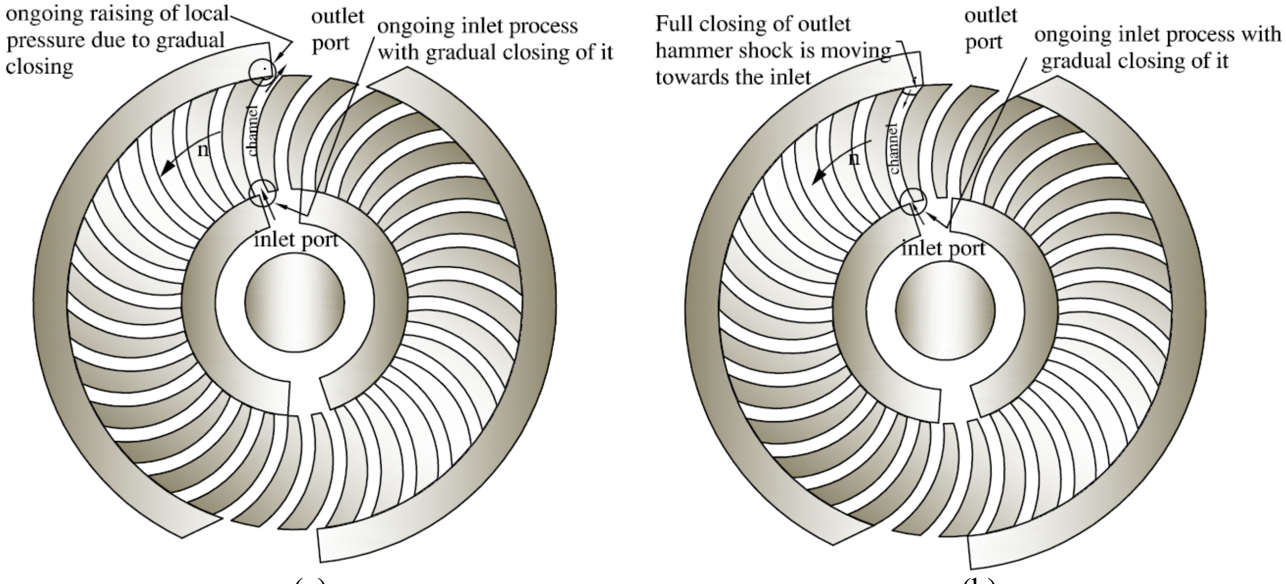

(a) (b)

Figure 1-4: Intake process and early stage of Compression process

The next process is combustion. The outlet and inlet ports of the channel are closed, and the combustion happens in an enclosed channel. Therefore, it is called constant volume combustion (Figure 1-5 (a) and (b)). The time available for combustion is constrained by the geometry of the engine and the rotational velocity. Thus, complete combustion of the mixture is limited by this time allotted.

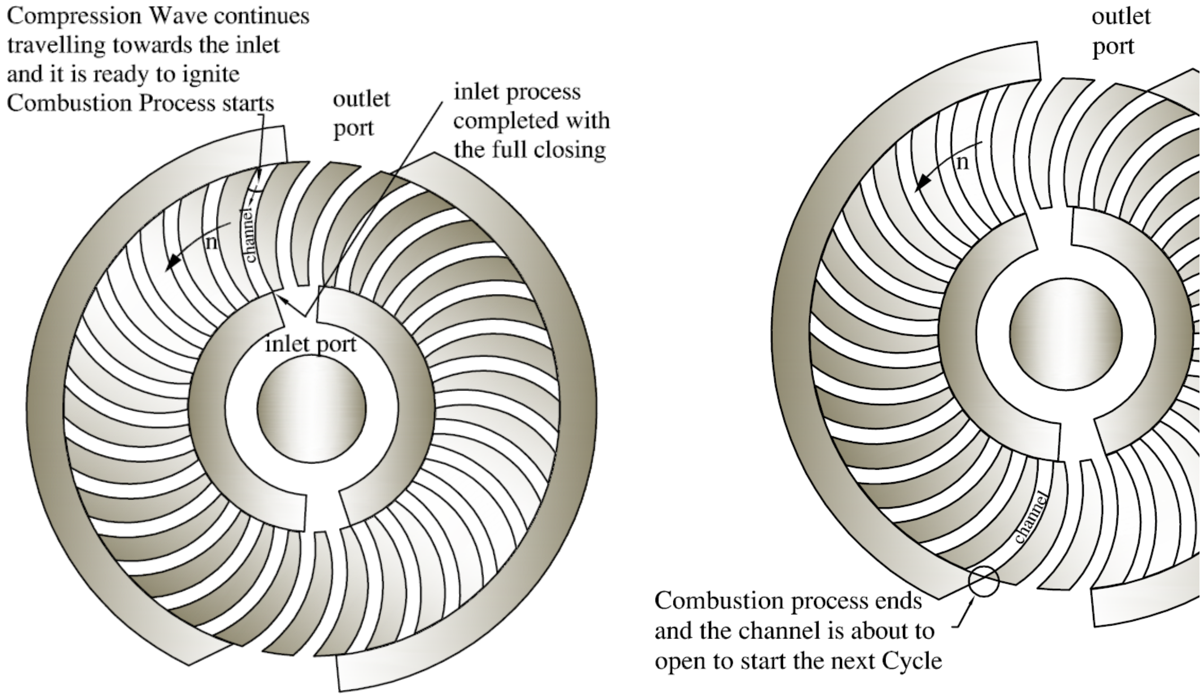

(a) (b)

Figure 1-5: Beginning and end of the Combustion process

The unsteady expansion is the final process in the cycle and torque generation begins with gradual opening of the channel outlet (Figure 1-6(a)). This process is limited as well by the available geometric time of the engine at a particular rpm. The scavenging overlaps the intake process and begins; following a short interval, the front of the expansion wave strikes the inlet wall of the channel (Figure 1-6 (b)).

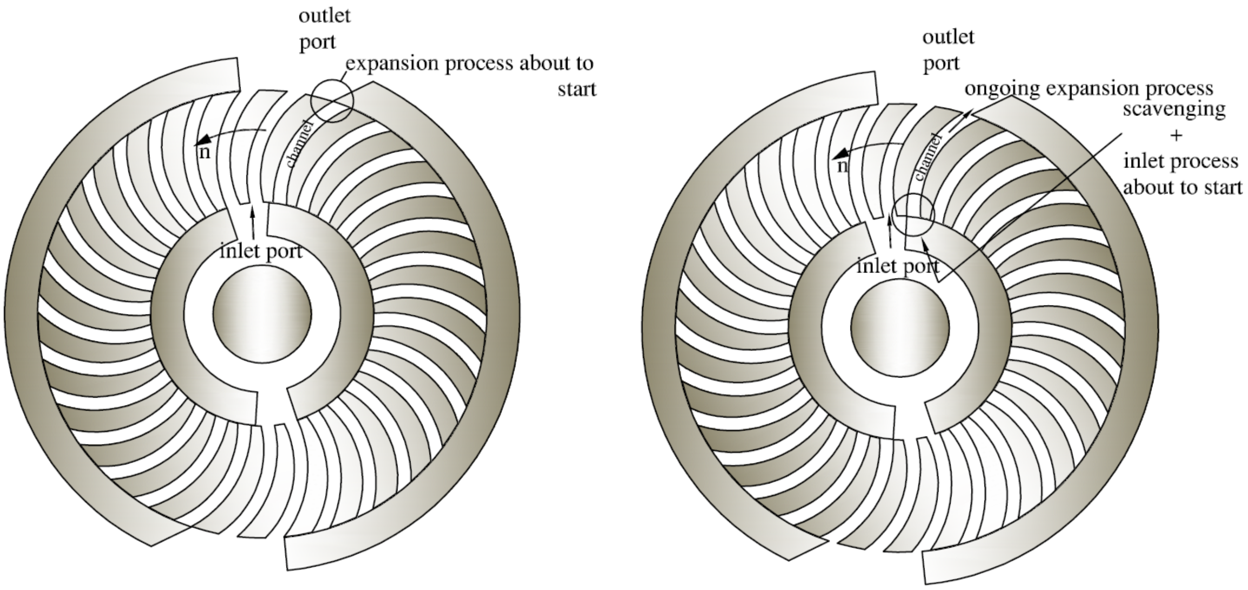

(a) (b)

Figure 1-6: Unsteady expansion process

Figure 1-8 shows an example of the available geometric time per cycle. The available time was calculated based on the WDE-II rotor design built by the WDE research group at MSU (Figure 1-7) and is valid only for this particular rotor. It appears the available geometric time for Combustion and Expansion + scavenging + Inlet (P0) are 68.6% and 24.4%, respectively, of the total cycle time. These percentages are kept constant as the rpm increases but the absolute time for each processes decreases.

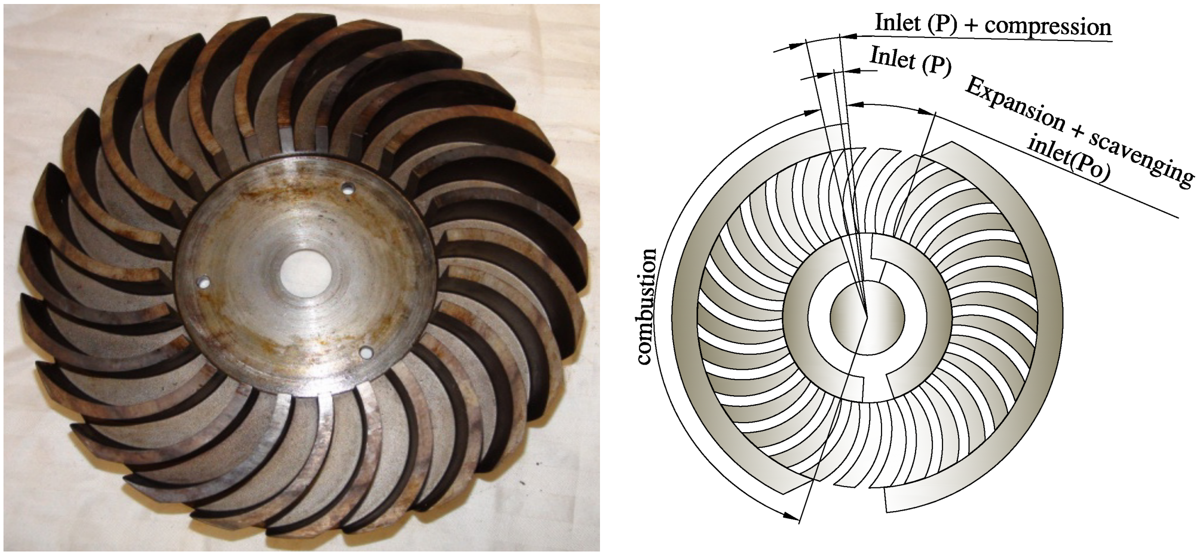

(a) (b)

Figure 1-7: (a) WDE-II Rotor designed and built by the MSU WDE research group & (b) space distribution for processes

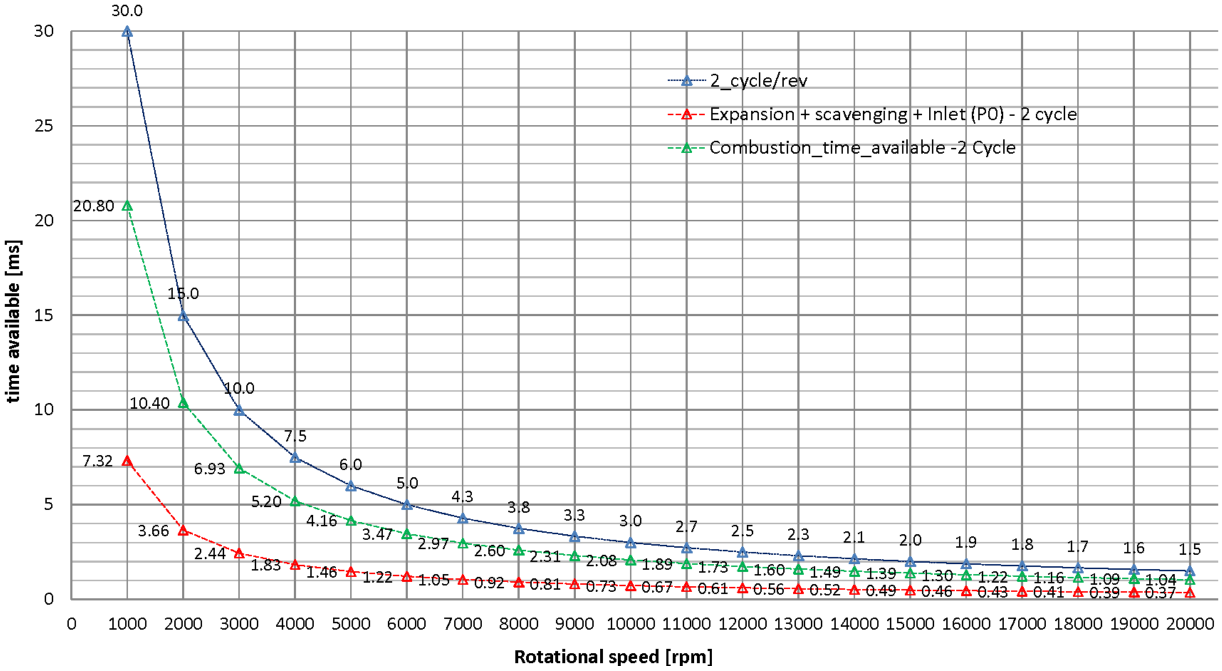

Figure 1-8: Geometric time available per cycle for the Unsteady Expansion Process for a 2 cycle per revolution WDE-II Rotor

1.6. Previous work on the WDE

1.6.1. Thermodynamic Cycle of the WDE

A transient thermodynamic model was proposed to explicitly calculate the cycle efficiency of the WDE. The formula was stated to calculate the work produced by the burned gas during the expansion process [6]:

$$W_e = -\int_{t_3}^{t_4} \dot{m}_{out} h_{tot.out} dt + E_{t_3} - E_{t_4}$$

Where t_3 and t_4 represent the initial and final state of the pure expansion process. This equation was used to derive the final expression of the thermal efficiency in terms of mass-average temperature.

$$\eta = 1 - \gamma \frac{\bar{T}_4 - \bar{T}_1}{\bar{T}_3 - \bar{T}_2}$$

The unsteadiness of the expansion process was considered in this formula but the expression was changed to have as a function of mass-average temperature values.

1.6.2. Mechanism for Torque Generation

Previous work on studying the mechanism was presented by Sun [7]. It stated the torque generation principle for a traditional steady turbine is not valid for the WDE operating in unsteady flow conditions. This principle refers to a fluid particle passing through a blade passage; centrifugal force creates a pressure gradient toward the center of the curvature; as a result of this, force is applied to the blade. According to Newton’s Law, the normal direction for steady state conditions:

$$\frac{\partial \mathrm{p}}{\partial n} = \frac{\rho . {V_\theta}^2}{\mathrm{R}} \qquad (1\text{-}1)$$

The principle was tested for steady and unsteady conditions using the concept from Equation (1-1). Unsteady condition test did not prove the validity in the two channel shapes tested. Thus, it was concluded the steady state principle does not apply for torque generation under unsteady state conditions [7] and more factors need to be considered for torque generation mechanism.

Another topic in this study was the direction of the pressure gradient when the expansion wave travels inside the channel [7]. A positive pressure gradient is generated when the expansion wave moves toward the inlet and the pressure decreases from the inlet to the outlet. A negative pressure gradient generates an opposite effect. Conclusions were summarized in Table 1-1 and blade angles refers to the inlet or outlet angles of the blade [7].

	Blade angle<90 deg	Blade angle>90 deg
+ pressure gradient	[+]	[-]
- pressure gradient	[-]	[+]

Table 1-1: General principle of torque generation according to the travelling direction of expansion wave [7]

Another conclusion from this research [7], was the influence of the outlet opening in channel geometries. The efficiency of the expansion increased with the extension of the expansion duration, and these higher values were the result of having a smaller outlet opening. This was defined as the smallest distance from the trailing upper wall to the lower wall of the suction surface.

1.6.3. Unsteady Expansion in channels

Previous work shows efficiency is reduced for two primary reasons: Kinetic Energy leaving the channel outlet and incomplete work extraction from the burned gases [7]. Preliminary research was conducted for a hypothetical variation of the average density in the channel, considering different time duration of the expansion process (Figure 1-3). In this figure, the magnitude of the outlet velocity in the channel decreases as the duration time of the expansion process increases.

A work extraction investigation by Sun [7] concludes greater work is generated in the WDE during the expansion process. The work generated is negligible in other WDE processes during the CFD simulation. Therefore, focusing on the unsteady expansion process for work generation is valuable. For this investigation, the performance of channel geometry (efficiency) was calculated using the energy heat addition as ideal (maximum) work: the net internal energy-the difference between initial and final state of the expansion process-through the patching of pressure and temperature.

Sun [7], focusing on the CFD investigation of unsteady expansion, concluded that, in a single channel, the source of losses were primarily from Kinetic Energy leaving the channel, and under-expansion of exhaust gases. The next finding was that convergent channels show the best performance, from 2.2% to 3.3%.

1.6.4. Re-utilization of exhaust gases

Options to re-utilize exhaust gases to improve engine efficiency are found in the literature:

1.6.4.1. Return channel

Re-directing the pressure and kinetic energy of the gases for additional work extraction, to take advantage of the exhaust gases during the unsteady expansion, to the entrance of a lower pressure contiguous channel, is the return channel's purpose.

Several works have been done on this concept. A numerical study by Sun [7] found that efficiency increases 56.1% by re-using the exhaust energy in a return channel. This study was performed using a convergent channel, and the comparison with a base-line design configuration is provided in Table 1-2.

	Rotor Diameter [mm]	Power [kW]	Efficiency [%]
Convergent channel	200	2.48	3.96
Convergent + return channel	200	3.99	6.18

Table 1-2: Results from numerical simulation [7]

1.6.4.2. Parallel row of turbine blades

A MSU research team began investigating this new concept in 2010, sponsored by ARPA-E (Advanced Research Projects Agency-Energy) of the US Department of Energy. Using CFD, one study was accomplished for the WDE with the combination of re-injection passage and a second row of turbine blades [8]. This configuration delivered the highest efficiency (5.5% efficiency), but which of them made the greatest contribution was not stated. However, the exhaust gases did not yet fully expand within the external blade passages, and adding additional rows of turbine blades was suggested.

Another CFD investigation for two stage rotor configuration (first stage: a convergent channel/ second stage: a turbine blade) with guide vanes between them, found the efficiency increased from 3.96% to 11.01% for a 2 cycles per rotation engine [7]. See Table 1-3 for comparison with a single stage rotor (only convergent channel).

	Power [kW]	Efficiency [%]
1 stage rotor (only Convergent channel)	2.48	4.0
2 stage rotor (Convergent channel+GV+1 turbine blades)	8.29	11.0

Table 1-3: Comparison of a single stage and 2 stage rotors WDE

A multi-stage serial radial turbine, the hybrid wave engine, was investigated by Dyntar [9]. This proposed configuration was planned for use in MEMS technology (micro engines). The parallel flow configuration (Figure 1-9(a)) was dismissed because the mass flow rate of exhaust gases from the gas generator was high and therefore, not suitable for this application. The high flow rate passing through the blades do not properly transfer the energy into torque. Thus, this work proposed the serial flow configuration, where the exhaust gases expand in two steps in the same set of blades (Figure 1-9 (b)). The flow experiences two stages of expansion: at high-pressure and low-pressure, and the total maximum efficiency reported was 10% [9].

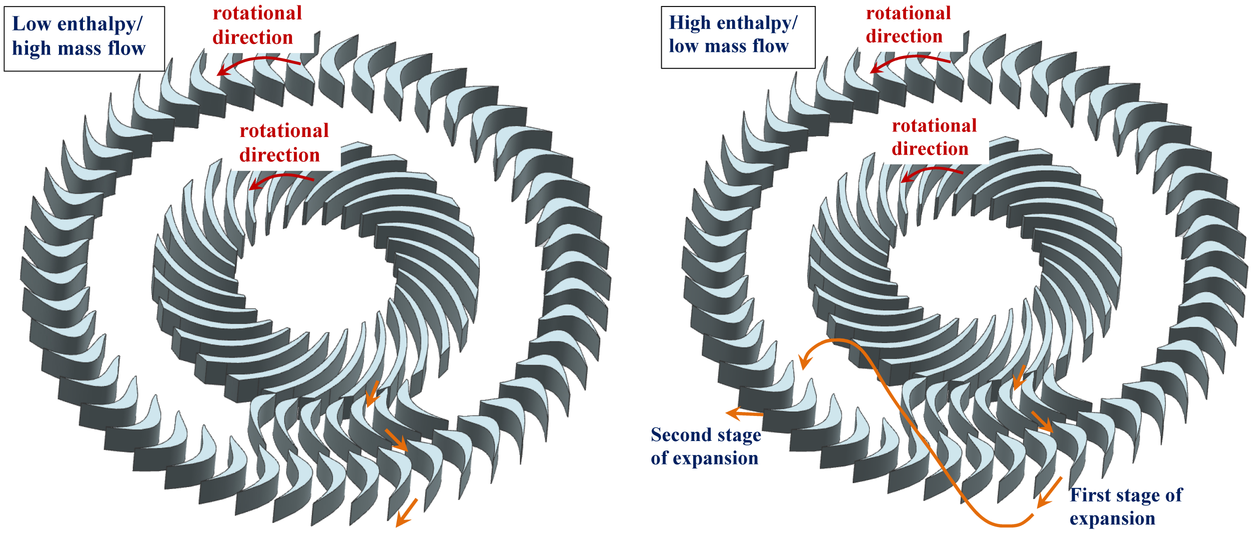

(a) Parallel flow configuration (b) Serial flow configuration

Figure 1-9: Parallel and Serial flow configuration of a radial turbine. Source [9]

1.7. Expansion efficiency

The isentropic efficiency of a turbine is one performance factor criteria to evaluate the performance of an expansion process, and is calculated in terms of the work done by the fluid passing through the blade passage [10]:

$$\eta_{isent} = \frac{Actual\ work}{Ideal\ (maximum) work} = \frac{W_a}{W_{isent}} \tag{1-2}$$

Equation (1-2) is used in turbomachines when the expansion process is at steady state conditions; this means all fluid particles passing through the turbine undergo the same thermodynamic conditions from inlet to outlet.

Previous work [7] defined a method to evaluate the unsteady expansion process:

$$\eta = \frac{Actual\ work}{Heat\ addition} = \frac{W_a}{Q} \tag{1-3}$$

The heat addition is calculated based on [7]:

$$Q = U_f - U_i \tag{1-4}$$

Where U_i is the internal energy in the channel before patching and U_f is after patching.

CHAPTER 2. INFLUENCE OF CHANNEL PARAMETERS: WIDTH, HEIGHT AND LENGTH AT CONSTANT CROSS-SECTION CHANNELS

This section determines torque generation influence by changing geometric parameters of cross-section (width and height) and length of the channel.

All channels initiate the unsteady expansion process at the same total energy. Due to the geometric parameter change, the kinetic energy of the fluid within the channel might vary but does not affect the results because they are negligible. Thus, the internal energy is the influential factor to preserve identical initial conditions of the fluid within the channel. The working fluid is air which follows the ideal gas law, and because of that, the internal energy contained in the channel depends on two factors: temperature and mass. To meet these two conditions, the unsteady expansion process in all cases starts at the same temperature and pressure (2100 [K] and 709275 [Pa], respectively). There is an additional requirement to keep the same mass: channel volume must be identical; to achieve this geometrical state, the length of the channel was varied to adjust to the volume-goal value.

Additional parameters such as outlet blade angle (β_{out}), tip speed (U), outer and inner radiuses (OR and IR) were kept constant (Figure 2-2(b)). Table 2-1 depicts a summary of the geometry characteristics for each case. All cases had channels rotating at 10,000 rpm, with channel outlet instantly opening.

Equation (1-3) was used to evaluate the performance of the unsteady expansion process in all cases.

In Table 2-1, cases 1 to 3 show the variation of height when theta angle is increased with channel width kept constant; and thus channel length becomes longer. The channel height was reduced to keep the volume-goal value constant. Figure 2-2 (a) schematically portrays the changes in Table 2-1 with the application of theta and beta angles (Figure 2-2(b)).

	θ	β_{out}	channel-height	channel-width	ch-center-length
Variation Height	[deg]	[deg]	[mm]	[mm]	[%] increase
case-1	40	30	25.00	8.5	0.0
case-2	50	30	22.83	8.5	9.2
case-3	60	30	20.98	8.5	18.5
Variation width					
case-4	50	30	25.00	7.74	9.4
case-5	60	30	25.00	7.09	19.3
Variation H & W					
case-6	40	30	28.28	7.5	0.0

Table 2-1: Geometry conditions for each constant cross-section channel

For cases 1 to 3, the expansion duration time was extended as theta increased (Figure 2-3) and this is linked to the channel length increase. The length increase is compared with respect to theta=40deg case-1 and is as follows: 9.2% and 18.5%, respectively. The same trend is observed in travel-time of expansion wave to reach the channel inlet wall (Figure 2-4 (b)), and as theta value increases, the head of the expansion waves has a greater distance to travel. Additionally, the combination of length increase with height decrease resulted in 1.6% and 3.6% rise of pressure side area with respect to case-1, respectively (Figure 2-1). However, suction side area decreased in 1.4% and 3.0% respectively. The results of increase and decrease of areas did not produce an important improvement on the net tangential force. Thus, those cases (1 to 3) produced similar values of expansion efficiency (Figure 2-4(a)). The biggest increase in efficiency was 0.7%. A gain based on extended duration of expansion process was counteracted by the reduced channel height to generate torque.

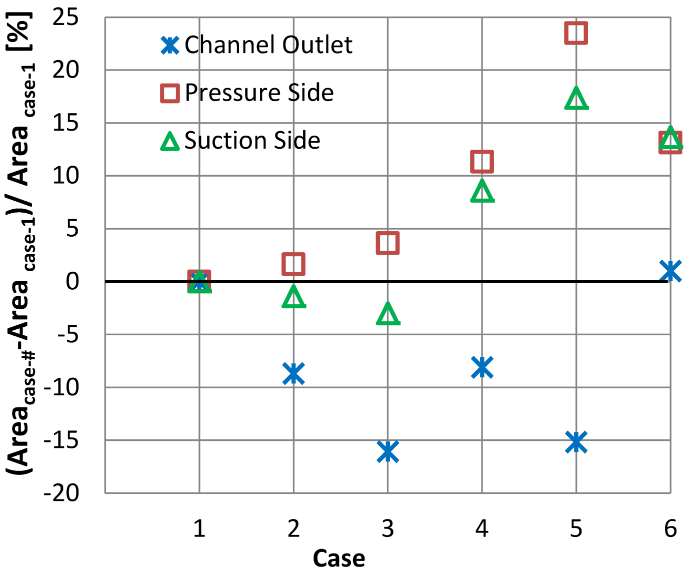

Figure 2-1: Comparison of channel outlet, pressure side and suction side areas with respect to reference case-1.

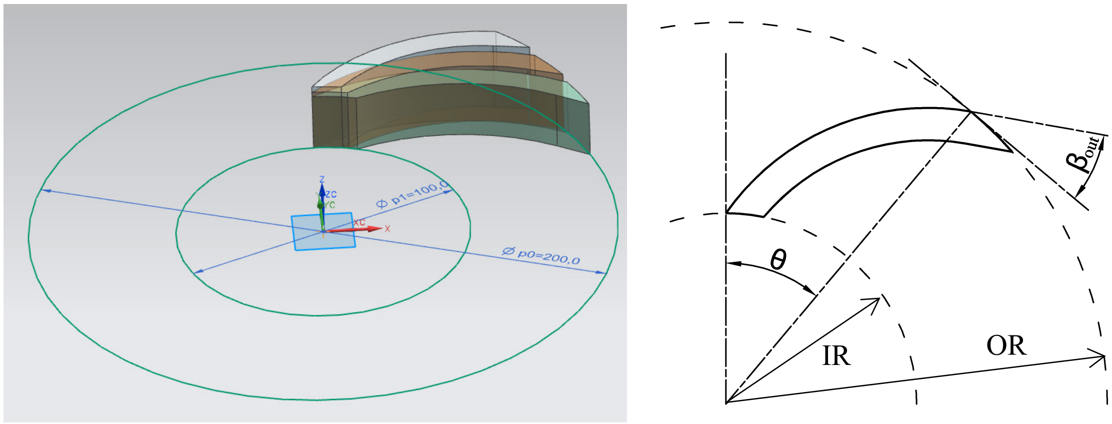

(a)

(b)

Figure 2-2: (a) Constant cross-section channel configurations for cases-1 to 3 and (b) meaning of θ and β_{out} angles.

In the following cases, (4 and 5) was considered the extension of the channel length but with the same channel height as case-1 (reference case). The changing parameter was the channel width. As a result of this, the areas of the pressure side were increased 11.3% and 23% with respect to the base line case, respectively. Also, the areas of the suction side were increased 8.6% and 17.3%, respectively. In addition, the expansion duration time and the EWTT were enlarged (Figure 2-3 and Figure 2-4 (b)). Another parameter to point out is expansion efficiency with an improvement of 1.4% and 3.7% in respect to the base line case-1 (Figure 2-4). The reduced width did not diminish significantly the case with the highest efficiency (3.7%) due to the boundary layer affecting more cross-sectional area if case-5 is compared to case-3.

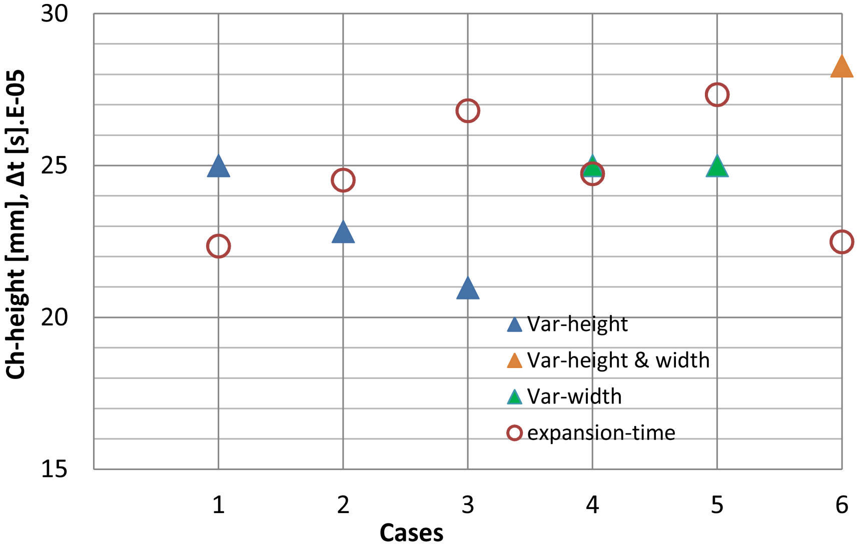

Figure 2-3: Duration of expansion process for constant cross-section channels varying their geometric parameters (Var =geometric parameter changed)

The last change in geometric dimension of the cross-section pertains to case-6, with the same theta value as the base line case-1, but with the width reduced to increase the height value and still preserve the volume-goal value. The modifications produced an increase in pressure and suction side areas of 13.1% and 13.6%, respectively. Results in Figure 2-4(a) show an improvement of 0.62%, in expansion efficiency. However, the duration of expansion process and EWTT carry the same value as in case-1 (Figure 2-4(b)). The contribution of additional pressure side area was not substantial enough to generate extra torque if the duration of expansion process is not extended.

The pressure side area increase produces a rise in the net tangential force if this condition is met: $P_{PS} > P_{SS}$. The rise of θ angle or channel length results in pressure side area increase even if height is either reduced or kept constant. However, the reduced height produced lower values of area increase. For example, 3.6% and 23.5% were the results for case-3 and -5 respectively.

The rise of the channel length extends the duration time of the unsteady expansion process and the head of the expansion wave will propagate longer distances. Thus, the duration increase of the expansion process contributes to extend the application time of the tangential force on the pressure and suction sides.

Results show that the highest efficiency happened when the duration time and the pressure side area, were increased. Therefore, the length of the channel and pressure side area, influence the expansion efficiency. Both parameters combine to raise efficiency. A method to improve it is by increasing geometric parameters: θ angle (channel length) and channel height.

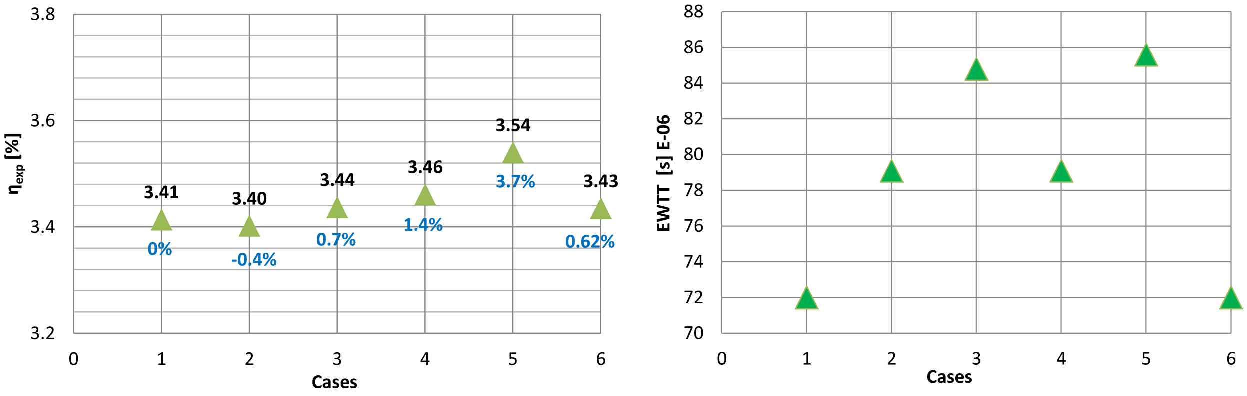

(a) (b)

Figure 2-4: (a) Expansion efficiency [%] and (b) Expansion wave travel time to reach channel inlet (EWTT) [s] for constant cross-section channels varying their geometric parameters.

Results of energy generated in Figure 2-5(a) refer to the gas expansion of one channel, and this value is translated into a rotor's specific number of channels. Thus, these results are interpreted as the power generated by the engine rotor and values are plotted in Figure 2-5.

A note from Figure 2-4(a) is concerned with the expansion efficiency results in which low values are based on the criterion of the internal energy change. Using a different approach to evaluate the unsteady expansion process is desirable, and this will be the next chapter topic.

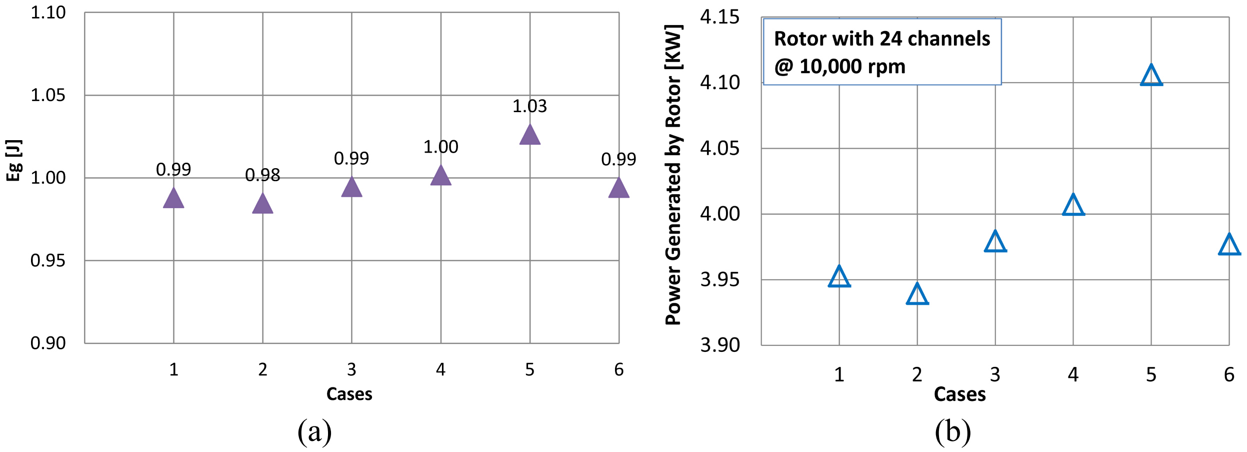

(a) (b)

Figure 2-5: (a) Energy generated by one channel, (b) Power generated by engine rotor of 24 channels rotating at 10,000 rpm

CHAPTER 3. EXERGY ANALYSIS OF THE UNSTEADY EXPANSION PROCESS

3.1. The necessity of an alternative method to evaluate the expansion efficiency

Typically for steady state processes in turbomachines, turbine or compressor efficiency is calculated based on the idea a unit of mass goes from an initial state at the inlet to final state at the outlet. All fluid elements experience the same trajectory in the thermodynamic diagram during a specific process (expansion or compression). Based on these conditions, the actual and the ideal (maximum) work are determined to calculate the efficiency. In the case of the WDE configuration for the expansion process, gases only leave the channel during the expansion and thus each fluid element traverses different paths along the channel. Therefore, every fluid particle undergoes different thermodynamic conditions. The application of the criterion above might give misleading results in the evaluation of the performance of the device.

In previous research [7], the performance of a single channel was approached based on the internal energy increased due to patching; this was considered as a heat addition. Thus, the work generated was compared to this value.

Up to now, all efficiency concepts were based on the energy approach of the First Law of thermodynamics. An alternative approach to evaluate the efficiency based on the combination of the First and Second law of thermodynamics, and this method is supported by Dincer and Rosen [11] (2013), Rosen and Etele [12] (2004), and many other researchers. Thermodynamic losses happening inside the system usually are not appropriately identified and evaluated with the energy analysis approach [11], and especially when the system is so highly unsteady it requires special attention. Exergy approach assists in overcoming the drawbacks of the energy analysis [11].

3.2. Exergy analysis of a single channel

Exergy is defined as: "… the maximum theoretical work obtainable from an overall system consisting of a system and the environment as the system comes into equilibrium with the environment (passes to the dead state)" [13]. Exergy concept does not specify the method to generate the work-either steady or unsteady-but only refers to the maximum potential associated with the initial state respect to a reference state (dead state). The dead state defined through all of this research is T_0=300 [K] and p_0= 101325 [Pa]. Exergy (E) is calculated based on Equation (3-1) [13]:

$$E = (U - U_0) - p_0(V - V_0) - T_0(S - S_0) + KE + PE \qquad (3\text{-}1)$$

For the case of a control volume in which fluid properties are not uniform, equation (3-1) is written in Integral form:

$$E = \left(\iiint_{CV} \rho(u - u_{ref})d\cancel{V} - \iiint_{CV} \rho(u_0 - u_{ref})d\cancel{V} \right) - p_0 \left(\iiint_{CV} dV - \iiint_{CV_0} dV \right)$$
$$- T_0 \left(\iiint_{CV} \rho(s - s_{ref})d\cancel{V} - \iiint_{CV} \rho(s_0 - s_{ref})d\cancel{V} \right) + \iiint_{CV} \rho \left(\frac{|\vec{V}|^2}{2} \right) d\cancel{V}$$
$$+ \iiint_{CV} \rho(z - z_0) g d\cancel{V}$$

And considering that the control volume does not change and all cell elements in the channel keep the same z-coordinate, it yields:

$$E = \left(\iiint\limits_{CV} \rho(u - u_{ref})d\cancel{V} - \iiint\limits_{CV} \rho(u_0 - u_{ref})d\cancel{V} \right) - T_0 \left(\iiint\limits_{CV} \rho(s - s_{ref})d\cancel{V} - \iiint\limits_{CV} \rho(s_0 - s_{ref})d\cancel{V} \right) + \iiint\limits_{CV} \rho \left(\frac{|\vec{V}|^2}{2} \right) d\cancel{V} \tag{3-2}$$

All terms in Equations (3-1) and (3-2) are based on a stationary control volume chosen according to Figure 3-1. All variables with the subscript "$_0$" are calculated at dead state conditions. Also, the subscript "$_{ref}$" means the variable is calculated at reference values of Temperature (288.16 [K]) and absolute pressure (101325 [Pa]).

As a starting point for this single channel analysis, Exergy was calculated based on Equation (3-1) and the gas initial conditions in the channel at different pressure ratios and results are plotted in Figure 3-2. These values should be considered as the upper limit value (maximum work) in the expansion process based on Exergy definition stated above. Thus, in Figure 3-2, the blue triangles are the maximum expected work at every specific pressure ratio for this channel.

Then, an expansion case is simulated numerically for the same geometry and gas initial conditions (10,000 rpm with instant opening at PR=7) and the work extracted is plotted in the graph as well. If this value is compared to the exergy at the same PR, it would result in 4.81% efficiency of expansion for this simulated case. The approach to determine the efficiency using the internal energy patching criteria predicts a lower value of 3.6%. Efficiency based on the exergy method predicts higher values and can be considered a more realistic value because the extracted reference work value is the maximum. Afterwards, exergetic efficiency will be defined to evaluate the performance of unsteady processes.

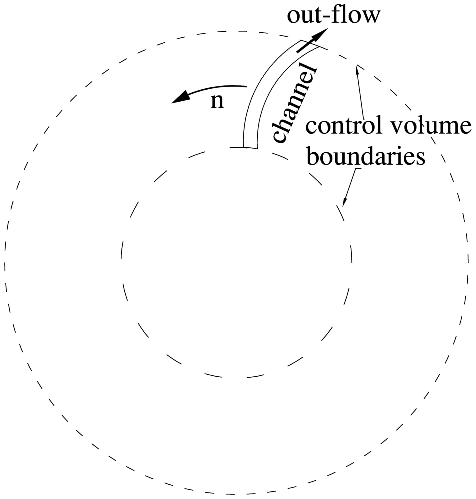

Figure 3-1: Control volume considered for exergy rate balance

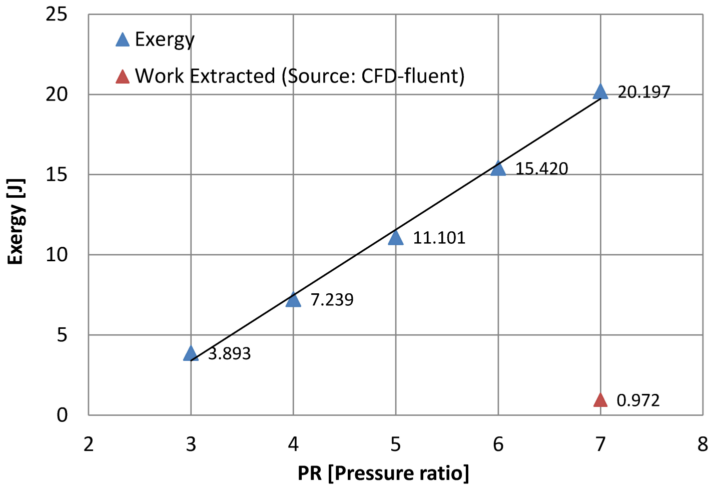

Figure 3-2: Exergy (maximum work available) for a constant cross-section curved channel at 10,000 rpm at several Pressure ratios (PR)

The next step is to monitor the exergy in the channel along with the flow time. Each exergy value was calculated at each time step interval of 1E-08 [s] using Equation (3-2) under these conditions: Instant Opening at 10,000 rpm (IO@10K); Gradual Opening at 10,000 (GO@10K), 20,000 (GO@20K), 30,000 (GO@30K), 40,000 (GO@40K) and 50,000 (GO@50K) rpm. The results are shown in Figure 3-3, and reveal the increase of initial exergy value as the tip speed of the channel increases. In the calculation for exergy, the kinetic energy component raises Exergy 7.2% (@50Krpm) compared to GO@10K. Two limits can be recognized, based on the conditions tested: at the lowest rotational velocity (GO@10K), and instant opening of the channel outlet (IO@10K). The history of exergy shows that as the rpm increases the behavior tends to resemble as the instant opening case.

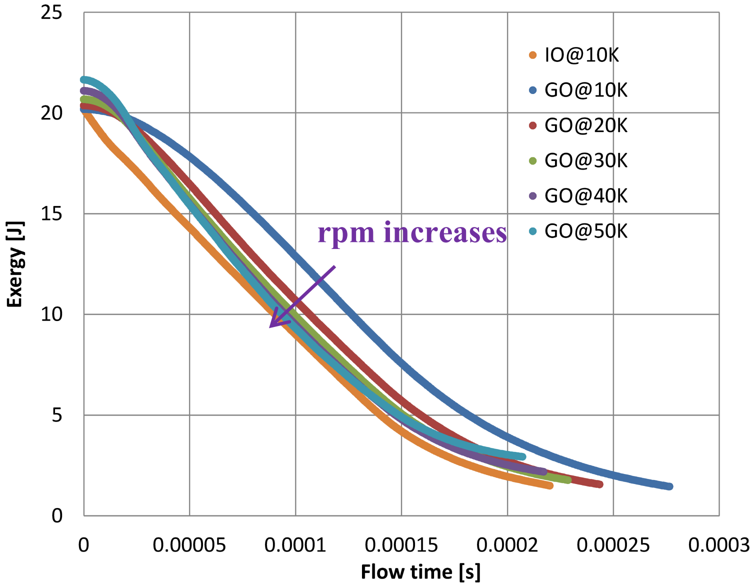

Figure 3-3: Exergy variation along expansion time for a constant cross-section channel at several rotational velocities and PR=7

3.3. Exergy rate analysis at transient state

Since the expansion is an unsteady process, tracking exergy variables as the expansion progresses, and as an overall value, is appropriate to consider the exergy rate analysis. The control volume is according to Figure 3-1, and the general exergy rate balance equation is [13]:

$$\frac{dE_{cv}}{dt} = \sum_j (1 - \frac{T_0}{T_j})\,\dot{Q}_j - \left(\dot{W}_{cv} + p\frac{dV_{cv}}{dt}\right) + \sum_i \dot{m}_i e_{fi} - \sum_e \dot{m}_e e_{fe} - \dot{E}_d \qquad (3\text{-}3)$$

Based on the working features of this engine and simplifications for the purpose of this analysis, some idealizations are applied:

(a) The boundaries of the control volume are considered adiabatic and channel walls are treated as if there is no heat flux through them during CFD simulations.

(b) The control volume size does not increase and stays stationary throughout the process

(c) There is only one outflow that goes through the channel outlet and no incoming flow.

After these constraints, Equation (3-3) becomes:

$$\frac{dE_{cv}}{dt} = -\dot{W}_{cv} - \dot{m}_e e_{fe} - \dot{E}_d \tag{3-4}$$

Equation (3-4) is the standard form that will be used for all calculations in this chapter. The final term ($\dot{E}_d$) in this equation is exergy destruction rate and represents the speed at which exergy is destroyed at a specific flow time, and must be equal or greater than zero but never a negative value. $\dot{E}_d$ is calculated indirectly when solving for it in Equation (3-4) and the other terms should be known:

$$\dot{E}_d = -\frac{dE_{cv}}{dt} - \dot{W}_{cv} - \dot{m}_e e_{fe} \tag{3-5}$$

The second term on the right hand side of (3-4) represents the flow exergy rate at exit (e):

$$\dot{E}_{fe} = \dot{m}_e e_{fe}$$

And is calculated based on Equation (3-6):

$$\dot{E}_{fe} = \dot{m}_e[h - h_0 - T_0(s - s_0) + \frac{V^2}{2} + gz] \tag{3-6}$$

Where:

$e_{fe} = h - h_0 - T_0(s - s_0) + \frac{V^2}{2} + gz$, is called specific flow exergy and all properties are taken at the channel outlet. All variables with the subscript “$_0$” are calculated at the dead state conditions.

Equations (3-4), (3-5), and (3-6) refer to uniform properties at every instant in time, but the unsteady expansion process demonstrates that properties are not uniform in the channel; for this reason two terms in those equations will be written in integral form:

(a) The term E_{cv} will be computed based on Equation (3-2)

(b) The term $\dot{m}_e e_{fe}$ will be computed based on:

$$\dot{m}_e e_{fe} = \dot{E}_{fe} = \left(\iint_{CS} \rho V_r (h - h_{ref}) dA - \iint_{CS} \rho V_r (h_0 - h_{ref}) dA \right) - T_0 \left(\iint_{CS} \rho V_r (s - s_{ref}) dA - \iint_{CS} \rho V_r (s_0 - s_{ref}) dA \right) + \iint_{CS} \rho V_r \left(\frac{|\vec{V}|^2}{2} \right) dA$$

$$\dot{E}_{fe} = \left(\iint_{CS} \rho V_r (h - h_{ref}) dA - \iint_{CS} \rho V_r (h_0 - h_{ref}) dA \right) - T_0 \left(\iint_{CS} \rho V_r (s - s_{ref}) dA - \iint_{CS} \rho V_r (s_0 - s_{ref}) dA \right) + \iint_{CS} \rho V_r \left(\frac{|\vec{V}|^2}{2} \right) dA \qquad (3\text{-}7)$$

Once values are calculated for each time step, a criterion is chosen to determine the end of the expansion process in order to calculate E_{cv}, E_d, E_{fe} and W_{cv}, which account for the entire process. This criterion will lead to the comparison of several cases and are as follows:

(a) When the absolute pressure at the channel inlet reaches the area-weighted average value of 101325 [Pa], or

(b) When all cases undergo the same net exergy change (ΔE)

The following formulas calculate values for the entire process:

$$\Delta E_{cv} = E_f - E_i \qquad (3\text{-}8)$$

Where E_f is determined based on criteria chosen above to terminate the expansion process.

$$E_{fe} = \int_0^t \dot{E}_{fe} dt = \sum_0^i \dot{E}_{fe,i} * \Delta t \tag{3-9}$$

$$W_{cv} = \int_0^t \dot{W}_{cv} dt = \sum_0^i \dot{W}_{cv,i} * \Delta t \tag{3-10}$$

$$E_d = \int_0^t \dot{E}_d dt = \sum_0^i \dot{E}_{d,i} * \Delta t \tag{3-11}$$

The exergy analysis follows to compare cases described by using variables which represent the overall process. In Figure 3-4, percentages of the overall variables are plotted based on the two criteria. All percentages are calculated based on the net exergy change for either criterion case. Both criteria to establish the termination of the expansion process show similar trends of the overall variables and percentage values as well. Therefore, equal net exergy is chosen as the criteria used in discussions (Figure 3-4 (b)).

The trend of the overall value percentage for E_d is opposite to W_{cv} (Figure 3-4). The increase in the rotational velocity enhances work generation but reduces the exergy destruction value. One factor associated with this effect is how quickly the outlet opens, and this will be discussed later.

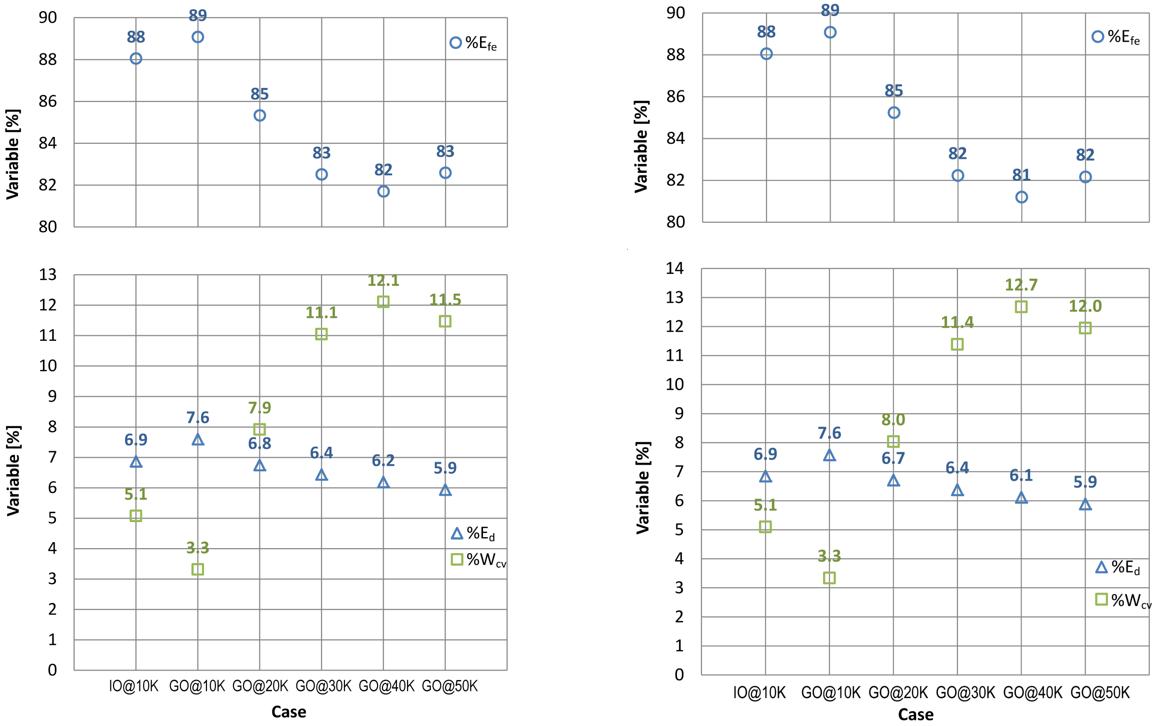

(a) End process based on inlet pressure (b) Equal ΔE

Figure 3-4: Percentage values of the W_{cv}, E_d and E_{fe} with respect to equal ΔE in several cases during the expansion process.

In the graph above, flow exergy has the highest percentages-ranging between 80 to 90% for this particular channel geometry-showing high potential to produce more power in subsequent stages. Another note of the graph is the increase in work generation due to gas expansion in the channel reducing the flow exergy value leaving the channel, indicating the production of work either in the channel or in further stages. However, results in Table 3-1 suggest converting the maximum possible available exergy into work because some exergy will be destroyed if not present in the flow exergy. An explanation of this follows.

	A_i	B_i	C_i	D_i
i	$\%W_i$-$\%W_{GO@10K}$	$\%E_{fe-i}$ + ($\%W_i$-$\%W_{GO@10K}$)	B_i-$B_{GO@10K}$	$\%E_{d-i}$+C_i
GO@10K	0.0	89.1	0.0	7.6
GO@20K	4.7	89.9	0.9	7.6
GO@30K	8.1	90.3	1.2	7.6
GO@40K	9.3	90.5	1.5	7.6
GO@50K	8.6	90.8	1.7	7.6

Table 3-1: Comparison of percentage values with respect to the GO@10K case

Column A_i shows produced work at case "i" with respect to GO@10K case (net difference). In column B_i, the A_i results is added to the % flow exergy of case "i", respectively, and is expected to have the same B_i for all cases if exergy is not destroyed (ideal condition). The justification for this idea is if exergy is not utilized in the channel then it will be used as flow exergy. According to Table 3-1, however, B_i increases with the rotational velocity. All B_i values are then compared with respect to GO@10K case ($B_{GO@10K}$), and results are shown in column C_i. These results are interpreted as the exergy not destroyed with respect to GO@10K, i.e. the value of $C_{GO@50K}$=1.7 is the exergy not destroyed if run at 50,000 rpm. If these results are added to the respective $\%E_d$ cases, then all cases result in the same value and are shown in column D_i.

The trend of overall variable values has been discussed. The next figure shows how these exergy variables change along the expansion process. The rate of each variable is used to describe the process. The rate of E (|dE/dt|) was calculated by using a second order finite difference of each value resulting from equation (3-2). Equations (3-5) and (3-7) are for $\dot{E}_d$ and $\dot{E}_{fe}$ respectively. Thus, in Figure 3-5, graphs for several rotational velocities are shown, and the blue arrow lines define the flow time when the channel outlet is fully open.

According to Figure 3-5, three regions can be approximately defined:

(a) The region immediately after opening (region-I)

(b) During the period of maximum work rate (region-II)

(c) When $\dot{E}_d$ starts to decrease until process completion (region-III)

In region I, the instant opening case shows that |dE/dt|, $\dot{E}_d$ & $\dot{E}_{fe}$ spike in their values due to the nature of channel outlet opening immediately. In the five other cases, as the rotational velocity increases, the spike tends to mirror the immediate opening case, i.e. GO@50K case tends to be as the sudden opening.

In region-II, the maximum work rate increases and shifts toward the left as the rotational velocity increases. The graph shows this effect is influenced by the time position when the channel outlet is fully open, allowing the fluid to follow a trajectory parallel to the channel walls. In region-III, all variable rates tend to converge and decrease to a close zero value.

As presented here, flow exergy at the outlet holds the biggest percentage-ranging between 80 to 90%-of the available potential energy to produce work, thus showing great potential to increase the total power in the wave engine if additional stages for expansion are considered.

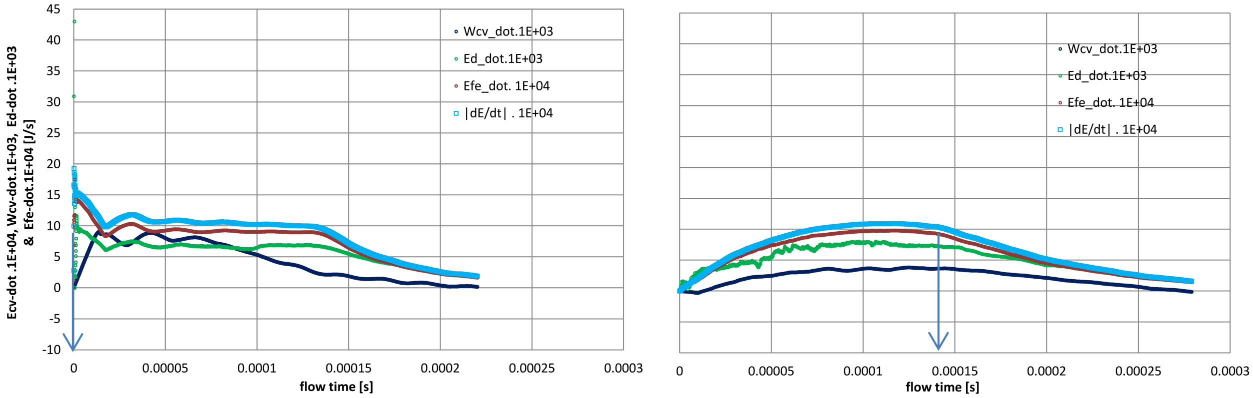

(a) IO@10K (b) GO@10K

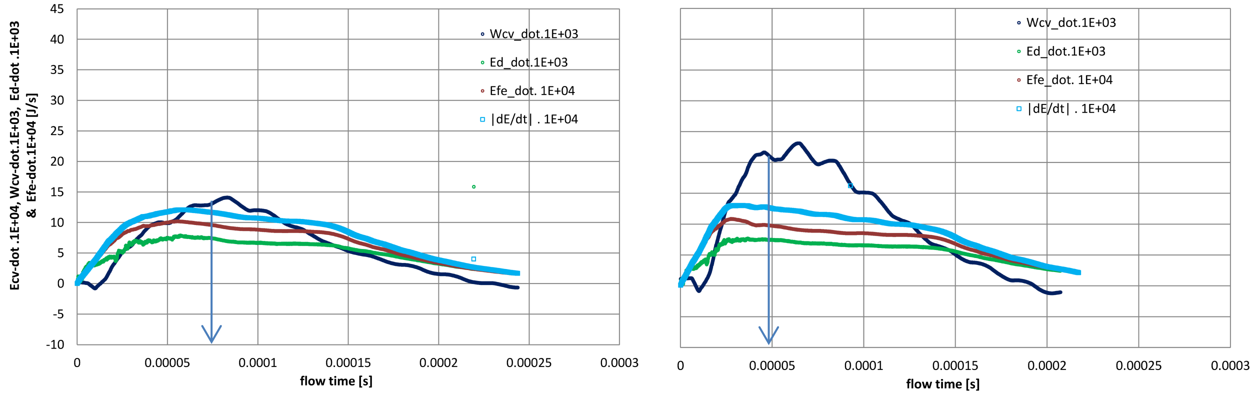

(c) GO@20K (d) GO@30K

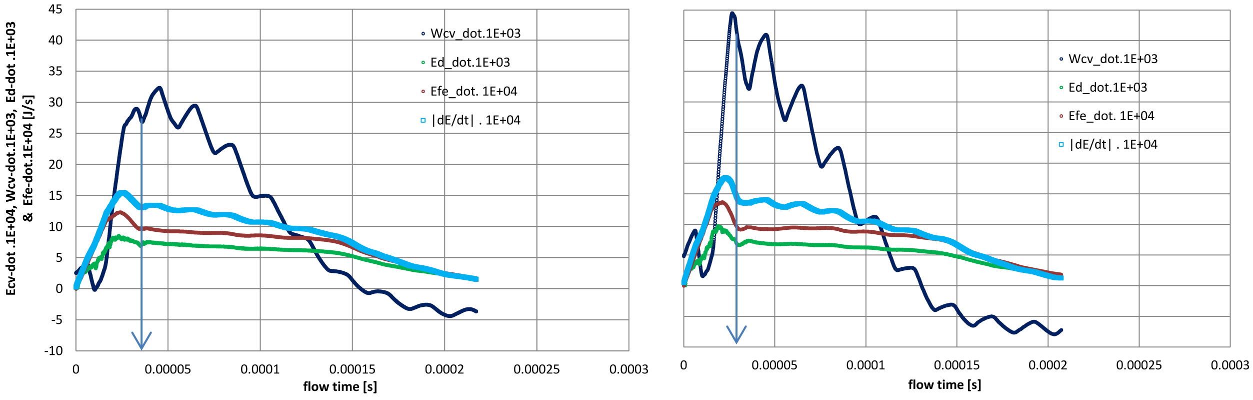

(e) GO@40K (f) GO@50K

Figure 3-5: Plots for |dE/dt|, $\dot{E}_{d}$, $\dot{W}_{cv}$, & $\dot{E}_{fe}$ for several rotational velocities in absolute values. Blue arrows represent the flow time when the channel outlet is fully open.

3.4. Exergetic efficiency for control volume under unsteady state

In this section, the channel geometry needs to be assessed to determine the effectiveness of the energy conversion of the overall expansion process. The exergy concept used to evaluate efficiency is called Exergetic Efficiency or Second Law Efficiency (ε). Equation (3-4) is the starting point for this discussion, where the idealization conditions still apply for the expansion process.

$$\frac{dE_{cv}}{dt} = -\dot{W}_{cv} - \dot{E}_{fe} - \dot{E}_d$$

To be considered for the overall process, the equation is integrated throughout the process time:

$$\int_0^t \frac{dE_{cv}}{dt}\, dt = -\int_0^t \dot{W}_{cv}\, dt - \int_0^t \dot{E}_{fe}\, dt - \int_0^t \dot{E}_d\, dt$$

The first integral term: $\int_0^t \frac{dE_{cv}}{dt} dt$ is equivalent to $\Delta E_{cv} = E_i - E_f$

$$\Delta E_{cv} = -W_{cv} - E_{fe} - E_d \qquad (3\text{-}12)$$

In aerospace engines where exhaust gases are ejected to the atmosphere at high temperatures and velocities to generate thrust, the large flow exergy leaving the system is accounted for as a loss [12], [11]. In this case exergetic efficiency is:

$$\varepsilon = \frac{W_{cv}}{|\Delta E_{cv}|} \times 100 \;\; [\%]$$

When the outlet port is opened the gases are released to generate work in the WDE, but work can still be generated in subsequent stages. Therefore, E_{fe} should not be included in the efficiency calculation. Thus, Equation (3-12) yields:

$$\Delta E_{cv} + E_{fe} = -W_{cv} - E_d$$

ΔE_{cv} has a negative value, meaning $|\Delta E_{cv}| > |\Delta E_{cv} + E_{fe}|$, and so the sum of the two LHS terms represents the exploited exergy in the channel during the expansion process. If RHS consists of work extraction and exergy destruction, the exploited exergy becomes reversible work or isentropic work, and is written as $W_{rev} = W_{cv} + E_d$ or $W_{rev} - W_{cv} = E_d$.

If $E_d = T_0 S_{gen}$, the equation results in the following expression:

$$W_{rev} - W_{cv} = T_0 S_{gen} \tag{3-13}$$

This Equation (3-13) is called the Gouy-Stodola theorem [14]. Thus, the Exergetic Efficiency for the expansion process yields:

$$\varepsilon = \frac{W_{cv}}{W_{rev}} \times 100\ [\%] \tag{3-14}$$

$Where\ W_{rev} = W_{cv} + E_d$

The Exergetic Efficiency is evaluated based on (3-14) and results are presented in Figure 3-6. The ratio of E_d/W_{cv} (Loss/Work) in percentages is included as well.

Based on Figure 3-6, exergy destruction takes place in three different conditions: instant opening, gradual opening at low rotational velocity, and gradual opening at high rotational velocity. The first two conditions show low exergetic efficiency values in contrast to the third condition, in which the efficiency increases to a quasi-constant value as the rotational velocity increases. Each of these three conditions produces different patterns of exergy destruction values based on the port outlet opening.

Bejan [15] performed a two dimensional analysis on a small fluid element dx dy as an open system by using the second law of thermodynamics. This tiny element was subjected to mass fluxes, energy transfer, and entropy transfer interactions, all going through the control surface. As a result an expression was derived to estimate the entropy generation rate per unit volume [W/m3.K]:

$$\dot{S}'''_{gen} = -\frac{1}{T^2}\vec{q}.\nabla T + \frac{\mu}{T}\Phi$$

And considering that $\vec{q} = -k\,\nabla T$, the equation above becomes:

$$\dot{S}'''_{gen} = \frac{1}{T^2}k\,[(\frac{\partial T}{\partial x})^2 + (\frac{\partial T}{\partial y})^2 + (\frac{\partial T}{\partial z})^2] + \frac{\mu}{T}\Phi \tag{3-15}$$

Based on (3-15), two actions produce local irreversibility: heat transfer and viscous effects. The first action is a tendency for a spontaneous energy transfer by conduction in the direction of decreasing temperature when spatial temperature varies. The second effect is related to velocity gradient in the fluid. Both effects will be used to interpret the destruction of exergy in the channel during gas expansion.

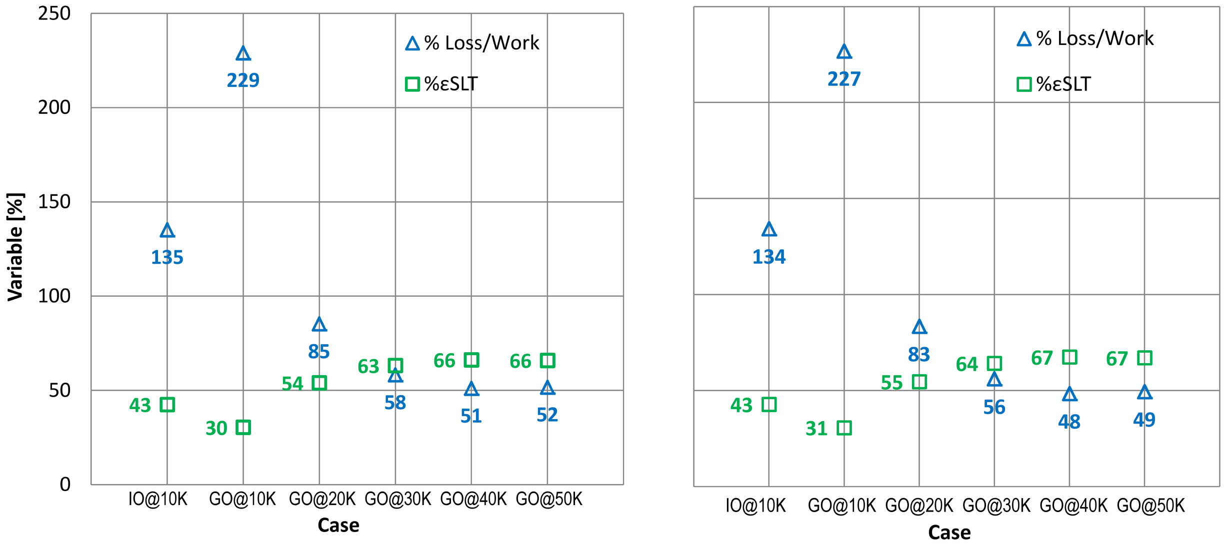

(a) Equal P-in (b) Equal ΔE

Figure 3-6: Exergetic Efficiency [%] and Loss/work generated for several rotational velocities

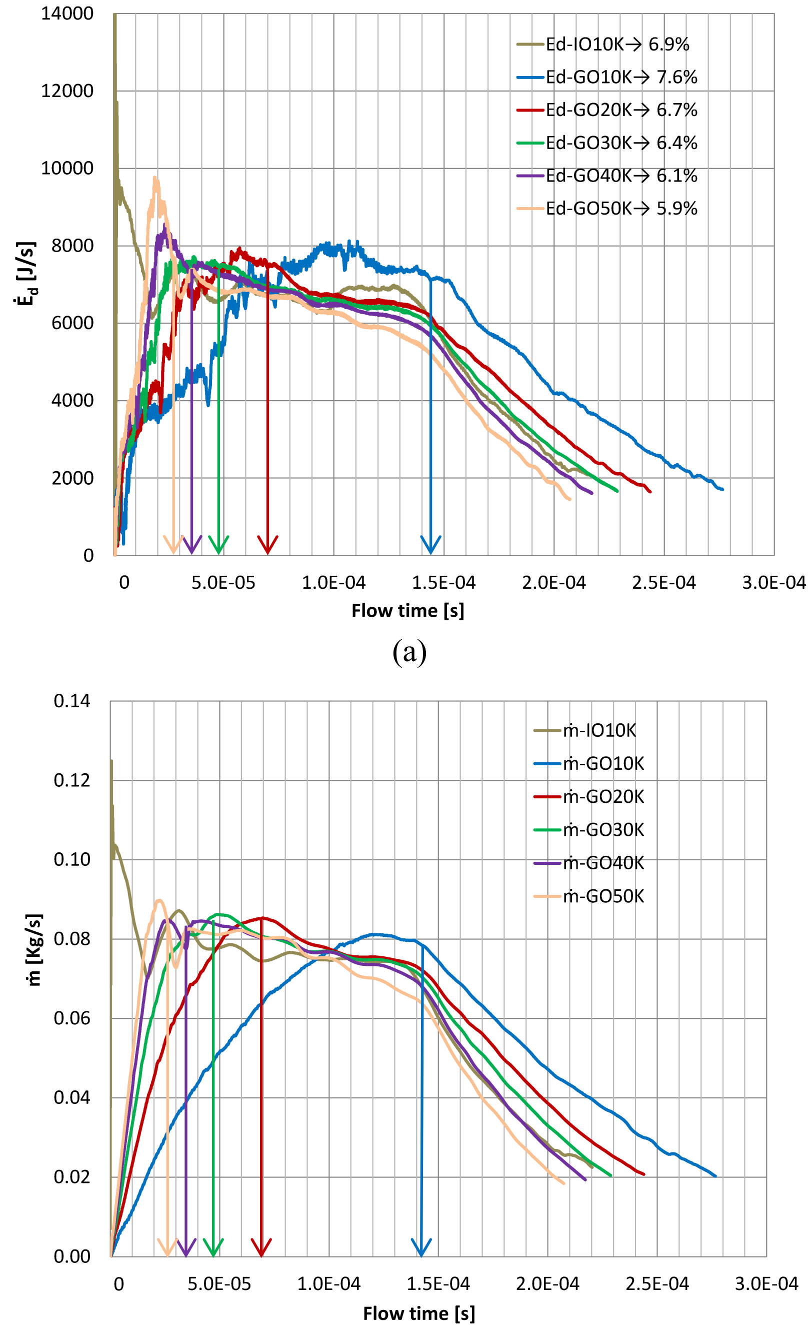

(a)

(b)

Figure 3-7: Comparison of % of exergy destruction (equal exergy for all cases) with mass flow rate. Arrows represent the time when the outlets fully open.

The rate of exergy destruction and mass flow rate plots are shown in Figure 3-7 for comparison; and an analogous trend between same case plots is found. Instant opening and high rotational velocity cases destroy exergy at higher rate at the beginning of the process but their overall exergy destruction values are smaller than the slow outlet opening case (see legend Figure 3-7(a)). The high $\dot{m}$ is linked with the full or faster outlet opening area. This condition generates high spatial temperature gradients along with viscous losses which cause a spike in the exergy destruction rate when the channel outlet opens instantly. A sharp increase in the exergy destruction rate is also produced in the quick outlet opening cases. The slow opening case -10000 rpm- destroys exergy at very low rates in the beginning, but continues destroying for longer time which results in the highest overall value of exergy destruction.

Based on results, the operation of the rotor at high velocities reduces losses or destroys less exergy.

CHAPTER 4. ENERGY ANALYSIS OF THE UNSTEADY EXPANSION PROCESS

4.1. Zero-dimensional Macroscopic Analytical Model of the Unsteady Expansion Process

Figure 4-1 depicts all four processes of the wave engine. The unsteady expansion process, the final process of the WDE cycle, is analyzed.

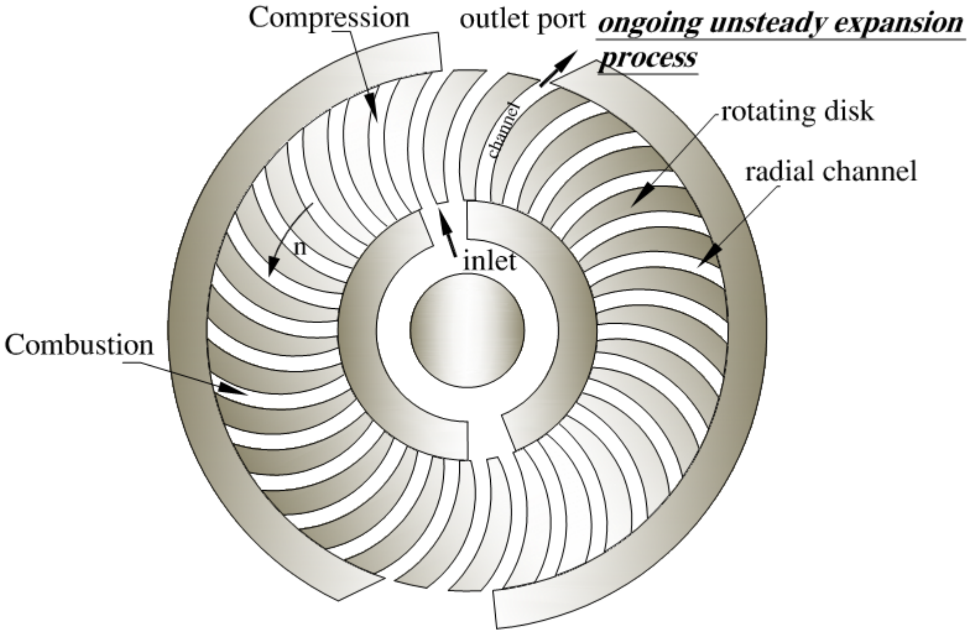

Figure 4-1: Schematic of the wave disc engine with curved channels (two cycles per revolution).

Energy analysis is performed using the rate form of the general energy balance equation for a transient-flow process considering the inertial control volume from Figure 6-1: the control volume is the area surrounded by the two dotted concentric circles. During the expansion process the control volume only exchanges mass through the outlet port. This process starts when the outlet port begins to open, either quickly or gradually.

The rate of energy change in the system is equivalent to the rate of net energy transfer through the control volume [16]:

$$\frac{dE_{system}}{dt} = \dot{E}_{in} - \dot{E}_{out} \tag{4-1}$$

Where:

Specific total energy of the system:

$$\mathrm{e} = \mathrm{u} + \mathrm{ke} + \mathrm{pe} = \mathrm{u} + \frac{\mathrm{V}^2}{2} + \mathrm{gz} \tag{4-2}$$

The total energy of the system:

$$E_{system} = \mathrm{m}_{sys}.\,\mathrm{e} \tag{4-3}$$

The specific total energy for a flowing fluid:

$$\Theta = \mathrm{h} + \mathrm{ke} + \mathrm{pe} = \mathrm{h} + \frac{\mathrm{V}^2}{2} + \mathrm{gz} \tag{4-4}$$

Amount of energy transport:

$$\dot{\mathrm{E}}_{\mathrm{mass,b}} = \dot{\mathrm{m}}\Theta = \dot{\mathrm{m}}(\mathrm{h} + \frac{\mathrm{V}^2}{2} + \mathrm{gz}\,) \tag{4-5}$$

Rate of energy transfer by heat, work and mass:

$$\dot{E}_b = \dot{Q}_b + \dot{W}_b + \dot{\mathrm{E}}_{\mathrm{mass,b}} \tag{4-6}$$

Where: $b = in\ or\ out$

Replacing (4-2), (4-5) and (4-6) in Equation (4-1):

$$\frac{d(\mathrm{m}_{sys}.\,[\mathrm{u}_{sys} + \frac{{\mathrm{V}_{sys}}^2}{2} + \mathrm{gz}_{sys}])}{dt} = [\dot{Q}_{in} + \dot{W}_{in} + \dot{\mathrm{m}}_{in}(\mathrm{h}_{in} + \frac{{\mathrm{V}_{in}}^2}{2} + \mathrm{gz}_{in}\,)\ ] - [\dot{Q}_{out} + \dot{W}_{out} + \dot{\mathrm{m}}_{out}(\mathrm{h}_{out} + \frac{{\mathrm{V}_{in}}^2}{2} + \mathrm{gz}_{out}\,)\ ] \tag{4-7}$$

In Equation (4-7), macroscopic properties of the fluid within the channel or the incoming/outgoing flow streams are considered to be uniform but properties actually change with the position. Having representative values for the fluid within the channel or flow streams at the outlet port is necessary to derive a zero-dimensional macroscopic balance equation. Thus, mass-weighted average or volume-weighted average will be used accordingly.

For the representative property $\widehat{\emptyset}$ at the surface boundary [17]:

$$\widehat{\emptyset} = \frac{\int \emptyset\rho|\vec{v}_i.\vec{A}_i|}{\int \rho|\vec{v}_i.\vec{A}_i|} = \frac{\sum_{i=1}^{n}\emptyset_i\rho_i|\vec{v}_i.\vec{A}_i|}{\sum_{i=1}^{n}\rho_i|\vec{v}_i.\vec{A}_i|} \tag{4-8}$$

For the representative property $\widehat{\emptyset}$ of the control volume [17]:

$$\widehat{\emptyset} = \frac{\int \emptyset\rho\, d\cancel{V}}{\int \rho\, d\cancel{V}} = \frac{\sum_{i=1}^{n}\emptyset_i\rho_i|\cancel{V}_i|}{\sum_{i=1}^{n}\rho_i|\cancel{V}_i|} \tag{4-9}$$

Temperature, internal energy, enthalpy and velocity magnitude will be calculated based on Equations (4-8) and (4-9) for volume and surface, respectively. Volume-weighted average will be used to calculate the representative pressure and density values in the channel according to equation (4-10) [17].

$$\widehat{\emptyset} = \frac{1}{\cancel{V}}\int \emptyset d\cancel{V} = \frac{1}{\cancel{V}}\sum_{i=1}^{n}\emptyset_i|\cancel{V}_i| \tag{4-10}$$

Changing to representative variables in (4-7):

$$\frac{d(\mathrm{m}_{sys}.[\hat{\mathrm{u}}_{sys} + \frac{\hat{\mathrm{V}}_{sys}^{\;2}}{2} + \mathrm{g}\hat{\mathrm{z}}_{sys}])}{dt} = [\dot{Q}_{in} + \dot{W}_{in} + \dot{\mathrm{m}}_{in}(\hat{\mathrm{h}}_{in} + \frac{\hat{\mathrm{V}}_{in}^{\;2}}{2} + \mathrm{g}\hat{\mathrm{z}}_{in}\ )\ ] - [\dot{Q}_{out} + \dot{W}_{out} + \dot{\mathrm{m}}_{out}(\hat{\mathrm{h}}_{out} + \frac{\hat{\mathrm{V}}_{in}^{\;2}}{2} + \mathrm{g}\hat{\mathrm{z}}_{out}\ )\ ] \tag{4-11}$$

Several conditions are applied to Equation (4-11) based on ideal WDE working conditions of a single channel and fixed control volume chosen.

Condition-1:

(a) The rotor is flat (2-D), then variables $\hat{\mathrm{z}}_{sys}, \hat{\mathrm{z}}_{in}\ and\ \hat{\mathrm{z}}_{out} = 0$

(b) There is not work done on the system or work input, $\dot{W}_{in} = 0$

(c) The control volume chosen does not exchange heat with the surroundings. Thus, $\dot{Q}_{in}\ or\ \dot{Q}_{out} = 0$. The same condition applies as well to channel walls.

(d) There is not incoming flow to the control volume and to the channel.

Based on condition-1, equation (4-11) becomes:

$$\frac{d(\mathrm{m}_{sys}.[\hat{\mathrm{u}}_{sys}+\frac{\hat{\mathrm{V}}_{sys}^{\ 2}}{2}])}{dt} = -[\dot{W}_{out}+\dot{\mathrm{m}}_{out}(\hat{\mathrm{h}}_{out}+\frac{\hat{\mathrm{V}}_{out}^{\ 2}}{2})\ ] \tag{4-12}$$

Solving Equation (4-12) for the generated work:

$$\dot{W}_{out} = -\ \frac{d(\mathrm{m}_{sys}.[\hat{\mathrm{u}}_{sys}+\frac{\hat{\mathrm{V}}_{sys}^{\ 2}}{2}])}{dt} - \dot{\mathrm{m}}_{out}(\hat{\mathrm{h}}_{out}+\frac{\hat{\mathrm{V}}_{out}^{\ 2}}{2})$$

Expressing the rate equation for a finite interval of time δt:

$$\frac{\delta \mathrm{W}_{out}}{\delta t} = -\ \frac{\delta(\mathrm{m}_{sys}.[\hat{\mathrm{u}}_{sys}+\frac{\hat{\mathrm{V}}_{sys}^{\ 2}}{2}])}{\delta t} - \frac{\delta \mathrm{m}_{out}}{\delta t}(\hat{\mathrm{h}}_{out}+\frac{\hat{\mathrm{V}}_{out}^{\ 2}}{2})$$

Removing δt from the denominator:

$$\delta \mathrm{W}_{out} = -\ \delta(\mathrm{m}_{sys}.[\hat{\mathrm{u}}_{sys}+\frac{\hat{\mathrm{V}}_{sys}^{\ 2}}{2}]) - \delta \mathrm{m}_{out}(\hat{\mathrm{h}}_{out}+\frac{\hat{\mathrm{V}}_{out}^{\ 2}}{2}) \tag{4-13}$$

Considering that:

$\delta E_{sys} = E_{sys,j+1} - E_{sys,j}$ Or

$$\delta\left(\mathrm{m}_{sys}.\left[\hat{\mathrm{u}}_{sys}+\frac{\hat{\mathrm{V}}_{sys}^{\ 2}}{2}\right]\right) = m_{\mathrm{sys,j+1}}\left(\hat{\mathrm{u}}_{\mathrm{j+1}}+\frac{\hat{\mathrm{V}}_{\mathrm{j+1}}^{2}}{2}+g\hat{\mathrm{z}}_{\mathrm{j+1}}\right) - m_{\mathrm{sys,j}}\left(\hat{\mathrm{u}}_{\mathrm{j}}+\frac{\hat{\mathrm{V}}_{\mathrm{j}}^{2}}{2}+g\hat{\mathrm{z}}_{\mathrm{j}}\right)$$

Convention of symbols:

j = beginning of the process (j=1)

j+1= end of the process (j=2)

Then:

$$\delta\left(\mathrm{m}_{sys}\cdot\left[\hat{\mathrm{u}}_{sys}+\frac{\hat{\mathrm{V}}_{sys}{}^{2}}{2}\right]\right)=m_{\mathrm{sys},2}\left(\hat{\mathrm{u}}_{2}+\frac{\hat{\mathrm{V}}_{2}^{2}}{2}\right)-\ m_{\mathrm{sys},1}\left(\hat{\mathrm{u}}_{1}+\frac{\hat{\mathrm{V}}_{1}^{2}}{2}\right) \tag{4-14}$$

Replacing result of (4-14) into Equation (4-13):

$$\delta\mathrm{W}_{out}=m_{\mathrm{sys},1}\left(\hat{\mathrm{u}}_{1}+\frac{\hat{\mathrm{V}}_{1}^{2}}{2}\right)-\ m_{\mathrm{sys},2}\left(\hat{\mathrm{u}}_{2}+\frac{\hat{\mathrm{V}}_{2}^{2}}{2}\right)-\delta\mathrm{m}_{out}(\hat{\mathrm{h}}_{out}+\frac{\hat{\mathrm{V}}_{out}{}^{2}}{2}) \tag{4-15}$$

Now, the conservation of mass principle is applied to the fixed control volume:

$$\dot{m}_{\mathrm{in}}-\dot{m}_{out}=\frac{dm_{sys}}{dt}$$

With the condition-1 that no incoming flow entering the control volume $\dot{m}_{\mathrm{in}}=0$, it yields:

$$-\dot{m}_{out}=\frac{dm_{sys}}{dt}$$

Expressing this instantaneous equation for a finite time δt:

$$-\frac{\delta m_{out}}{\delta t}=\frac{\delta m_{sys}}{\delta t} \tag{4-16}$$

Taking into account that:

$$\delta m_{sys}=m_{sys,j+1}-m_{sys,j}=m_{sys,2}-m_{sys,1}$$

Replacing in (4-16):

$$-\delta m_{out}=m_{sys,2}-m_{sys,1} \tag{4-17}$$

Replacing (4-17) into (4-15):

$$\delta\mathrm{W}_{out}=m_{\mathrm{sys},1}\left(\hat{\mathrm{u}}_{1}+\frac{\hat{\mathrm{V}}_{1}^{2}}{2}\right)-\ m_{\mathrm{sys},2}\left(\hat{\mathrm{u}}_{2}+\frac{\hat{\mathrm{V}}_{2}^{2}}{2}\right)+(m_{sys,2}-m_{sys,1})(\hat{\mathrm{h}}_{out}+\frac{\hat{\mathrm{V}}_{out}{}^{2}}{2}) \tag{4-18}$$

Equation (4-18) is the energy balance for a finite time "δt" during the unsteady expansion process. To describe the progress of the process, the criteria of "Finite Stages" for intervals of Δt time, is applied by using the concept in Figure 4-2.

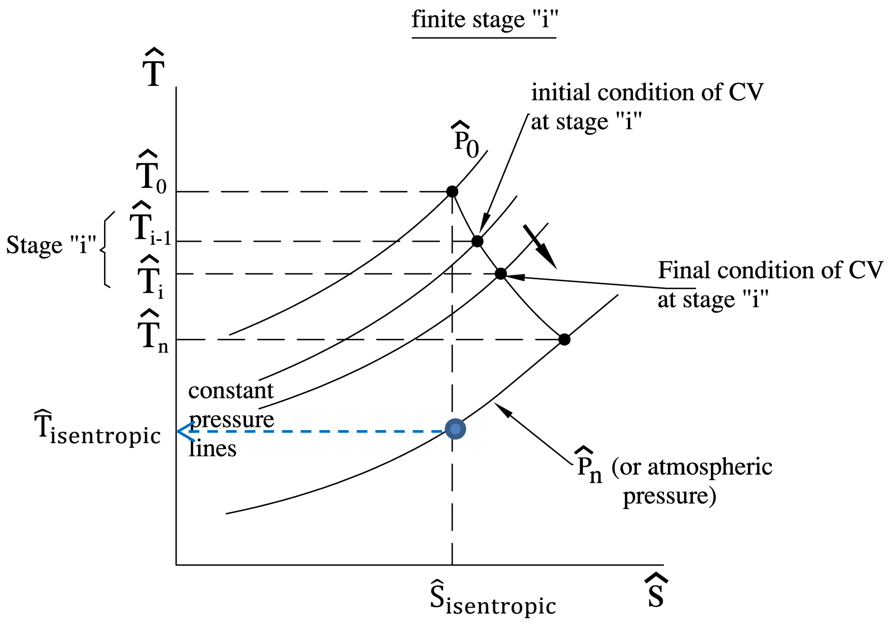

Figure 4-2: Unsteady expansion process for stage “i”

Considering an arbitrary finite stage “i” and dropping the index “sys” to simplify the expression, equation (4-18) becomes:

$$\delta W_{out,i} = m_{1,i}\left(\hat{u}_{1,i} + \frac{\hat{V}_{1,i}^2}{2}\right) - m_{2,i}\left(\hat{u}_{2,i} + \frac{\hat{V}_{2,i}^2}{2}\right) + (m_{2,i} - m_{1,i})\left(\hat{h}_{out,i} + \frac{\hat{V}_{out,i}^{\;2}}{2}\right) \tag{4-19}$$

Describing every time-step of the unsteady expansion process from the beginning to the end:

stage "i"	Finite work done
1	$\delta W_{out,1} = m_{1,1}\left(\hat{\mathrm{u}}_{1,1} + \frac{\hat{\mathrm{V}}_{1,1}^2}{2}\right) - m_{2,1}\left(\hat{\mathrm{u}}_{2,1} + \frac{\hat{\mathrm{V}}_{2,1}^2}{2}\right) + (m_{2,1} - m_{1,1})(\hat{\mathrm{h}}_{out,1} + \frac{\hat{\mathrm{V}}_{out,1}^2}{2})$
2	$\delta W_{out,2} = m_{1,2}\left(\hat{\mathrm{u}}_{1,2} + \frac{\hat{\mathrm{V}}_{1,2}^2}{2}\right) - m_{2,2}\left(\hat{\mathrm{u}}_{2,2} + \frac{\hat{\mathrm{V}}_{2,2}^2}{2}\right) + (m_{2,2} - m_{1,2})(\hat{\mathrm{h}}_{out,2} + \frac{\hat{\mathrm{V}}_{out,2}^2}{2})$
3	$\delta W_{out,3} = m_{1,3}\left(\hat{\mathrm{u}}_{1,3} + \frac{\hat{\mathrm{V}}_{1,3}^2}{2}\right) - m_{2,3}\left(\hat{\mathrm{u}}_{2,3} + \frac{\hat{\mathrm{V}}_{2,3}^2}{2}\right) + (m_{2,3} - m_{1,3})(\hat{\mathrm{h}}_{out,3} + \frac{\hat{\mathrm{V}}_{out,3}^2}{2})$
4	$\delta W_{out,4} = m_{1,4}\left(\hat{\mathrm{u}}_{1,4} + \frac{\hat{\mathrm{V}}_{1,4}^2}{2}\right) - m_{2,4}\left(\hat{\mathrm{u}}_{2,4} + \frac{\hat{\mathrm{V}}_{2,4}^2}{2}\right) + (m_{2,4} - m_{1,4})(\hat{\mathrm{h}}_{out,4} + \frac{\hat{\mathrm{V}}_{out,4}^2}{2})$
5	$\delta W_{out,5} = m_{1,5}\left(\hat{\mathrm{u}}_{1,5} + \frac{\hat{\mathrm{V}}_{1,5}^2}{2}\right) - m_{2,5}\left(\hat{\mathrm{u}}_{2,5} + \frac{\hat{\mathrm{V}}_{2,5}^2}{2}\right) + (m_{2,5} - m_{1,5})(\hat{\mathrm{h}}_{out,5} + \frac{\hat{\mathrm{V}}_{out,5}^2}{2})$
	. . .
n-1	$\delta W_{out,n-1} = m_{1,n-1}\left(\hat{\mathrm{u}}_{1,n-1} + \frac{\hat{\mathrm{V}}_{1,n-1}^2}{2}\right) - m_{2,n-1}\left(\hat{\mathrm{u}}_{2,n-1} + \frac{\hat{\mathrm{V}}_{2,n-1}^2}{2}\right) + (m_{2,n-1} - m_{1,n-1})(\hat{\mathrm{h}}_{out,n-1} + \frac{\hat{\mathrm{V}}_{out,n-1}^2}{2})$
n	$\delta W_{out,n} = m_{1,\mathrm{n}}\left(\hat{\mathrm{u}}_{1,\mathrm{n}} + \frac{\hat{\mathrm{V}}_{1,\mathrm{n}}^2}{2}\right) - m_{2,\mathrm{n}}\left(\hat{\mathrm{u}}_{2,\mathrm{n}} + \frac{\hat{\mathrm{V}}_{2,\mathrm{n}}^2}{2}\right) + (m_{2,n} - m_{1,n})(\hat{\mathrm{h}}_{out,n} + \frac{\hat{\mathrm{V}}_{out,n}^2}{2})$

Table 4-1: Detailed description of the unsteady expansion process at each stage "i"

Matching parameters between two consecutives stages: the final state of the system during stages "i" will have the same conditions for the initial state of the system in the following stage "i+1". For instance, if stage 1 and 2 are matched, it yields:

$$m_{2,1}\left(\hat{\mathrm{u}}_{2,1} + \frac{\hat{\mathrm{V}}_{2,1}^2}{2}\right) = m_{1,2}\left(\hat{\mathrm{u}}_{1,2} + \frac{\hat{\mathrm{V}}_{1,2}^2}{2}\right)$$

Because: $m_{2,1} = m_{1,2}$; $\hat{\mathrm{u}}_{2,1} = \hat{\mathrm{u}}_{1,2}$; $\hat{\mathrm{V}}_{2,1}^2 = \hat{\mathrm{V}}_{1,2}^2$, and the same condition is applied for process 2 and 3, 3 and 4 … n-1 and n processes.

Then the summation of all the $\delta W_{out,i}$ in Table 4-1 yields:

$$\begin{aligned}\sum_{i=1}^{n}(\delta W_{out,i}) = {} & m_{1,1}\left(\hat{\mathrm{u}}_{1,1} + \frac{\hat{\mathrm{V}}_{1,1}^2}{2}\right) - m_{2,\mathrm{n}}\left(\hat{\mathrm{u}}_{2,\mathrm{n}} + \frac{\hat{\mathrm{V}}_{2,\mathrm{n}}^2}{2}\right) \\ & + \left(m_{2,1} - m_{1,1}\right)\left(\hat{\mathrm{h}}_{out,1} + \frac{\hat{\mathrm{V}}_{out,1}^2}{2}\right) + \left(m_{2,2} - m_{1,2}\right)\left(\hat{\mathrm{h}}_{out,2} + \frac{\hat{\mathrm{V}}_{out,2}^2}{2}\right) \\ & + \left(m_{2,3} - m_{1,3}\right)\left(\hat{\mathrm{h}}_{out,3} + \frac{\hat{\mathrm{V}}_{out,3}^2}{2}\right) + \left(m_{2,4} - m_{1,4}\right)\left(\hat{\mathrm{h}}_{out,4} + \frac{\hat{\mathrm{V}}_{out,4}^2}{2}\right) \\ & + \left(m_{2,5} - m_{1,5}\right)\left(\hat{\mathrm{h}}_{out,5} + \frac{\hat{\mathrm{V}}_{out,5}^2}{2}\right) \ldots\ldots\ldots + (m_{2,n-1} \\ & - m_{1,n-1})(\hat{\mathrm{h}}_{out,n-1} + \frac{\hat{\mathrm{V}}_{out,n-1}^2}{2}) + (m_{2,n} - m_{1,n})(\hat{\mathrm{h}}_{out,n} + \frac{\hat{\mathrm{V}}_{out,n}^2}{2})\end{aligned} \qquad (4\text{-}20)$$

The mass of the system is expressed in terms of volume-weighted average:

$$m_{1,\mathrm{i}} = \hat{\rho}_{1,\mathrm{i}}\mathrm{V\!\!\!-} \qquad\qquad m_{2,\mathrm{i}} = \hat{\rho}_{2,\mathrm{i}}\mathrm{V\!\!\!-} \qquad (4\text{-}21)$$

The volume $\mathrm{V\!\!\!-}$ of the channel is constant at all stages. Replacing (4-21) into (4-20):

$$\begin{aligned}W_{out} = {} & \sum_{i=1}^{n}(\delta W_{out,i}) \\ = {} & \hat{\rho}_{1,1}\mathrm{V\!\!\!-}\left(\hat{\mathrm{u}}_{1,1} + \frac{\hat{\mathrm{V}}_{1,1}^2}{2}\right) - \hat{\rho}_{2,\mathrm{n}}\mathrm{V\!\!\!-}\left(\hat{\mathrm{u}}_{2,\mathrm{n}} + \frac{\hat{\mathrm{V}}_{2,\mathrm{n}}^2}{2}\right) + \mathrm{V\!\!\!-}\left(\hat{\rho}_{2,1} - \hat{\rho}_{1,1}\right)\left(\hat{\mathrm{h}}_{out,1} + \frac{\hat{\mathrm{V}}_{out,1}^2}{2}\right) \\ & + \mathrm{V\!\!\!-}\left(\hat{\rho}_{2,2} - \hat{\rho}_{1,2}\right)\left(\hat{\mathrm{h}}_{out,2} + \frac{\hat{\mathrm{V}}_{out,2}^2}{2}\right) + \mathrm{V\!\!\!-}\left(\hat{\rho}_{2,3} - \hat{\rho}_{1,3}\right)\left(\hat{\mathrm{h}}_{out,3} + \frac{\hat{\mathrm{V}}_{out,3}^2}{2}\right) \\ & + \mathrm{V\!\!\!-}\left(\hat{\rho}_{2,4} - \hat{\rho}_{1,4}\right)\left(\hat{\mathrm{h}}_{out,4} + \frac{\hat{\mathrm{V}}_{out,4}^2}{2}\right) + \mathrm{V\!\!\!-}\left(\hat{\rho}_{2,5} - \hat{\rho}_{1,5}\right)\left(\hat{\mathrm{h}}_{out,5} + \frac{\hat{\mathrm{V}}_{out,5}^2}{2}\right) \ldots\ldots\ldots \\ & + \mathrm{V\!\!\!-}(\hat{\rho}_{2,n-1} - \hat{\rho}_{1,n-1})(\hat{\mathrm{h}}_{out,n-1} + \frac{\hat{\mathrm{V}}_{out,n-1}^2}{2}) + \mathrm{V\!\!\!-}(\hat{\rho}_{2,n} - \hat{\rho}_{1,n})(\hat{\mathrm{h}}_{out,n} + \frac{\hat{\mathrm{V}}_{out,n}^2}{2})\end{aligned}$$

The index notation of the above expression will be translated into the flow time notation as follows:

(a) Index “0” corresponds to the initial state of stage 1 and “1” to the end state of stage 1.

(b) Index “1” correspond to the initial state of stage 2 and “2” to the end state of stage 2

(c) Index “2” correspond to the initial state of stage 3 and “3” to the end state of stage 3, and so on.

Condition-2:

Parameters at the outlet boundary ($\hat{\mathrm{h}}_{out,i}$, $\hat{\mathrm{V}}_{out,i}$) are regarded as constant values during each finite stage “i” but varies at each finite stage.

$$
\begin{aligned}
W_{out} = \text{¥}\Bigg\{ & \hat{\rho}_0\left(\hat{\mathrm{u}}_0+\frac{\hat{\mathrm{V}}_0^2}{2}\right)-\hat{\rho}_\mathrm{n}\left(\hat{\mathrm{u}}_\mathrm{n}+\frac{\hat{\mathrm{V}}_\mathrm{n}^2}{2}\right)+(\hat{\rho}_1-\hat{\rho}_0)\left(\hat{\mathrm{h}}_{out,1}+\frac{\hat{\mathrm{V}}_{out,1}^2}{2}\right) \\
& +(\hat{\rho}_2-\hat{\rho}_1)\left(\hat{\mathrm{h}}_{out,2}+\frac{\hat{\mathrm{V}}_{out,2}^2}{2}\right)+(\hat{\rho}_3-\hat{\rho}_2)\left(\hat{\mathrm{h}}_{out,3}+\frac{\hat{\mathrm{V}}_{out,3}^2}{2}\right) \\
& +(\hat{\rho}_4-\hat{\rho}_3)\left(\hat{\mathrm{h}}_{out,4}+\frac{\hat{\mathrm{V}}_{out,4}^2}{2}\right)+(\hat{\rho}_5-\hat{\rho}_4)\left(\hat{\mathrm{h}}_{out,5}+\frac{\hat{\mathrm{V}}_{out,5}^2}{2}\right)\dots\dots.\dots \\
& +(\hat{\rho}_{n-1}-\hat{\rho}_{n-2})\left(\hat{\mathrm{h}}_{out,n-1}+\frac{\hat{\mathrm{V}}_{out,n-1}^2}{2}\right) \\
& +(\hat{\rho}_{n}-\hat{\rho}_{n-1})\left(\hat{\mathrm{h}}_{out,n}+\frac{\hat{\mathrm{V}}_{out,n}^2}{2}\right)\Bigg\}
\end{aligned}
\tag{4-22}
$$

Series Taylor expansion is applied for the density parameter to simplify Equation (4-22):

$$\hat{\rho}_{(\mathrm{t}+\Delta\mathrm{t})}=\hat{\rho}_\mathrm{t}+(\frac{\partial\hat{\rho}}{\partial\mathrm{t}})_t\Delta t+(\frac{\partial^2\hat{\rho}}{\partial\mathrm{t}^2})_t\frac{(\Delta t)^2}{2}+(\frac{\partial^3\hat{\rho}}{\partial\mathrm{t}^3})_t\frac{(\Delta t)^3}{6}+\ \dots+(\frac{\partial^\mathrm{n}\hat{\rho}}{\partial\mathrm{t}^\mathrm{n}})_t\frac{(\Delta t)^n}{n!}+\cdots$$

The volume-weighted average density will be considered for a second order-accurate, and higher order terms will be a truncation error:

$$\hat{\rho}_{(\mathrm{t}+\Delta\mathrm{t})}=\hat{\rho}_\mathrm{t}+(\frac{\partial\hat{\rho}}{\partial\mathrm{t}})_t\Delta t+(\frac{\partial^2\hat{\rho}}{\partial\mathrm{t}^2})_t\frac{(\Delta t)^2}{2}$$

Translating the stage “i” in terms of time step:

Time step		
0	At t_0=0	$\hat{\rho}_{(t_0=0)} = \hat{\rho}_0$
1	At $t_1 = t_0 + \Delta t = 0 + \Delta t = 1\Delta t$	$\hat{\rho}_{\Delta t} = \hat{\rho}_{(0+\Delta t)} = \hat{\rho}_0 + (\frac{\partial \hat{\rho}}{\partial t})_0 \Delta t + (\frac{\partial^2 \hat{\rho}}{\partial t^2})_0 \frac{(\Delta t)^2}{2}$
2	At $t_2 = t_1 + \Delta t = \Delta t + \Delta t = 2\Delta t$	$\hat{\rho}_{2\Delta t} = \hat{\rho}_{(\Delta t+\Delta t)} = \hat{\rho}_{\Delta t} + (\frac{\partial \hat{\rho}}{\partial t})_{\Delta t} \Delta t + (\frac{\partial^2 \hat{\rho}}{\partial t^2})_{\Delta t} \frac{(\Delta t)^2}{2}$
3	At $t_3 = t_2 + \Delta t = 2\Delta t + \Delta t = 3\Delta t$	$\hat{\rho}_{3\Delta t} = \hat{\rho}_{(2\Delta t+\Delta t)}$ $= \hat{\rho}_{2\Delta t} + (\frac{\partial \hat{\rho}}{\partial t})_{2\Delta t} \Delta t$ $+ (\frac{\partial^2 \hat{\rho}}{\partial t^2})_{2\Delta t} \frac{(\Delta t)^2}{2}$
4	At $t_4 = t_3 + \Delta t = 3\Delta t + \Delta t = 4\Delta t$	$\hat{\rho}_{4\Delta t} = \hat{\rho}_{(3\Delta t+\Delta t)}$ $= \hat{\rho}_{3\Delta t} + (\frac{\partial \hat{\rho}}{\partial t})_{3\Delta t} \Delta t$ $+ (\frac{\partial^2 \hat{\rho}}{\partial t^2})_{3\Delta t} \frac{(\Delta t)^2}{2}$
…	…..	….
…	…..	….
n	At $t_n = t_{(n-1)} + \Delta t = (n-1)\Delta t + \Delta t = n\Delta t$	$\hat{\rho}_{((n-1)\Delta t+\Delta t)} = \hat{\rho}_{(n-1)\Delta t} + (\frac{\partial \hat{\rho}}{\partial t})_{(n-1)\Delta t} \Delta t$ $+ (\frac{\partial^2 \hat{\rho}}{\partial t^2})_{(n-1)\Delta t} \frac{(\Delta t)^2}{2}$

Table 4-2: Development of the $\hat{\rho}$ according to Series Taylor expansion for each t_i

Expressions from Table 4-2 are replaced into the $\hat{\rho}$ variable of equation (4-22):

i	
1	$\hat{\rho}_1 - \hat{\rho}_0 = (\hat{\rho}_0 + (\frac{\partial\hat{\rho}}{\partial t})_0 \Delta t + (\frac{\partial^2\hat{\rho}}{\partial t^2})_0 \frac{(\Delta t)^2}{2}) - \hat{\rho}_0 = (\frac{\partial\hat{\rho}}{\partial t})_0 \Delta t + (\frac{\partial^2\hat{\rho}}{\partial t^2})_0 \frac{(\Delta t)^2}{2}$
2	$\hat{\rho}_2 - \hat{\rho}_1 = (\hat{\rho}_{\Delta t} + (\frac{\partial\hat{\rho}}{\partial t})_{\Delta t} \Delta t + (\frac{\partial^2\hat{\rho}}{\partial t^2})_{\Delta t} \frac{(\Delta t)^2}{2}) - \hat{\rho}_{\Delta t} = (\frac{\partial\hat{\rho}}{\partial t})_{\Delta t} \Delta t + (\frac{\partial^2\hat{\rho}}{\partial t^2})_{\Delta t} \frac{(\Delta t)^2}{2}$
3	$\hat{\rho}_3 - \hat{\rho}_2 = (\hat{\rho}_{2\Delta t} + (\frac{\partial\hat{\rho}}{\partial t})_{2\Delta t} \Delta t + (\frac{\partial^2\hat{\rho}}{\partial t^2})_{2\Delta t} \frac{(\Delta t)^2}{2}) - \hat{\rho}_{2\Delta t} = (\frac{\partial\hat{\rho}}{\partial t})_{2\Delta t} \Delta t + (\frac{\partial^2\hat{\rho}}{\partial t^2})_{2\Delta t} \frac{(\Delta t)^2}{2}$
4	$\hat{\rho}_4 - \hat{\rho}_3 = (\hat{\rho}_{3\Delta t} + (\frac{\partial\hat{\rho}}{\partial t})_{3\Delta t} \Delta t + (\frac{\partial^2\hat{\rho}}{\partial t^2})_{3\Delta t} \frac{(\Delta t)^2}{2}) - \hat{\rho}_{3\Delta t} = (\frac{\partial\hat{\rho}}{\partial t})_{3\Delta t} \Delta t + (\frac{\partial^2\hat{\rho}}{\partial t^2})_{3\Delta t} \frac{(\Delta t)^2}{2}$
	…
n-1	$\hat{\rho}_{n-1} - \hat{\rho}_{n-2} = (\hat{\rho}_{(n-2)\Delta t} + (\frac{\partial\hat{\rho}}{\partial t})_{(n-2)\Delta t} \Delta t + (\frac{\partial^2\hat{\rho}}{\partial t^2})_{(n-2)\Delta t} \frac{(\Delta t)^2}{2}) - \hat{\rho}_{(n-2)\Delta t} = (\frac{\partial\hat{\rho}}{\partial t})_{(n-2)\Delta t} \Delta t + (\frac{\partial^2\hat{\rho}}{\partial t^2})_{(n-2)\Delta t} \frac{(\Delta t)^2}{2}$
n	$\hat{\rho}_n - \hat{\rho}_{n-1} = (\hat{\rho}_{(n-1)\Delta t} + (\frac{\partial\hat{\rho}}{\partial t})_{(n-1)\Delta t} \Delta t + (\frac{\partial^2\hat{\rho}}{\partial t^2})_{(n-1)\Delta t} \frac{(\Delta t)^2}{2}) - \hat{\rho}_{(n-1)\Delta t} = \frac{\partial\hat{\rho}}{\partial t})_{(n-1)\Delta t} \Delta t + (\frac{\partial^2\hat{\rho}}{\partial t^2})_{(n-1)\Delta t} \frac{(\Delta t)^2}{2}$

Table 4-3: Detailed development of $\hat{\rho}$ for each stage “i”

The next step is to insert results from Table 4-3 into Equation (4-22).

$$
\begin{aligned}
W_{out} = \text{¥}\Bigg\{ & \hat{\rho}_0\left(\hat{u}_0+\frac{\hat{V}_0^2}{2}\right)-\hat{\rho}_n\left(\hat{u}_n+\frac{\hat{V}_n^2}{2}\right)+((\frac{\partial\hat{\rho}}{\partial t})_0\Delta t+(\frac{\partial^2\hat{\rho}}{\partial t^2})_0\frac{(\Delta t)^2}{2})\left(\hat{h}_{out,1}+\frac{\hat{V}_{out,1}^2}{2}\right)\\
&+(\,(\frac{\partial\hat{\rho}}{\partial t})_{\Delta t}\Delta t+(\frac{\partial^2\hat{\rho}}{\partial t^2})_{\Delta t}\frac{(\Delta t)^2}{2})\left(\hat{h}_{out,2}+\frac{\hat{V}_{out,2}^2}{2}\right)+(\,(\frac{\partial\hat{\rho}}{\partial t})_{2\Delta t}\Delta t\\
&+(\frac{\partial^2\hat{\rho}}{\partial t^2})_{2\Delta t}\frac{(\Delta t)^2}{2}\,)\left(\hat{h}_{out,3}+\frac{\hat{V}_{out,3}^2}{2}\right)+(\;(\frac{\partial\hat{\rho}}{\partial t})_{3\Delta t}\Delta t\\
&+(\frac{\partial^2\hat{\rho}}{\partial t^2})_{3\Delta t}\frac{(\Delta t)^2}{2})\left(\hat{h}_{out,4}+\frac{\hat{V}_{out,4}^2}{2}\right)+(\,(\frac{\partial\hat{\rho}}{\partial t})_{4\Delta t}\Delta t\\
&+(\frac{\partial^2\hat{\rho}}{\partial t^2})_{4\Delta t}\frac{(\Delta t)^2}{2}\,)\left(\hat{h}_{out,5}+\frac{\hat{V}_{out,5}^2}{2}\right)\dots\dots\dots+(\,(\frac{\partial\hat{\rho}}{\partial t})_{(n-2)\Delta t}\Delta t\\
&+(\frac{\partial^2\hat{\rho}}{\partial t^2})_{(n-2)\Delta t}\frac{(\Delta t)^2}{2}\,)\left(\hat{h}_{out,n-1}+\frac{\hat{V}_{out,n-1}^2}{2}\right)+(\frac{\partial\hat{\rho}}{\partial t})_{(n-1)\Delta t}\Delta t\\
&+(\frac{\partial^2\hat{\rho}}{\partial t^2})_{(n-1)\Delta t}\frac{(\Delta t)^2}{2}\,)\left(\hat{h}_{out,n}+\frac{\hat{V}_{out,n}^2}{2}\right)\Bigg\}
\end{aligned}
$$

Gathering terms as a summation:

$$
\begin{aligned}
W_{out} = {} & \text{¥}\hat{\rho}_0\left(\hat{u}_0+\frac{\hat{V}_0^2}{2}\right)-\text{¥}\hat{\rho}_n\left(\hat{u}_n+\frac{\hat{V}_n^2}{2}\right)\\
&+\text{¥}\,\Delta t\,\{\sum_{i=1}^{n}[(\frac{\partial\hat{\rho}}{\partial t})_{(i-1)}+(\frac{\partial^2\hat{\rho}}{\partial t^2})_{(i-1)}(\frac{\Delta t}{2})\,][\hat{h}_{out,i}+\frac{\hat{V}_{out,i}^2}{2}]\,\}
\end{aligned}
$$

$$
\begin{aligned}
W_{out} = {} & m_0\left(\hat{u}_0+\frac{\hat{V}_0^2}{2}\right)-m_n\left(\hat{u}_n+\frac{\hat{V}_n^2}{2}\right)\\
&+(\frac{1}{2})\,\text{¥}\,\Delta t\,\{\sum_{i=1}^{n}[(\frac{\partial\hat{\rho}}{\partial t})_{(i-1)}+(\frac{\partial^2\hat{\rho}}{\partial t^2})_{(i-1)}(\frac{\Delta t}{2})\,][2\,\hat{h}_{out,i}+\hat{V}_{out,i}^2\,]\,\}
\end{aligned}
\tag{4-23}
$$

Equation (4-23) is the approximate general equation to calculate work extraction during the unsteady expansion process based on conditions -1 and -2.

4.2. Analysis of the approximate general equation for extracted work

Equation (4-23) is an approximate mathematical expression derived from the energy balance equation with conditions -1 and -2 to calculate the work of the unsteady expansion process.

The right hand side of Equation (4-23) has three terms: the first and second terms represent the total energy of the fluid within the control volume at the initial and final state of the process, respectively. The third term expresses the total fluid energy leaving the channel thru the outlet, depicted as a summation term dependent of time and therefore, this third term represents the unsteadiness of the expansion process. Equation (4-23) demonstrates the physics as follows:

$$\begin{pmatrix} Work \\ extracted \end{pmatrix} = \begin{pmatrix} Total\ energy \\ at\ initial\ state \end{pmatrix} - \begin{pmatrix} Total\ energy \\ at\ final\ state \end{pmatrix} + \begin{pmatrix} Total\ energy\ thru \\ channel\ outlet \end{pmatrix} \qquad (4\text{-}24)$$

When Total energy is mentioned, it primarily implies the û value because the magnitude of $\frac{\widehat{V}_0^2}{2}$ is small compared to û. The work extracted according to Equation (4-24) is mainly dependent on flowing energy leaving the channel and the final state because the total energy at initial state is a fixed condition. The û value at final state must be the lowest for maximum work extraction and occurs when the process trajectory follows a constant entropy line obtaining $\hat{u}_{n,isentropic}$ value for the fluid within the control volume (Figure 4-2).

The flowing energy is negative due to the decreasing rate of density change, diminishing the net value of the first two terms, and the lower this rate, the greater the generation of torque. Thus, maximizing work extraction will depend on how this third term is modulated by the geometry of the channel.

4.2.1. The flowing energy in the summation term

The summation in Equation (4-23) contains constant parameters (Ꝟ and Δt) and the time-dependent variables (the rate of $\hat{\rho}$ change, $\hat{h}_{out,i}$ and $\hat{V}_{out,i}$). The rotational speed (ω_i) is considered constant in the analysis as in the actual operation of the engine.

The first and second partial derivatives of the density function, $\left(\frac{\partial \hat{\rho}}{\partial t}\right)$ and $\left(\frac{\partial^2 \hat{\rho}}{\partial t^2}\right)$, play an influential role in the value and symbol of the summation term. The first derivative captures the slope of the curve and the second derivative accounts for the curvature, but the focus will be on the first derivative because the second derivative is a higher order term.

During the actual unsteady expansion process, the density decreases throughout the whole process (emptying process). Thus, the rate of density change in the channel has a negative value ranging from $-fv < \frac{\partial \hat{\rho}}{\partial t} \leq 0$. The physical effect refers to the speed of fluid mass being expelled from the channel. Higher rates produce bigger values of $\frac{\partial \hat{\rho}}{\partial t}$, thus higher flowing energy diminishes the work generated. For this reason, fast discharging process can have a negative effect on torque generation.

4.3. Unsteady generated work for isentropic process

The isentropic process produces maximum values of torque, and this section investigates the influence of the time dependent variables under isentropic conditions.

The unsteady expansion is a complex process in the operation of an actual engine; inheriting the effects of compression waves, created during the combustion process, propagating back and forth inside the channel. The expansion process starts with a gradual opening of the outlet port, expelling the fluid from the channel with a gradual increase in the fluid's relative velocity. This opening creates an expansion wave that spreads toward the channel inlet. During this period, the magnitude of the absolute velocity of the gases at the outlet reaches a maximum value, and then decreases. Subsequently, the inlet port opens and fresh mixture starts to fill the channel again. An overlapping period happens between the end of the expansion and beginning of the inlet processes. The inlet process benefits from the effect of gases leaving the channel, which draw the incoming fluid. The outlet port closes when most of the gases have already left the channel, and is the end of the Unsteady Expansion Process.

A number of constraints are applied to simplify the complexity of this process: there is no influence from the combustion process and the relative gas velocity within the channel is zero (at rest) until the outlet port opens instantly and the fluid accelerates through the channel toward the outlet. At the final step of the process, the mass-weighted average value of fluid velocity reduces to the channel velocity, and the volume-weighted average value of pressure within the channel is equalized with surroundings.

At every finite stage, the flow expands to the same mass-weighted average value of the isentropic temperature ($\widehat{\mathrm{T}}_{out,isentropic}$) at the channel outlet. Thus, it yields:

$$\hat{T}_{out,1} = \hat{T}_{out,2} = \hat{T}_{out,3} = \hat{T}_{out,4} = \cdots = \hat{T}_{out,isentropic} \tag{4-25}$$

Then:

$$\hat{h}_{out,1} = \hat{h}_{out,2} = \hat{h}_{out,3} = \hat{h}_{out,4} = \cdots = \hat{h}_{out,isentropic} \tag{4-26}$$

To investigate the influence of density on the torque generation some idealizations are applied. The fluid in this idealization is air and behaves as an ideal gas. A density function is built to imitate how the volume-weighted average value of density changes within the channel during the process. This function depicts the channel’s instant opening and the density's decreasing rate. This rate value starts at zero, falls to a negative value, and continues decreasing.

It reaches the lowest negative value (called inflection point at the density curve), and begins increasing until reaching zero value again when the pressure inside the channel is equalized to the surrounding pressure and thus, the outlet relative velocity is zero.

The summation term of Equation (4-23) appears as a function of Δt as well. This parameter depends on the number of finite stages according to Equation (4-27):

$$\Delta t = \frac{t_{2s}}{n} \tag{4-27}$$

Based on this statement, several calculations were performed using different number of finite stages in Equation (4-23). Results in Figure 4-3 indicate the unsteady work value converges at around 1,000 finite stages. Thus, all calculations are considered to have more than 5,000 finite stages.

To determine any impact on the torque generation based on Equation (4-23), two options are considered in the density function variation:

(a) Same duration of expansion process but the inflection point of the density function increases (Figure 4-4).

(b) Duration of expansion time increases but the inflection point remains constant and occurs in the middle of each duration time (Figure 4-5).

For both options of the density function is plotted the density, magnitude of the outlet velocity and the rate of density change (Figure 4-4and Figure 4-5).

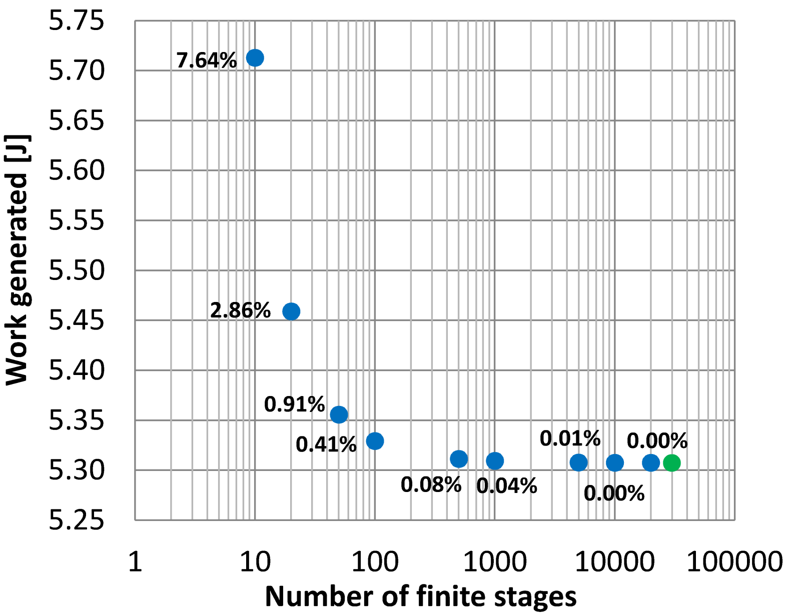

Figure 4-3: Convergence of the Unsteady Isentropic Work as a function of Number of finite stages at PR=7 with 10,000 rpm.

Shifting the position of the inflection point in the density function toward the right causes both a concentration of higher outlet velocities and rate of density change toward the right (Figure 4-4 (b) and (c)).

The curves of the rate of density change show the earlier and later inflexion points produce the highest negative values (Figure 4-4 (c)). These results predict trends of channel outlet velocity and rate of density change if the volume-weighted average results of density from numerical simulation produce similar plots to Figure 4-4(a).

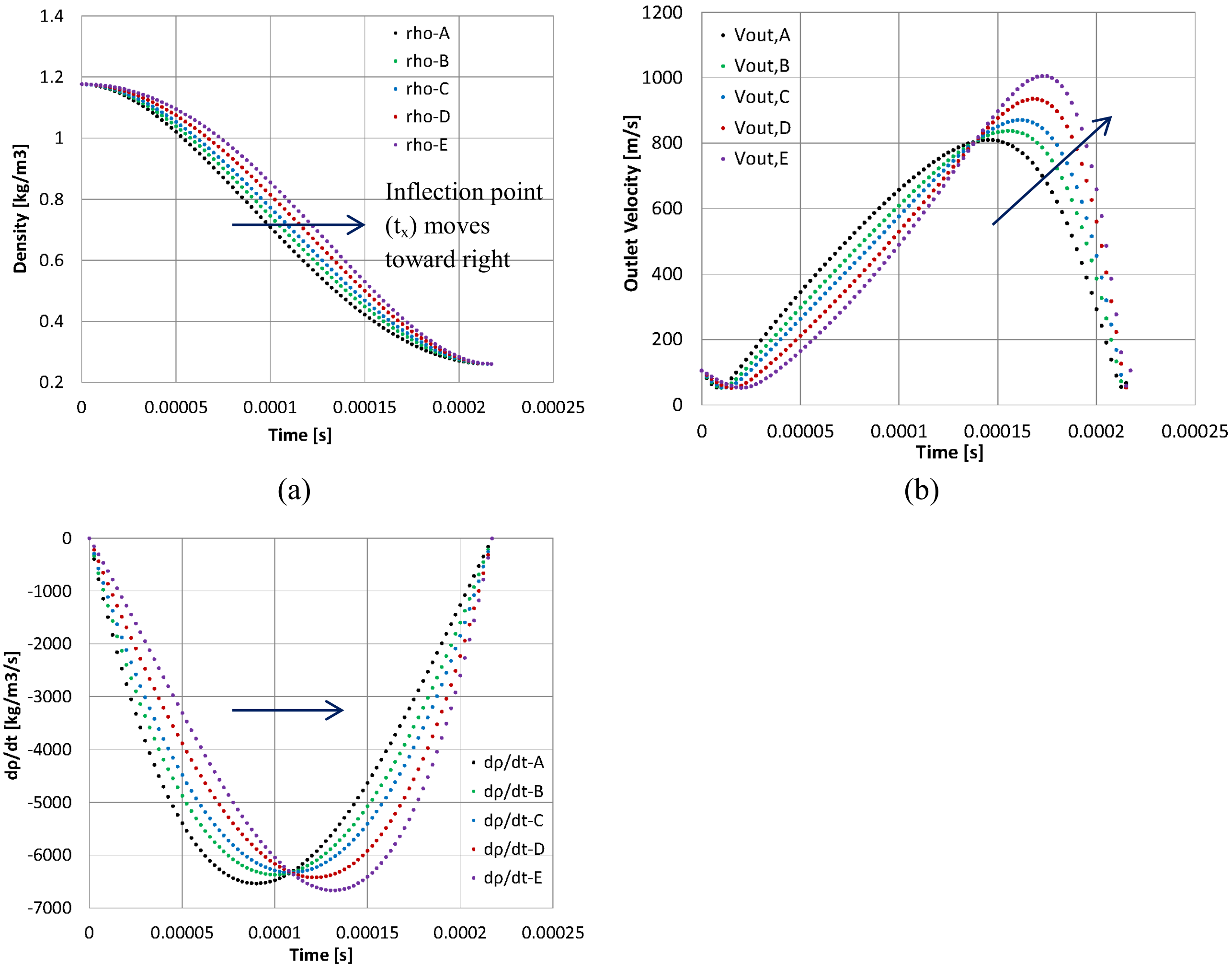

(a) (b)

(c)

Figure 4-4: Density (a), magnitude of outlet velocity (b) and dρ/dt (c) with several inflection-time during the unsteady expansion process (PR=7 and 10,000 rpm)

The second option considers the influence of the total duration time of the unsteady expansion process on work generation (Figure 4-5 and Figure 4-6). The extension of the expansion process duration causes lower rates of density change and thus, lower channel outlet velocities. According to Equation (4-23), the unsteady work is the result of net positive contribution of both first terms, and by the negative contribution of the summation term. This last term is negative due to the decreasing rate of density change (first partial derivative with respect to time). With shorter expansion duration, the rate of density change increases, and the summation term also increases and thus, reduces the unsteady isentropic generated work. In addition to this change, the summation term contains the outlet velocity which increases as well, having a greater effect of this summation term in the unsteady isentropic generated work. The increase in the channel outlet velocity can be interpreted as fast outgoing of kinetic energy that was not exploited in the generation of work.

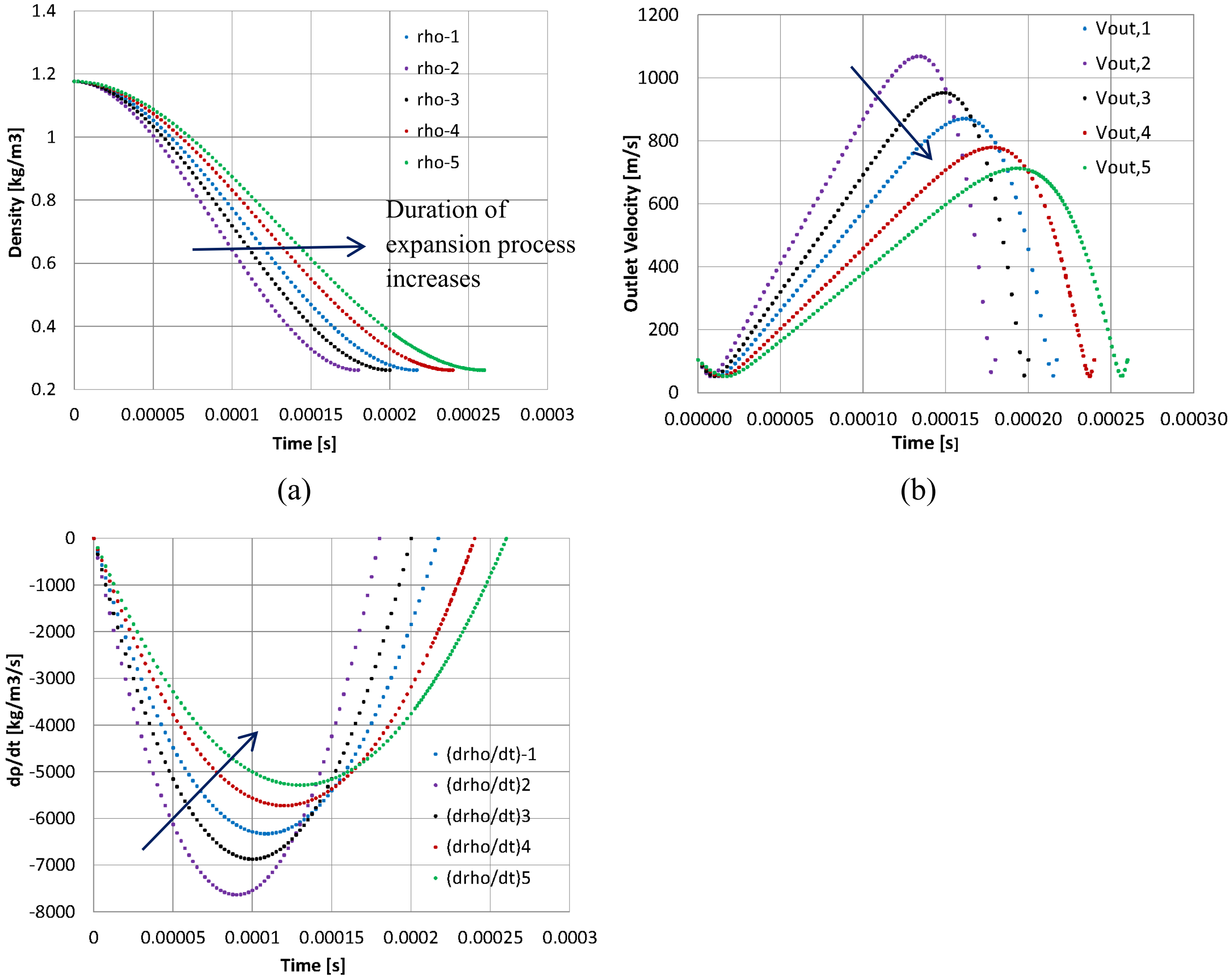

(a) (b)

(c)

Figure 4-5: Density (a), magnitude of outlet velocity (b), and dρ/dt (c), with several duration-times of the unsteady expansion process (PR=7 and 10,000 rpm)

The initial and final conditions (the first two terms in Equation (4-23)) become fixed in the isentropic process, then, the work generated will be higher as long as the summation term becomes smaller. Therefore, extending the duration of the unsteady expansion process appears as a controlling parameter to maximize the unsteady work extraction. This conclusion is consistent with that in Chapter 2, but channel side areas are not included in these findings because thermodynamic energy analysis does not provide evidence of the influence on the unsteady work due to the area of pressure and suction sides.

In Figure 4-6 the unsteady isentropic generated work is plotted at different pressure ratios (PR). Each point indicates the maximum isentropic work expected (y-coordinate) according to the process duration, respectively (x- coordinate). The values of t1, t2 and t3 are the threshold flow times, and following that point the production of unsteady isentropic work starts to decrease. The graph depicts the increase of expansion duration produces the increase of work extraction in all plots.

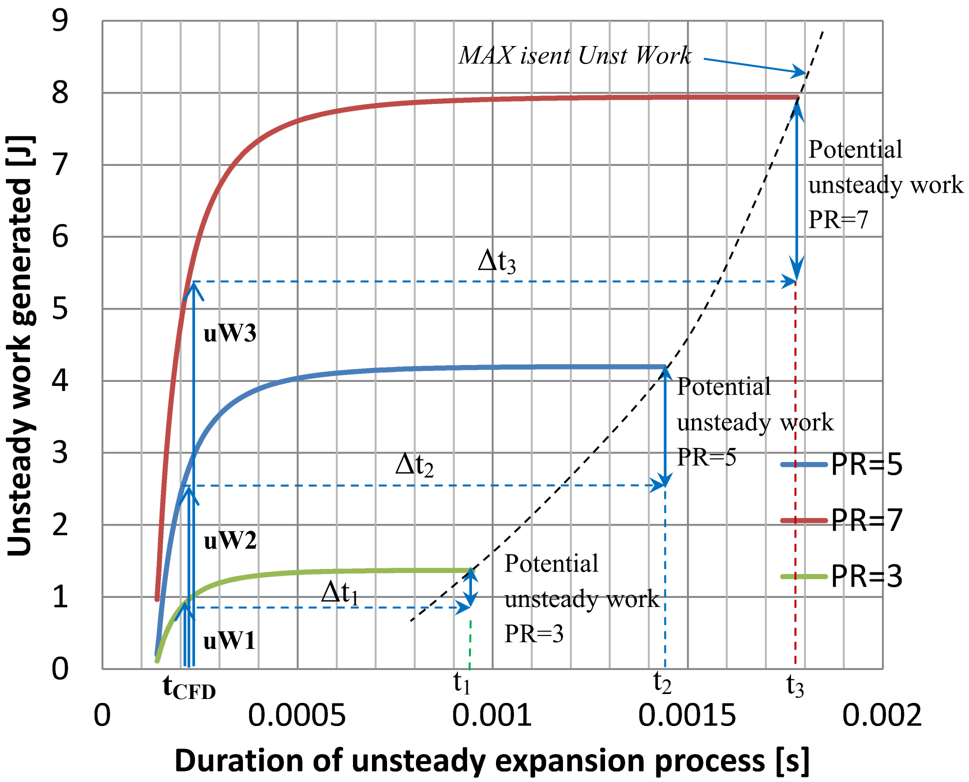

Figure 4-6: Unsteady Isentropic Work vs time at several PR= 3, 5 and 7, discharging to surrounding environment pressure of 101325 Pa.

Table 4-4 provides a summary of the actual unsteady generated work results from numerical simulations. The corresponding unsteady isentropic generated work values are determined in Figure 4-6 as uW1, uW2 and uW3 at PR= 3, 5 and 7, respectively, based on the duration of the actual extracted work. The graph indicates additional unsteady work can be extracted if the expansion process duration is extended. In addition, Table 4-4 provides expansion efficiencies and indicates work generation at lower pressure ratio is more efficient. The unsteady expansion efficiencies were calculated based on two criteria: same duration time and maximum unsteady isentropic work.

PR	Actual UnstW (numerical simulation)	UnstW_isent	Duration (actual process)	η_{exp} (same duration)	η_{exp} (max isent-work)
	[J]	[J]	[ms]	[%]	[%]
3	0.40	0.90	0.20897	44.6	29.2
5	0.73	2.62	0.21057	27.9	17.4
7	0.97	5.31	0.21717	18.3	12.2

Table 4-4: Results for PR=3, 5 and 7 ("same duration" refers to the isentropic unsteady work produced according to the duration of the actual work extracted. "maximum isentropic work" refers to the maximum value at different duration time than the actual work extracted).

Expansion efficiency based on the energy approach does not distinguish between losses that generate entropy and potential energy to produce work in subsequent stages. Exergy approach considers all aspects.

CHAPTER 5. ROLE OF PRESSURE AND FORCE IN TORQUE GENERATION

This chapter focuses on the role of pressure and force in the generation of torque. A constant cross-section curved channel is chosen for an unsteady expansion process, at instant and gradual openings, both with rotational velocity of 10,000 rpm. The torque coefficient through the flow time is plotted. Cm is calculated based on equation:

$$C_m = \frac{T}{\frac{1}{2}\rho_{ref}V_{ref}^2 A_{ref} L_{ref}} \tag{5-1}$$

Torque value (T) is calculated based on the cross product summation of pressure and viscous force vectors together with position vector, with respect to the center of the channel rotation.

For the purpose of analysis, the focus will be on the effect of pressure forces in torque generation. Viscous forces are very small compared with pressure forces, and are negligible in this study. Therefore, results are not affected when torque due to pressure forces is compared with cm or torque history values provided by CFD simulation.

5.1. Unsteady Expansion Process at Instant Opening

5.1.1. Pressure distribution on channel walls

A step by step description of the unsteady expansion in the channel during torque generation is performed. According to Figure 5-1, 9 points at different flow time locations are selected to analyze this case.

In Figure 5-2, Figure 5-7, and Figure 5-8, the pressure distribution on the pressure and suction side of the channel are plotted for each point selected from Figure 5-1, the abscissa on the graphs refers to radial coordinate locations. Additionally, the circumferential average of the velocity magnitude in radial coordinates was included in each graph. On the right hand side of graphs were plotted line-contours of pressure, and radial coordinates are indicated.

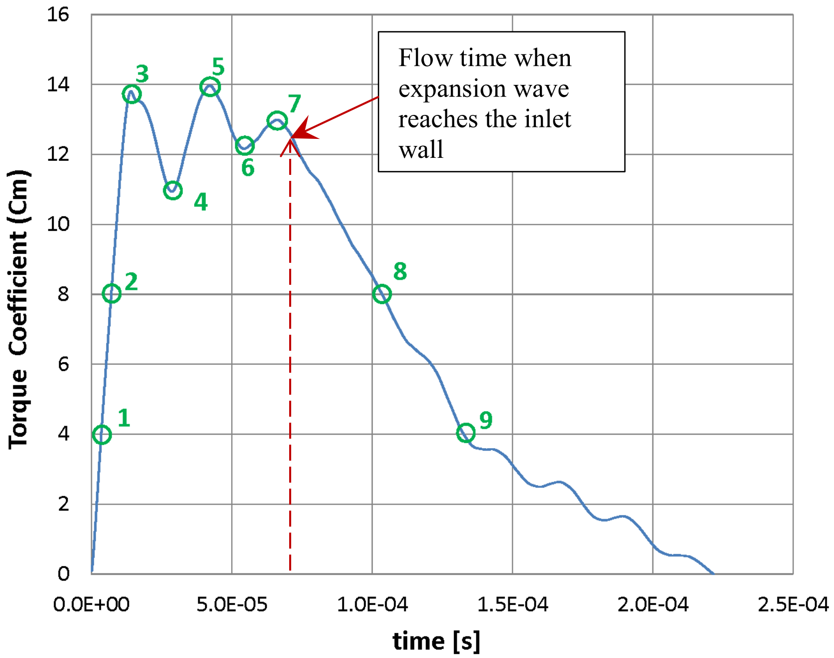

Figure 5-1: Torque coefficient (cm) history of a constant-cross section curved channel for instant opening

Figure 5-1 shows the increasing trend of the torque coefficient (points 1-3) reaching a maximum value at point 3. The slope of the curve plotted (approximately a line) by the three initial points has a high steep value due to the instant opening condition imposed during the simulation. A less steep trend will be observed for a gradual opening situation. The instant opening forces the fluid to leave the channel in a radial direction. During this initial time (Figure 5-2), the head of the expansion wave at point 1 is aligned approximately with the circumferential arc at radial coordinate 0.09638 [m] and modulates to relatively reach a perpendicular position with respect to the pressure and suction sides (Figure 5-2).

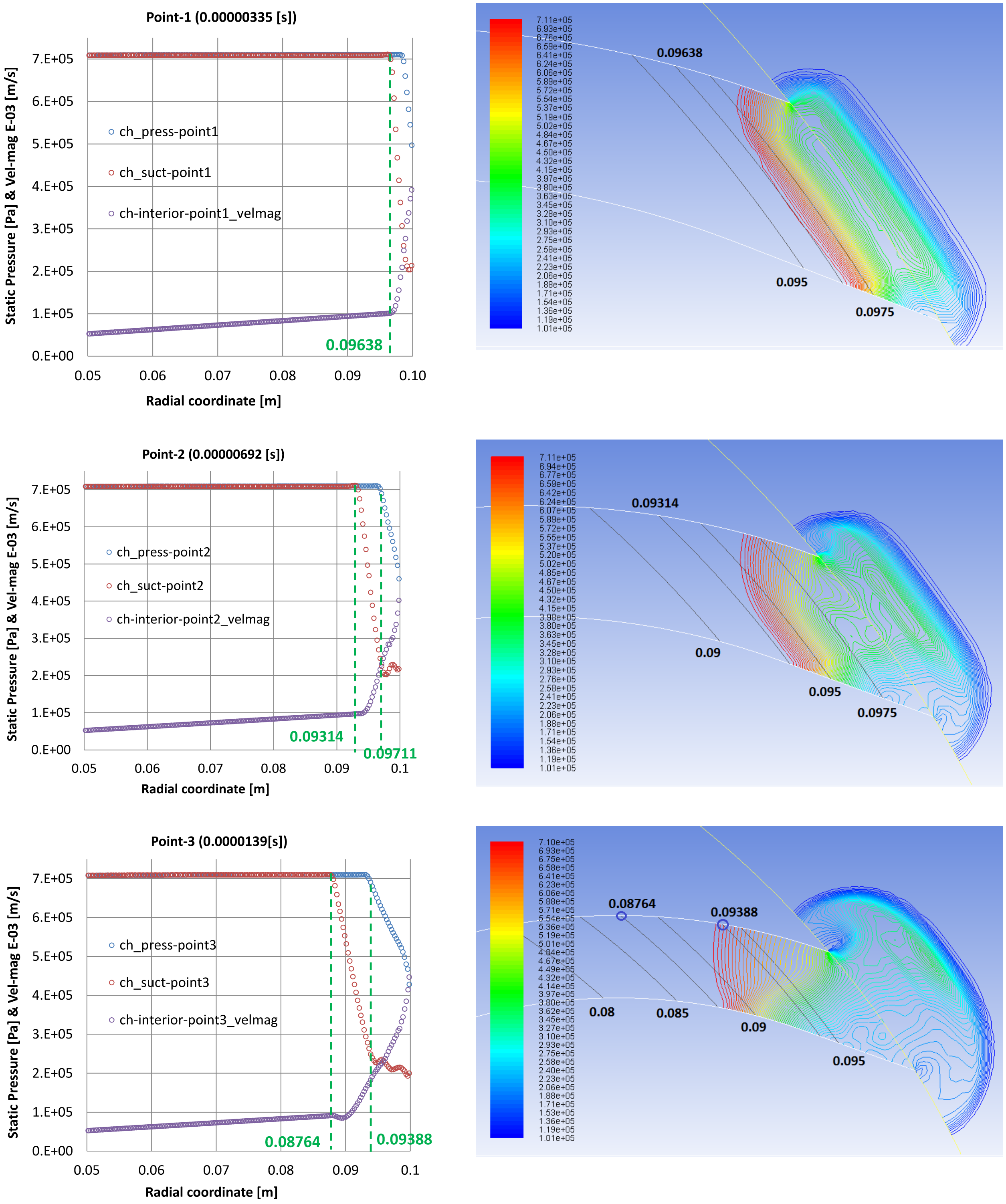

Figure 5-2: Pressure plot on the suction and pressure surface according to radial coordinates (left) and static pressure contour (right) for points 1 to 3.

During the unsteady expansion process, different pressures are exerted on the pressure and suction walls corresponding to the same radial coordinate; as a result, a differential pressure is exerted in, or against, the rotational direction, which is translated into generated torque. These different pressure values are due to pressure gradients generated by the expansion wave from head to tail when it propagates toward the channel inlet. The expansion wave produces line-contours of constant pressure from its head to tail, and these line-contours are expected to remain approximately perpendicular to the channel walls [18]. In some instances, this condition does not prevail, as seen later on. In general, the orientation of line-contours yields different pressure values at the pressure and suction sides with same radial coordinate (Equation (5-2) and Figure 5-3). This concept is used to explain results in this section.

$$P_{pw1} > P_{pw1} \;\; at\ radial\ coordinate\ r_1 \qquad (5\text{-}2)$$

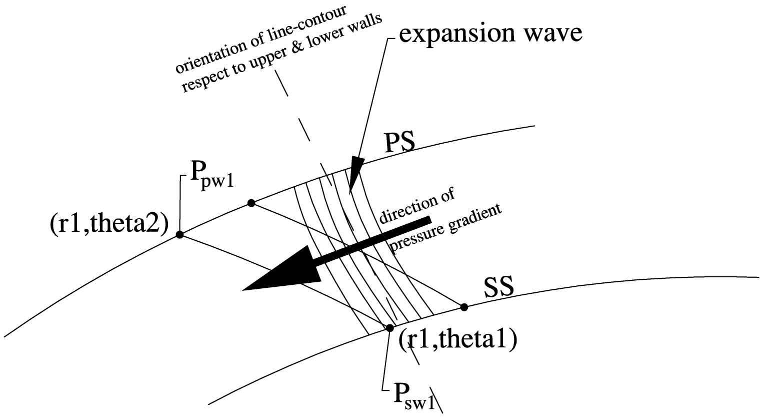

P_{pw1}=Pressure at the pressure wall P_{sw1}=Pressure at the suction wall

Figure 5-3: Pressure gradients and pressure on the suction and pressure walls

In the beginning of the process, two effects increase the differential pressure area (line-contour graphs in RHS of Figure 5-2 and Figure 5-4): the orientation change of the head of the expansion wave (first line-contour) going from point 1 to 3, and the pressure gradient along the expansion wave from head to tail. The change in orientation of the head of the expansion wave is one of the factors that causes “s” to gradually increase, and in consequence the net area grows from point 1 to 3 (Figure 5-4).

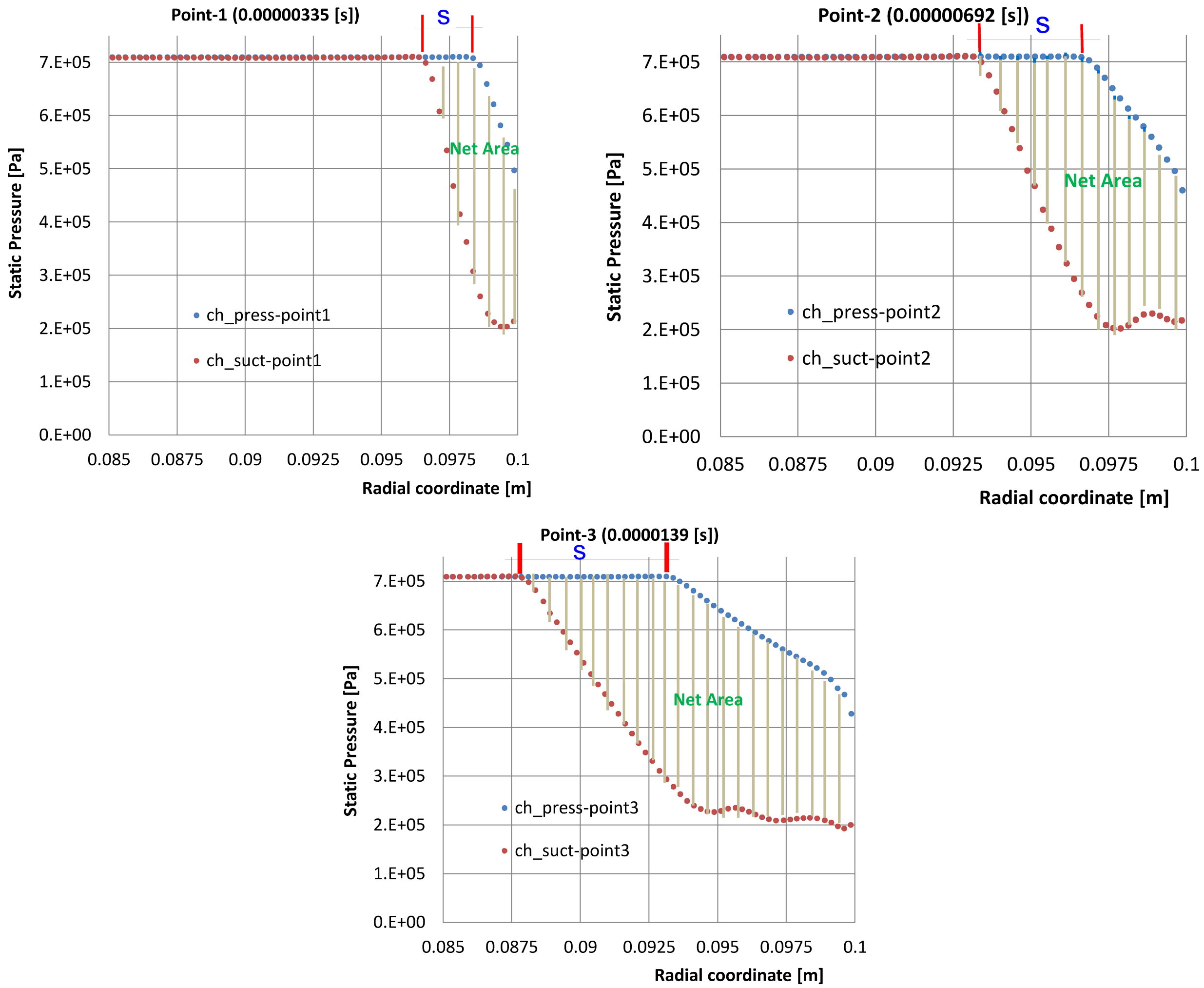
Point-1 (0.00000335 [s])

Point-2 (0.00000692 [s])

Point-3 (0.0000139 [s])

Figure 5-4: Increasing trend of the net pressure distribution for points 1 to 3.

In Figure 5-5, Velocity vector plots of velocity magnitude show the fluid closer to the suction side has higher local velocity magnitudes than the fluid closer to the pressure side during the period from point 1 to 3. Thus, it produces lesser pressure values on the suction side than the pressure side at the same radial coordinates as the expansion wave propagates from point 1 to 3.

After point 3, cm plot oscillates until point 7, and then decreases through the end of the expansion (Figure 5-1). Figure 5-7 shows pressure line-contours and pressure distribution on the walls for points from 4 to 6. Point 4 refers to the lowest cm value, which then goes up to point 5, and falls down again to point 6. As seen in Figure 5-7, the orientation of line-contours at the tail of the expansion wave changes from being almost perpendicular (in respect to upper and lower walls), inclines to the right, and returns to perpendicular. In point 4, the line-contours at radial locations 0.9 to 1.0 keep the vertical orientation, and then become less steep when moved to point 5 (maximum "cm" value). This effect projects more area on upper and lower walls for differential pressure. At point 6, the line-contours return to approximately the vertical position and the differential pressure is again reduced (last picture on the right of Figure 5-7).

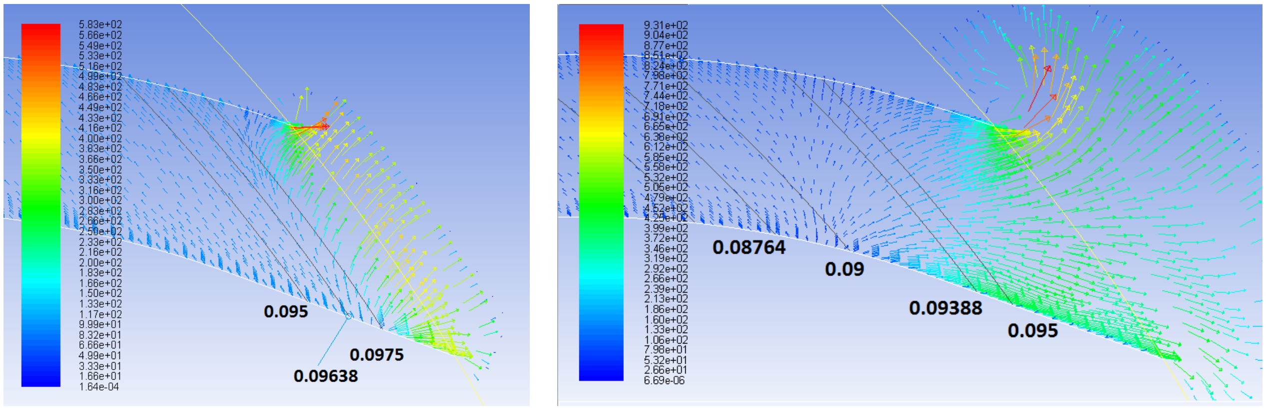

Point-1 Point-3

Figure 5-5: Velocity magnitude vectors for points 1 and 3

Next, at point 7, the line-contours of the channel outlet region inclines to the right again and covers more area of differential pressure, as seen in Figure 5-8. The head of the expansion wave impinges on the inlet wall of the channel between points 7 and 8 (0.07 [ms]) and the static pressure on both walls decreases abruptly until the end of the expansion, and an identical situation occurs with the differential pressure. The head of the expansion wave now becomes a right running wave that propagates through the incoming incident left running wave. This causes a distortion in line-contours and reduces the differential pressure to zero when the reflected wave travels back to the outlet port of the channel.

The oscillating behavior (Figure 5-6) of the cm plot from points 3 to 7 is caused by two effects: the orientation of the line-contours near the channel outlet and the net area increase of the differential pressure produced by the wave propagation. At point 4, cm decreases when the orientation of line-contours become perpendicular in the region near channel outlet and also reduces the differential pressure approximately at radius of 0.1 m and thus, the net area with respect to point 3 (Figure 5-6 (b)). At point 5, cm value is raised by the orientation of the line-contours in the region near the channel outlet where the slopes become less steep toward the right, causing an increase in differential pressure net area (Figure 5-6(b)). At point 6, cm diminishes due to the change in orientation of line-contours (returning to perpendicular again) but not at the level of point 4, because the net area increased and this positively compensates. At point 7, cm value does not recover, as in point 5, even when the orientation of line-contours benefits positively and the net area is similar (Figure 5-6 (a) & (b)). This result indicates that additional influential factors need to be considered.

Two extra factors are investigated in the next section: the component of the force due to pressure in the tangential direction and the impact on the torque distribution by the radial position.

In this section some conclusions are made: during the propagation of the incident head of the expansion wave around 62% of the total torque is extracted, approximately 80% of the length of the channel works actively for the generation of torque according to positive values of the differential pressure shown, and the remaining 20% corresponds to the channel zone length near the inlet wall.

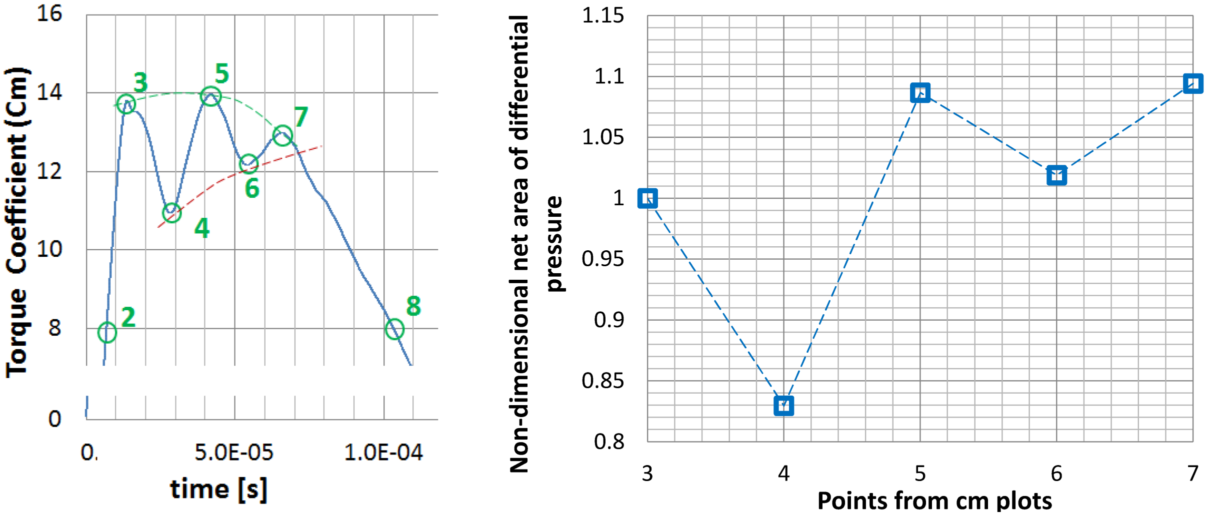

(a) (b)

Figure 5-6: (a) cm torque oscillation and (b) Non-dimensional net area of differential pressure.

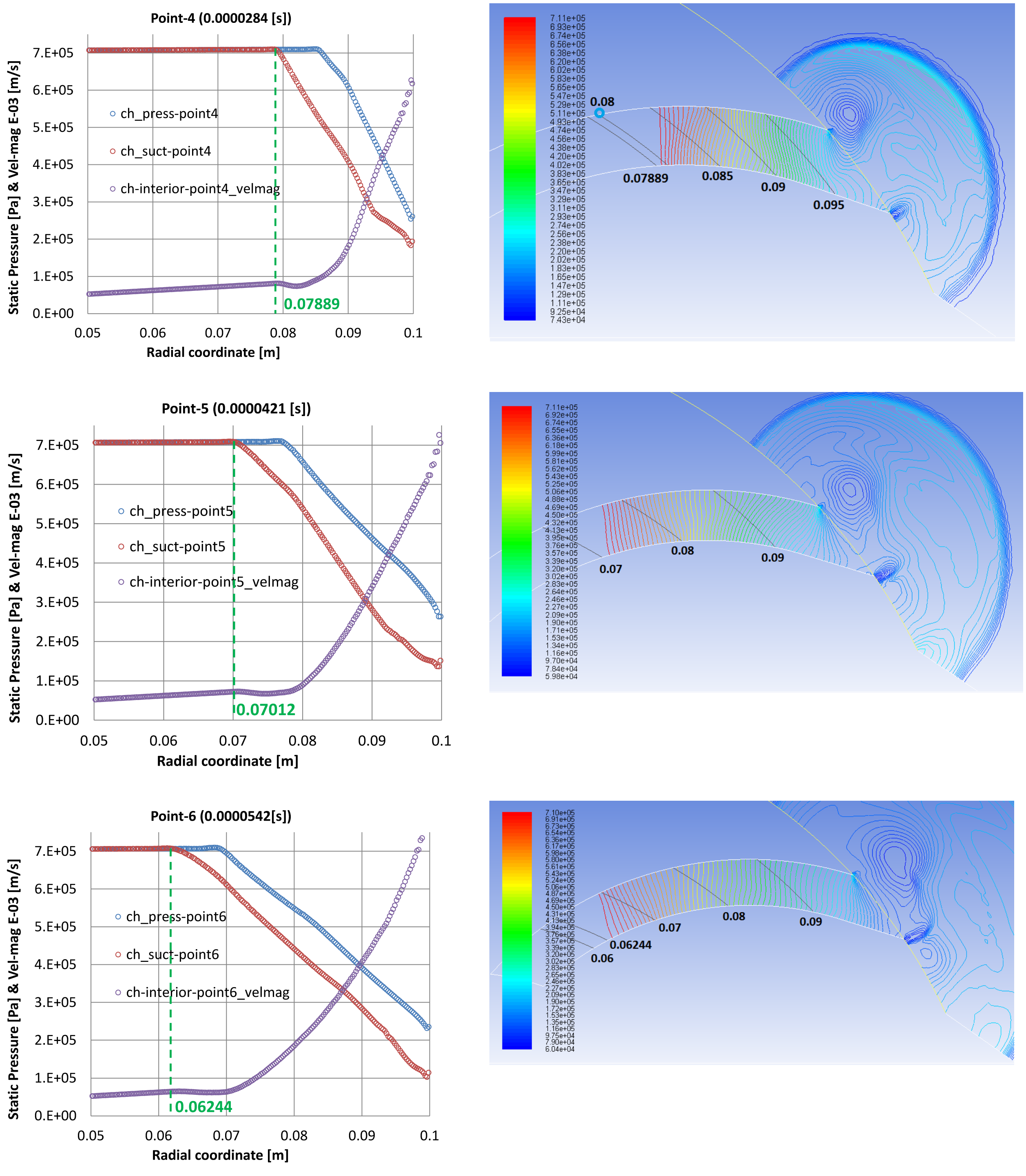

Figure 5-7: Pressure plot on the suction and pressure sides at each radial coordinates (left) and static pressure contour (right) for points 4 to 6.

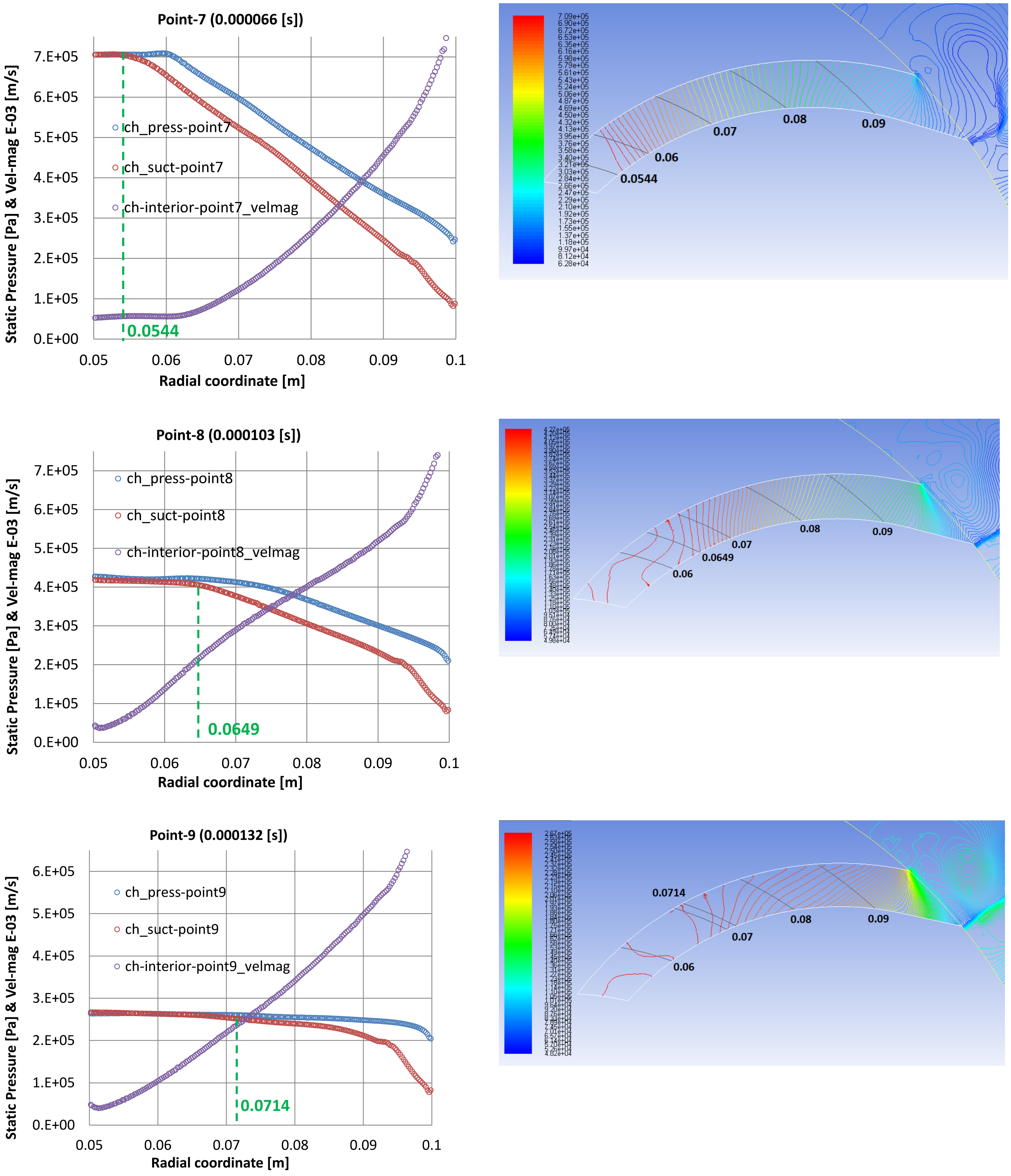

Figure 5-8: Pressure plot on the suction and pressure surface according to radial coordinates (left) and static pressure contour (right) for points 7 to 9.

5.1.2. Force and Torque distribution on channel walls

Force and torque distribution are presented in this section: the following convention is used. The expression for the Torque in a specific radial position is defined as:

$$\vec{T}_{rp} = \vec{r} \times \vec{F}_p + \vec{r} \times \vec{F}_v \tag{5-3}$$

As was stated at the beginning of this chapter, the moment due to viscous effect is considered negligible, then:

$$\vec{T}_{rp} = \vec{r} \times \vec{F}_p \tag{5-4}$$

The vector force component due to pressure:

$$\vec{F}_p = \vec{F}_{tan-p} + \vec{F}_{rad-p} \tag{5-5}$$

The force associated with the generation of torque:

$$\vec{F}_{tan-p} = (F_p)(sin\beta)\,\vec{e}_\theta$$

$$\vec{F}_{tan-p} = (P.A)(sin\beta)\,\vec{e}_\theta \tag{5-6}$$

Following the convention in Figure 5-9:

Pressure side:

$$\vec{F}_{tan-p-PS} = (p_{PS}.A_{PS})(sin\beta_{PS})\,\vec{e}_\theta \tag{5-7}$$

Suction side:

$$\vec{F}_{tan-p-SS} = (p_{SS}.A_{SS})(sin\beta_{SS})\,\vec{e}_\theta \tag{5-8}$$

Calculating the differential pressure for both at the same radial coordinate “r”:

$$\Delta\vec{F}_{tan-p} = [p_{PS}A_{PS}sin\beta_{PS} - p_{SS}A_{SS}sin\beta_{SS}]\,\vec{e}_\theta \tag{5-9}$$

If "Force − θ" is the force in the tangential direction:

And $\Delta(\text{Force} - \theta) = p_{PS}A_{PS}sin\beta_{PS} - p_{SS}A_{SS}sin\beta_{SS}$, then:

$$\Delta\vec{F}_{tan-p} = [\Delta(\text{Force} - \theta)]\,\vec{e}_\theta \tag{5-10}$$

So, the magnitude of Equation (5-10) when plotted in graphs:

$$\Delta F_{tan-p} = \Delta(\text{Force} - \theta) \tag{5-11}$$

Torque plots are now calculated based on Equation (5-4); but considering only the torque component in the rotation direction:

$$\vec{T}_{rp} = \vec{r} \times \vec{F}_p = rF_{tan-p}\,\vec{e}_k$$

Replacing results from Equation (5-11), which regards forces on pressure and suction walls, it yields:

$$\vec{T}_{rp} = r\Delta(\text{Force} - \theta)\,\vec{e}_k$$

$$T_{rp} = r.\Delta F_{tan-p} = \Delta(\text{r} * \text{Force} - \theta) \tag{5-12}$$

Then, Equation (5-12) is used to build torque plots.

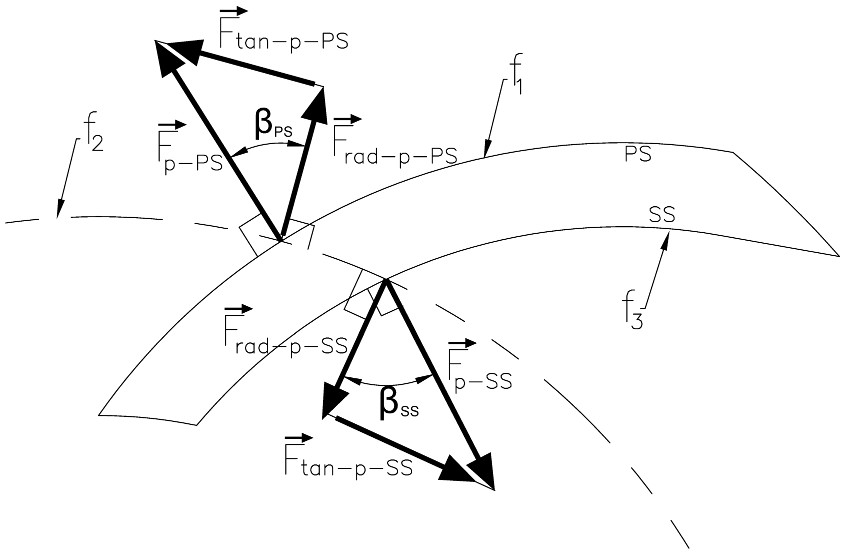

Figure 5-9: Nomenclature for forces, angles and channel walls

In previous section torque generation (or torque coefficient) based on pressure distribution on the channel walls was discussed. But tangential force directly contributes to gaining or losing torque. Thus, to calculate tangential forces, "β" angle must be known. At any specific radial coordinate, it is formed by the unit vector perpendicular to the channel wall area (f_1 or f_3) and the unit vector perpendicular to the circumference (f_2) (Figure 5-9). "β" angle favors a greater value of tangential component on the pressure or suction sides (Equations (5-7) or (5-8)) when approaching 90 degrees. β values closer to zero will result in low values of tangential force at the pressure or suction walls. Thus, values of β angle near 90° effects torque generation positively (Equation (5-9)) because of tangential force on the pressure side is responsible, but not for the tangential force component acting on the suction side, which counteracts the torque generation. In addition, values of β near 0° on the suction side work for the benefit of torque generation if the tangential component has this value. The influence of β angle in the orientation of the line-contours from head to tail of the expansion wave is a topic to discuss in Section 5.3.

The geometry of the constant cross section channel is plotted in Figure 5-10 (a). At the trailing edge of the suction side, the constant cross section is unchanged until the red curve ends and becomes a green straight line-this was added to reduce the adverse effect of a bigger outlet area during gradual opening. In Figure 5-10 (b), the sine of β changes from leading to trailing edge in a decreasing trend for this particular channel geometry. The green straight line added at the trailing edge generates higher sine of β values on the suction side. At 81.7 mm, on the suction side, higher values of sine of β are changed to lower values until 92.8 mm with respect to pressure side. Past this location, another change is made.

From Figure 5-11 to Figure 5-13, the net tangential force and torque distribution were plotted for points 1 to 9, according to Figure 5-1. To discuss figures in this section, $\Delta(\mathrm{Force} - \theta)$ or $\Delta(\mathrm{r} * \mathrm{Force} - \theta)$ will be referred to simply as force or torque. Positive values of force or torque are interpreted as torque production or gain, and negative values have the opposite meaning.

A crest appears at point 1 and continues moving and spreading to the left as the head of expansion wave travels toward the inlet wall for the following points in time. At point 1, negative values for force and torque are due to higher β values on the suction wall until "a1" position, where β values of pressure and suction sides are equalized (see Figure 5-10). At "a2" in Figure 5-11(a), force and torque both reach maximum values and begin to decrease due to the sine of β increase in the suction side. At "a3" location, both force and torque become zero, and sine of β of green straight (suction side) and blue curve (pressure side) have the same value. The decreasing trend of the force (or torque) is the result of increasing values of β for the green straight line (Figure 5-10 (b)). At the location of 96.38 mm (Figure 5-2 and Figure 5-11(a), point 1), force and torque reach the lowest value and begin increasing because of the action of the expansion wave on both walls.

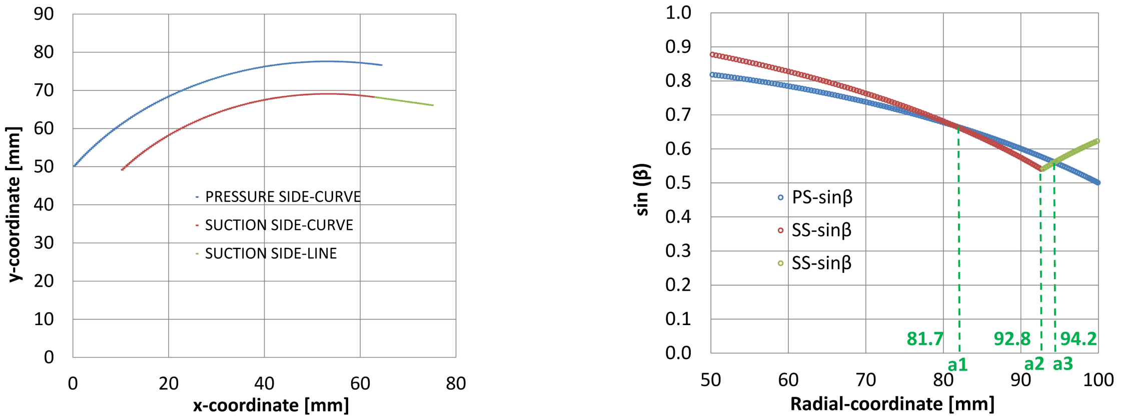

(a) (b)

Figure 5-10: Channel shape and sinβ variation along the radial coordinate of a constant cross section channel

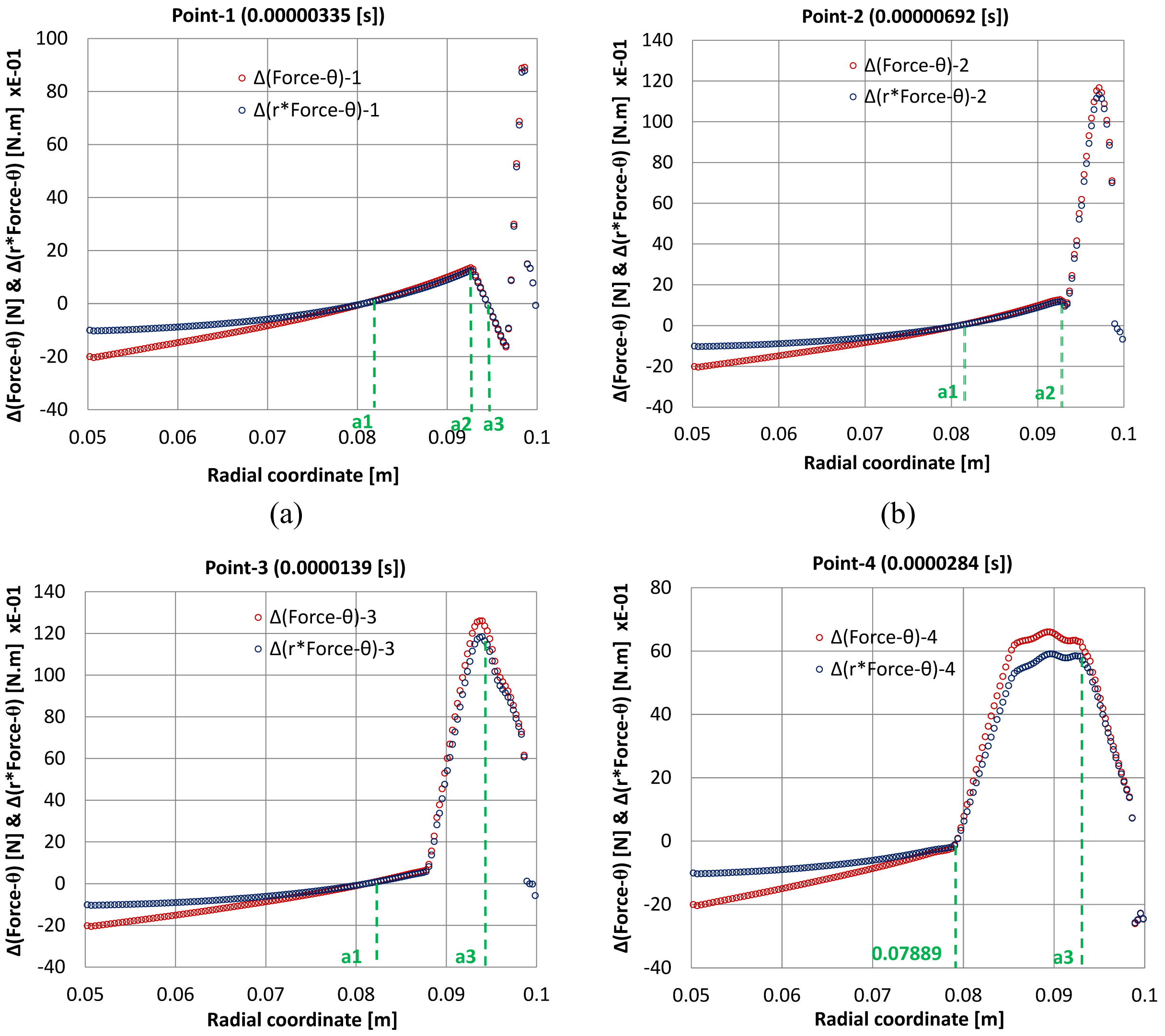

(a) (b)

(c) (d)

Figure 5-11: Δ(force-θ) and Δ(r*force-θ) plots at points 1, 2, 3 & 4 according to radial coordinates.

For points 2 to 7, the pressure and suction sides have the same pressure values in the channel region between the inlet wall and the head of the expansion wave (before it impinges the inlet wall), and β values cause a bigger component from the applied force on the suction side in the tangential direction, resulting in negative values of force and torque (Figure 5-11 and Figure 5-12). Based on this channel geometry, around 18% of the channel length does not produce positive force (or torque) because of bigger β angles in the suction side with respect to the pressure side. This percentage refers to the zone adjacent to the channel inlet.

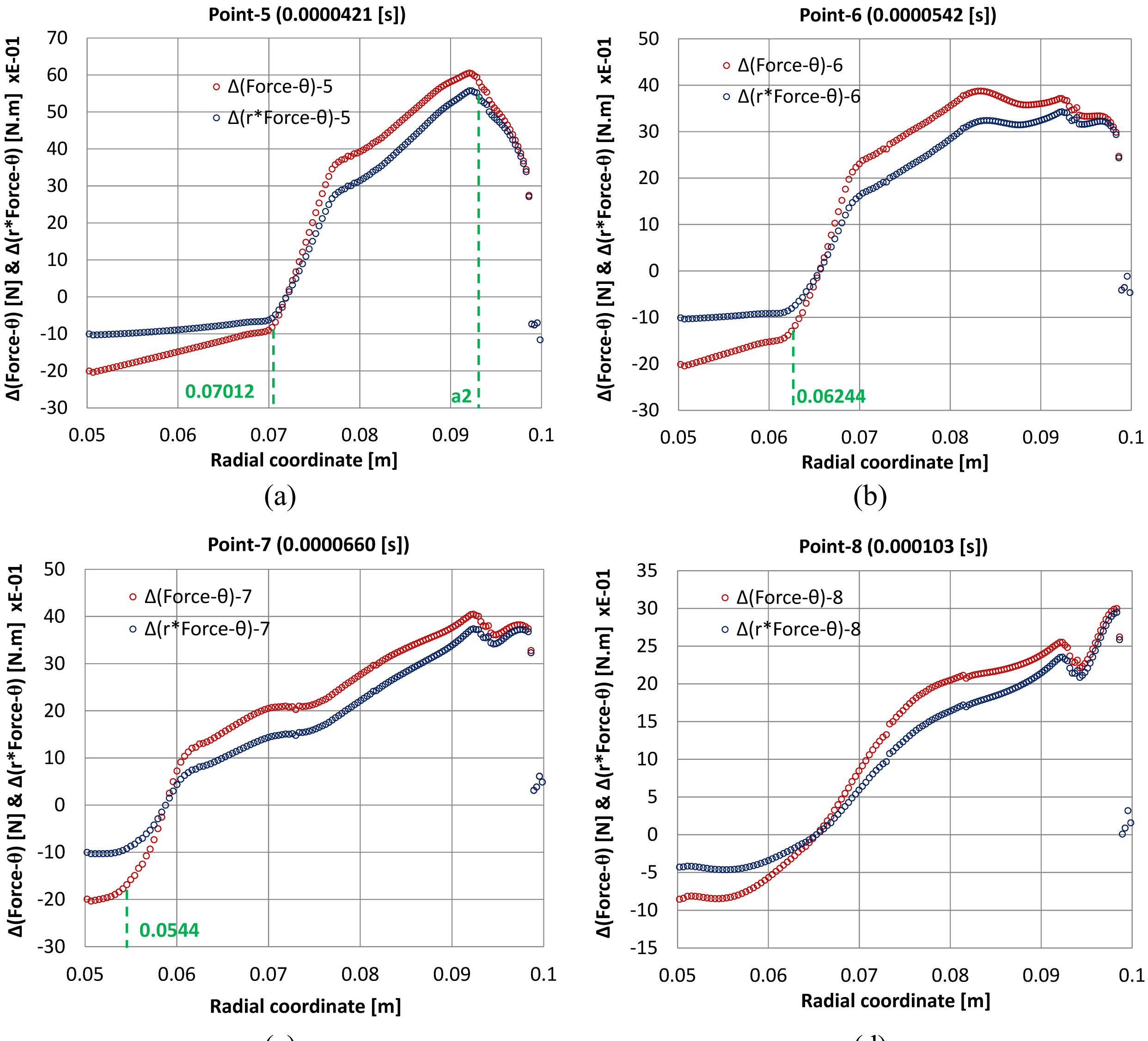

(a) (b)

(c) (d)

Figure 5-12: Δ(force-θ) and Δ(r*force-θ) plots at points 5, 6, 7 & 8 according to radial coordinates.

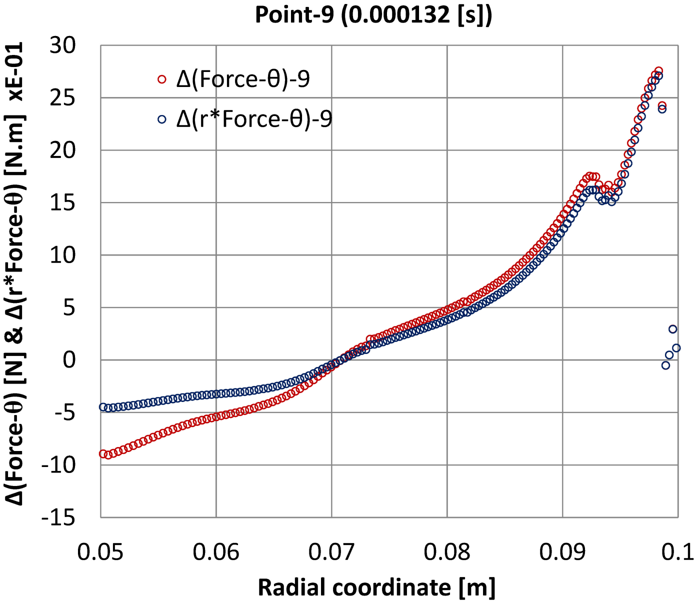

Figure 5-13: Δ(force-θ) and Δ(r*force-θ) plot at point 9, according to radial coordinates.

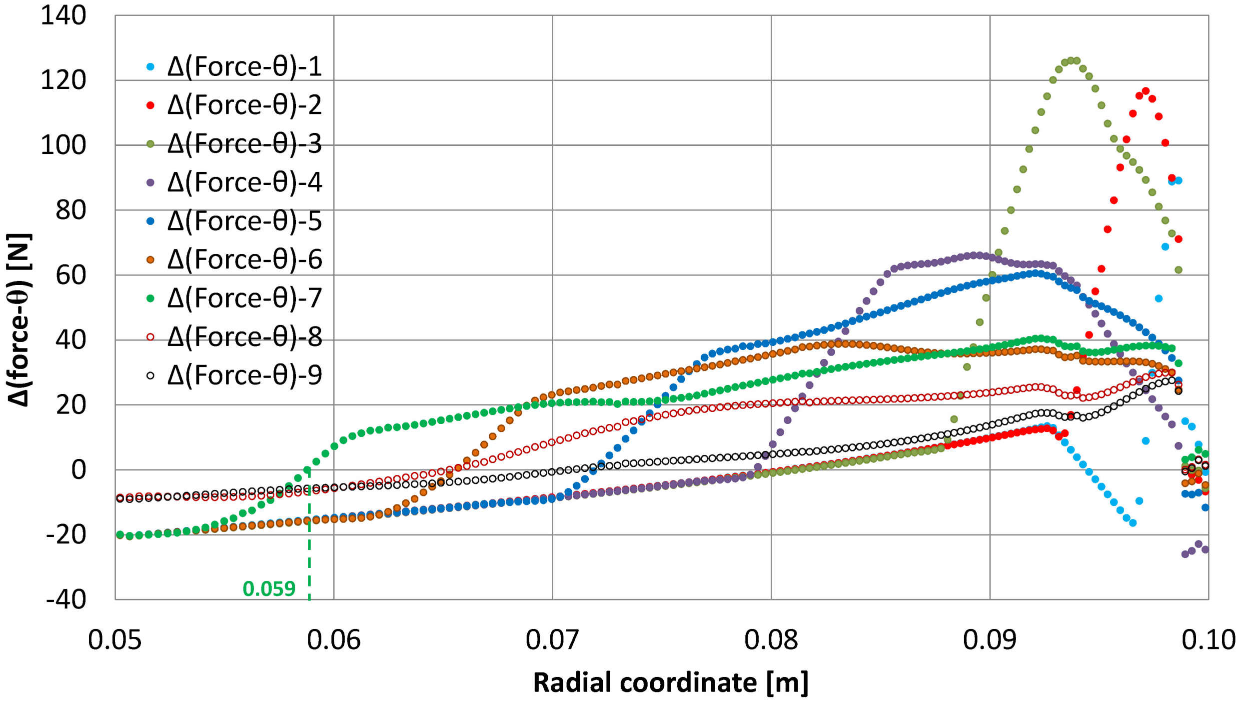

Figure 5-14: Δ(force-θ) at points 1, 2, 3, 4, 5, 6, 7, 8 & 9 along radial direction

Figure 5-14 and Figure 5-15 display the force and torque, respectively, as the expansion process propagates from point 1 to 9. The shape of the force distribution appears similar to the torque distribution along the radial coordinate, but with an order of magnitude around 10. The highest local values of torque (or force) are generated during the initial stage of the unsteady expansion process: points 1 to 3. As the head of expansion wave propagates toward the inlet wall, the torque (force) with smaller values is spread over the length of the channel. This fact can be called dissipation effect of the action of pressure because of $\beta_{SS} > \beta_{PS}$.

If a significant fraction of the torque is generated at the pressure and suction side of the region near the channel outlet, $\beta_{PS} > \beta_{SS}$ becomes a necessary design condition to maximize the work extraction.

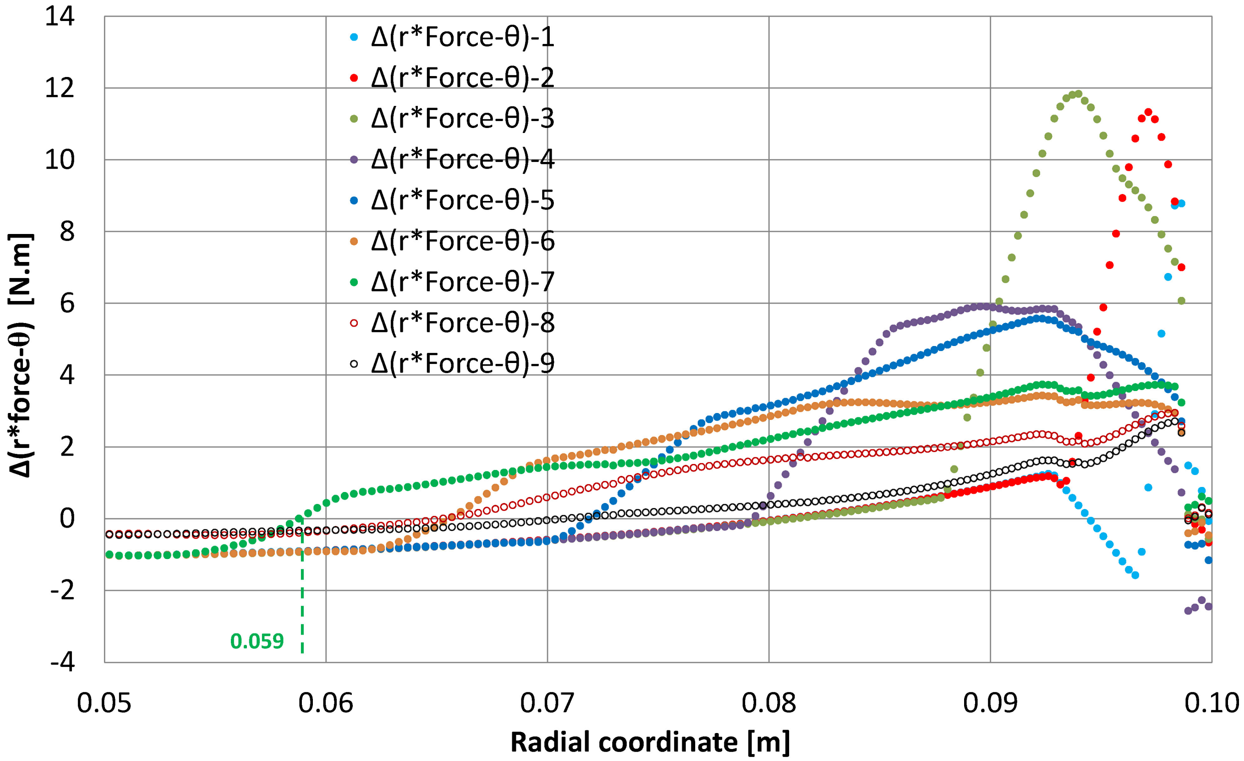

Figure 5-15: Δ(r*force-θ) at points 1, 2, 3, 4, 5, 6, 7, 8 & 9 along radial direction

5.2. Unsteady Expansion Process at gradual opening

5.2.1. Pressure distribution on channel walls

This section investigates the unsteady expansion process when the channel outlet opens gradually at 10,000 rpm. The torque coefficient history is shown in Figure 5-16, and 11 points are selected to analyze the process.

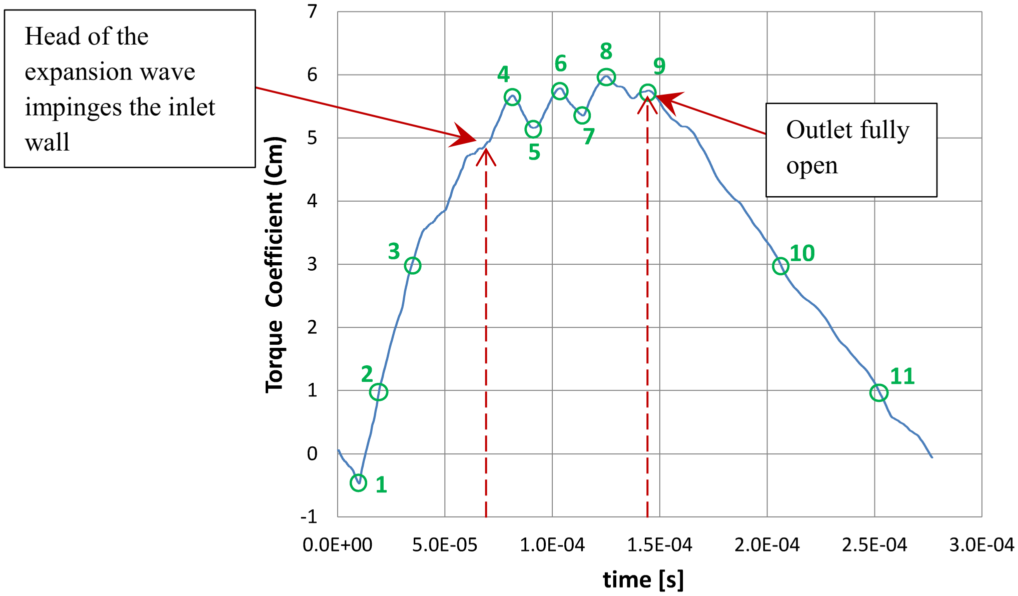

Figure 5-16: Torque coefficient (cm) history of a constant-cross section curved channel for gradual opening

At point 1, the fractional opening of the channel outlet creates an expansion wave made of concentric circle-contours of pressure. This configuration produces higher pressure on the suction side, which is why cm is negative (Figure 5-16 and Figure 5-17). Subsequently, at point 2, the effect of a slightly greater opening of the outlet causes the shape and position of the head of the expansion wave to become a front line perpendicular to the pressure and suction sides.

Positive torque is not produced in the region very close to the channel outlet until complete opening is achieved at point 9 (see left plots in Figure 5-17, Figure 5-18, and Figure 5-19). The gradual opening produces adverse effects on the pressure distribution on both pressure and suction sides, a disadvantageous condition with respect to instant opening because a significant portion of the generated torque comes from this region.

The head of the expansion wave impinges the inlet wall when the channel outlet is not yet fully opened; this causes the pressure to begin dropping, but not as rapidly as the instant opening case, slowing presure loss during the early stage. The pressure diferential between channel pressure and manifold pressure drives the acceleration of the fluid, thus the increase of the tangential velocity contributes to torque generation, and an explanation is given in Section 6.3.1. Therefore, cm values continue increasing till point 4 and then keep approximately the same value to point 9; this location in time marks the beginning of the cm decrease, the channel outlet has already been completely opened (point 9 in Figure 5-19), and these conditions appear to be correlated.

In all points in time, there is no positive net pressure area in the interval from r=0.05 [m] (at inlet wall) to r=0.06 [m] contributing to the generation of torque.

The results indicate instant opening of channel outlet with respect to the gradual opening creates more favorable conditions in the region near the channel outlet, maximizing torque generation. This positive condition indicates increasing the speed at which the outlet port opens are steps toward the optimal situation: instant opening.

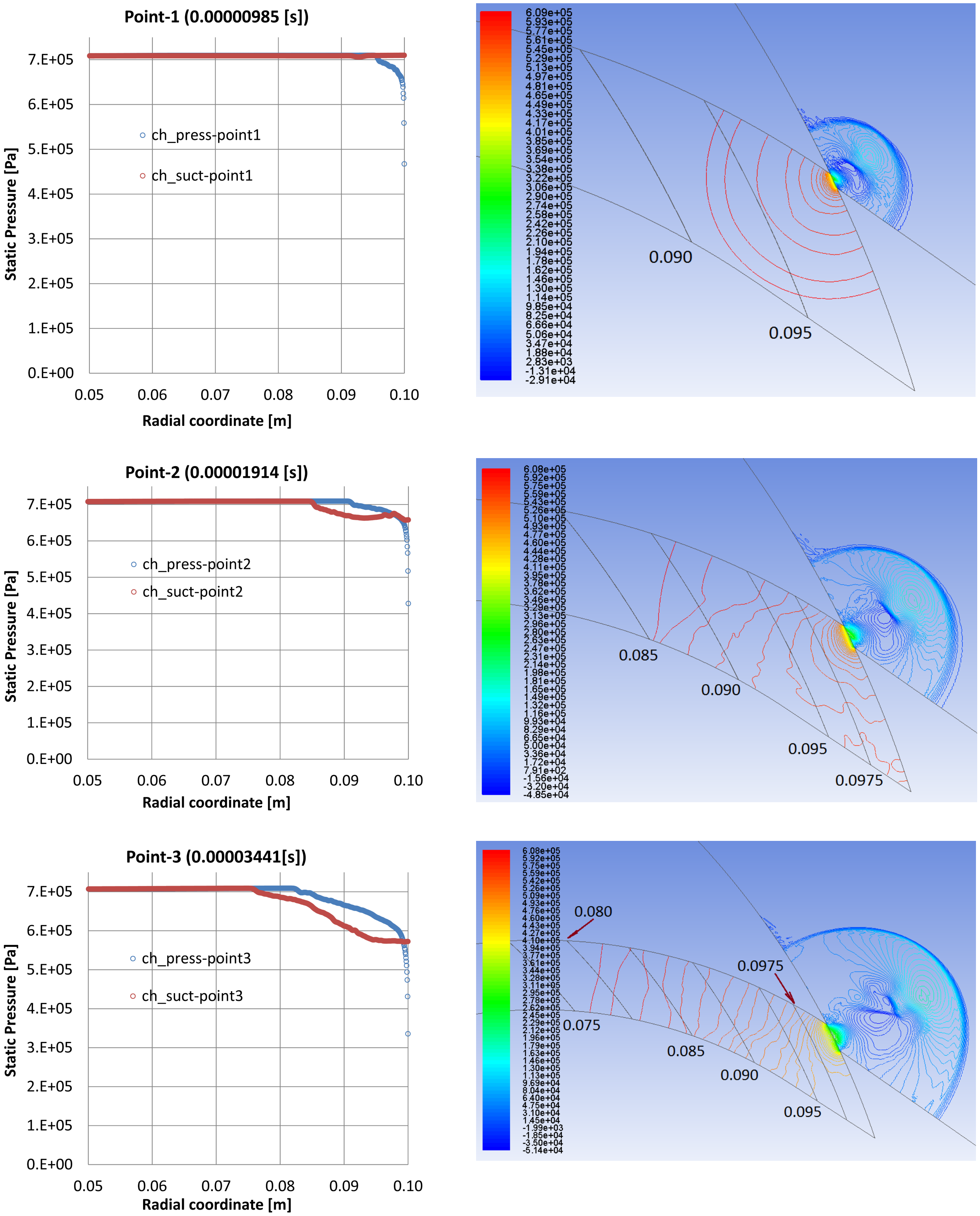

Figure 5-17: Pressure plot on the suction and pressure surface according to radial coordinates (left) and pressure contour (right) for points 1 to 3.

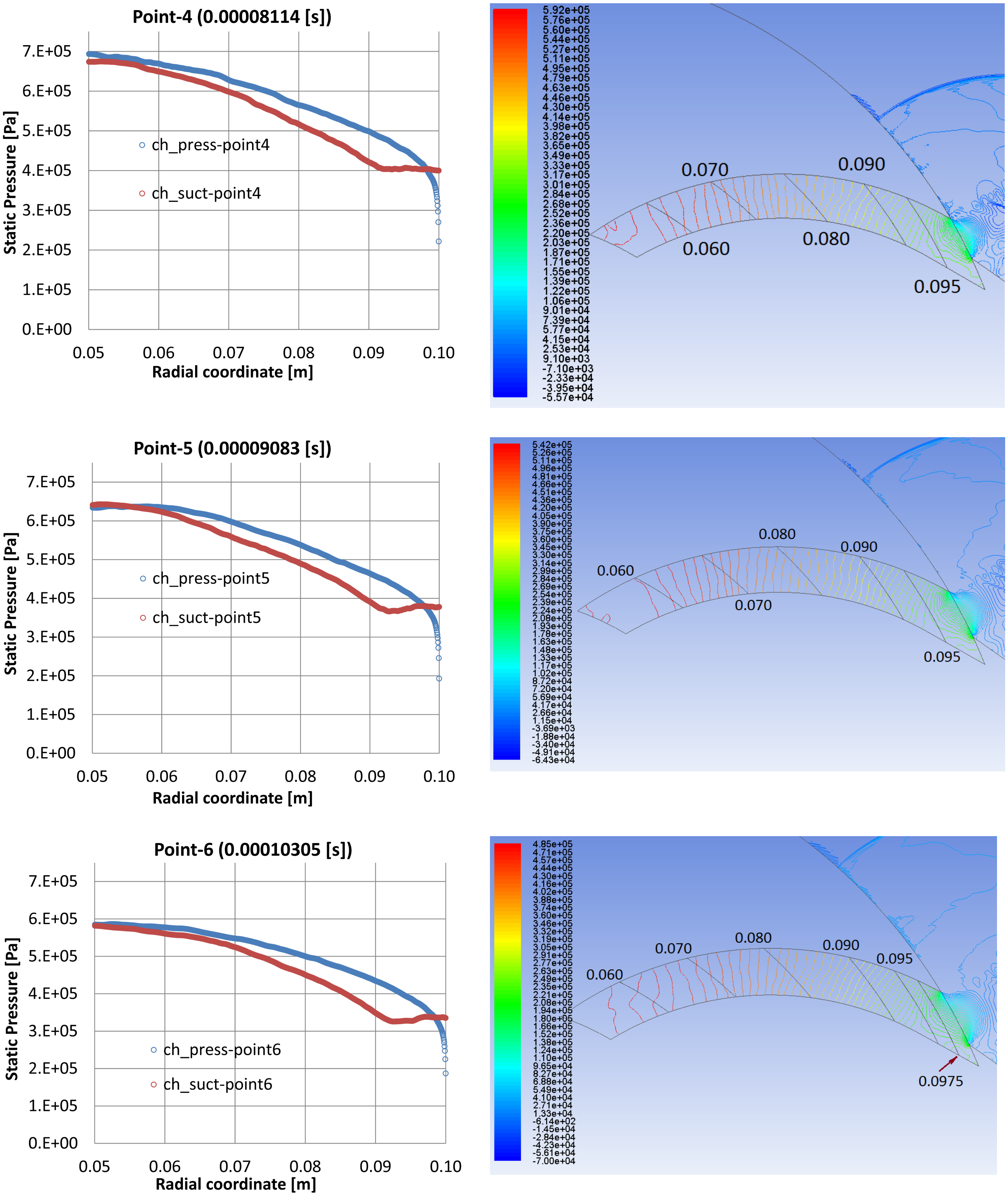

Figure 5-18: Pressure plot of the suction and pressure surface according to radial coordinates (left) and pressure contour (right) for points 4 to 6.

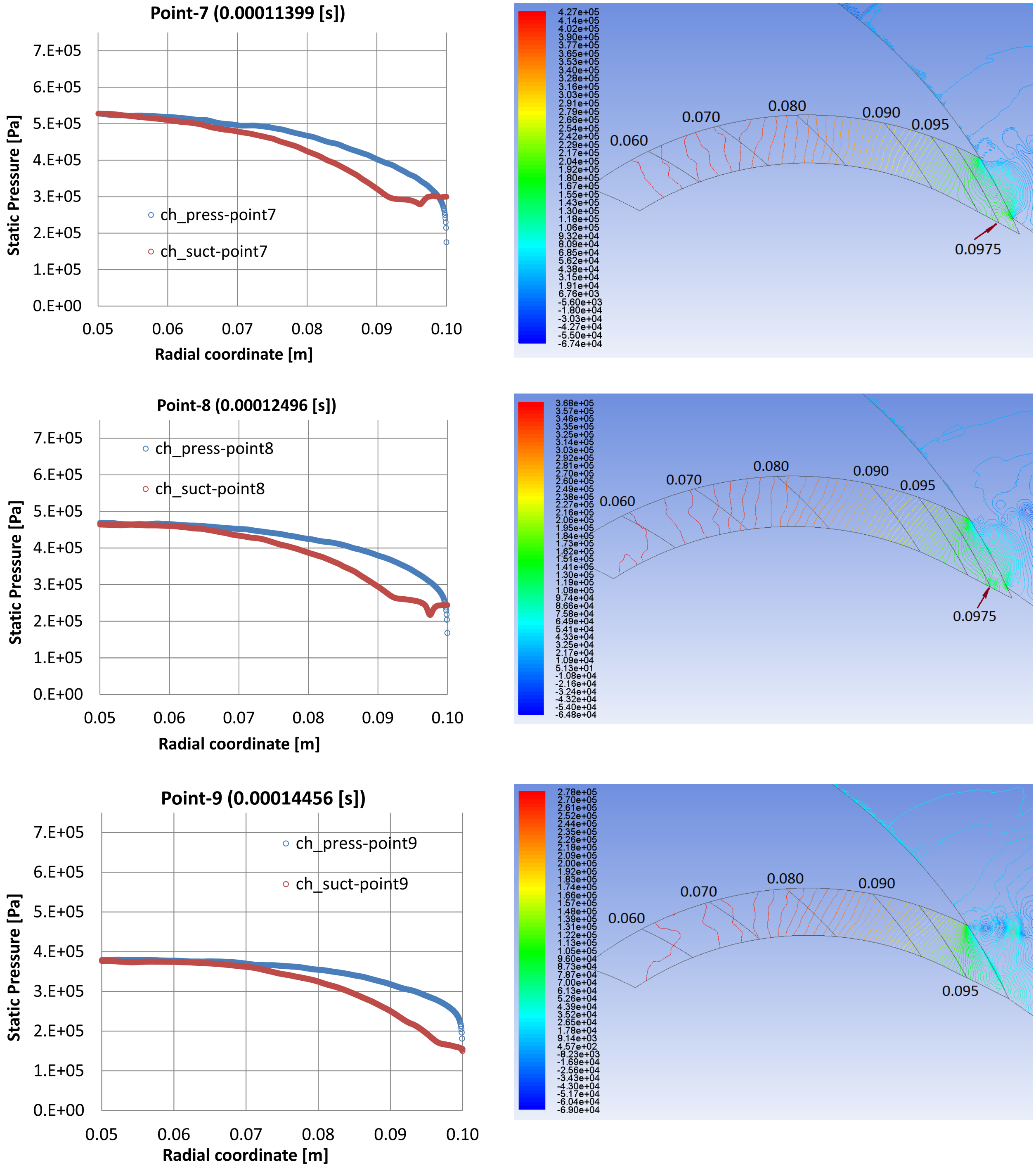

Figure 5-19: Pressure plot of the suction and pressure surface according to radial coordinates (left) and pressure contour (right) for points 7 to 9.

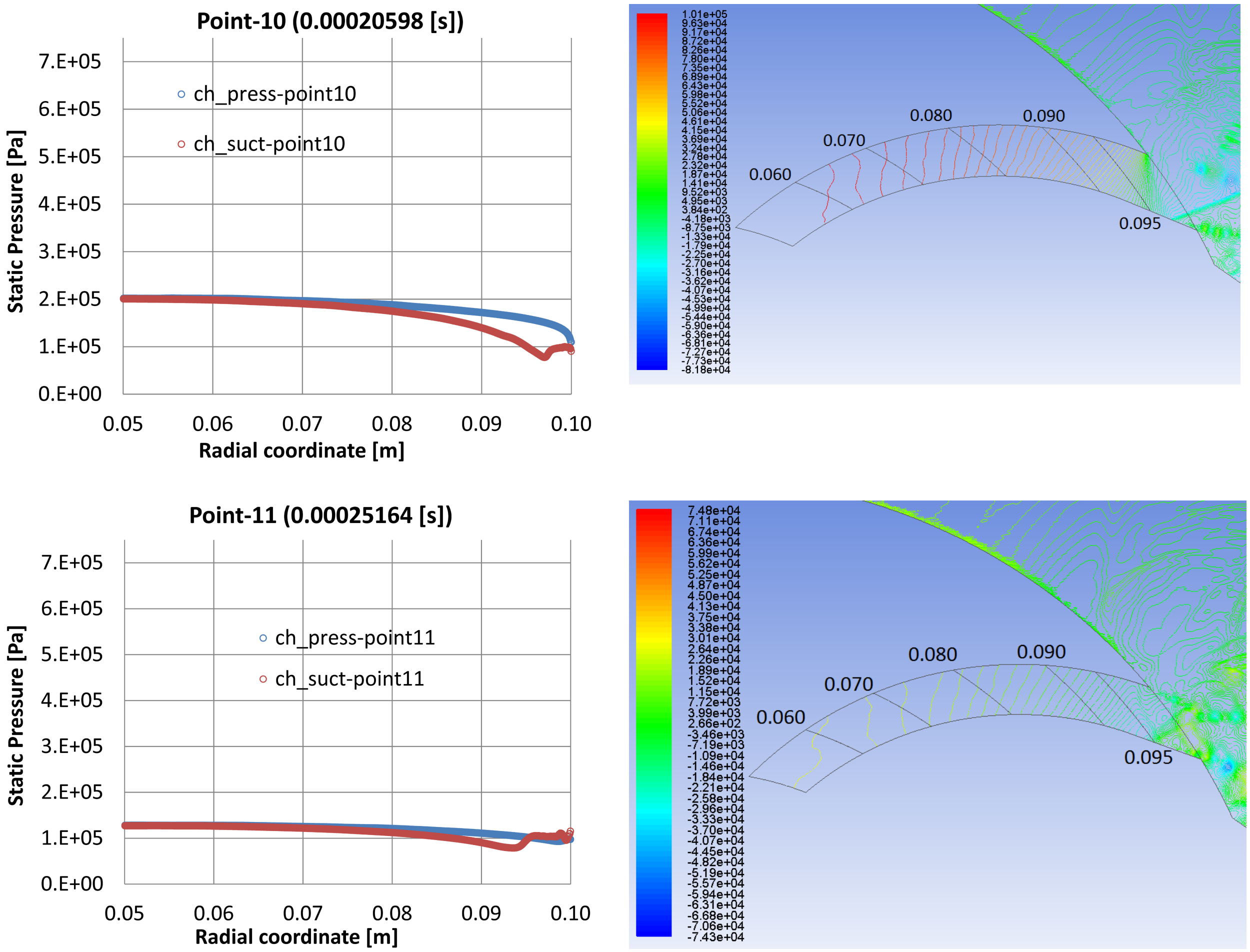

Figure 5-20: Pressure plot of the suction and pressure surface according to radial coordinates (left) and pressure contour (right) for points 10 to 11.

5.2.2. Force and Torque distribution on channel walls

In this section the force and torque differential distribution is presented in terms of pressure and sine of β. The magnitude of the force differential (Equation (5-9)) is proportional to the equation in terms of pressure and sine of β.

$$\Delta F_{tan-p} \approx [p_{PS} sin\beta_{PS} - p_{SS} sin\beta_{SS}]$$

Then:

$$\Delta(p * sin\beta) = [p_{PS} sin\beta_{PS} - p_{SS} sin\beta_{SS}] \qquad (5\text{-}13)$$

The same is done for the torque differential Equation (5-12):

$$T_{rp} = r.\Delta F_{tan-p} \approx \Delta(\mathrm{r} * \mathrm{p} * \sin\beta)$$

$$\Delta(r * p * sin\beta) = r.[p_{PS} sin\beta_{PS} - p_{SS} sin\beta_{SS}] \qquad (5\text{-}14)$$

Then, Equations (5-13) and (5-14) are used to plot curves of force (Figure 5-21 and Figure 5-22) and torque (Figure 5-23 and Figure 5-24), respectively.

Force plots present higher order of magnitude values with respect to the torque plots. Both force and torque graphs exhibit similar trends:

(a) Negative force and torque values near the channel outlet

(b) Positive force and torque values at the central region of the channel

(c) Negative force and torque near the channel inlet

These results show that gradual opening causes undesirable effects near the channel outlet, limiting torque extraction.

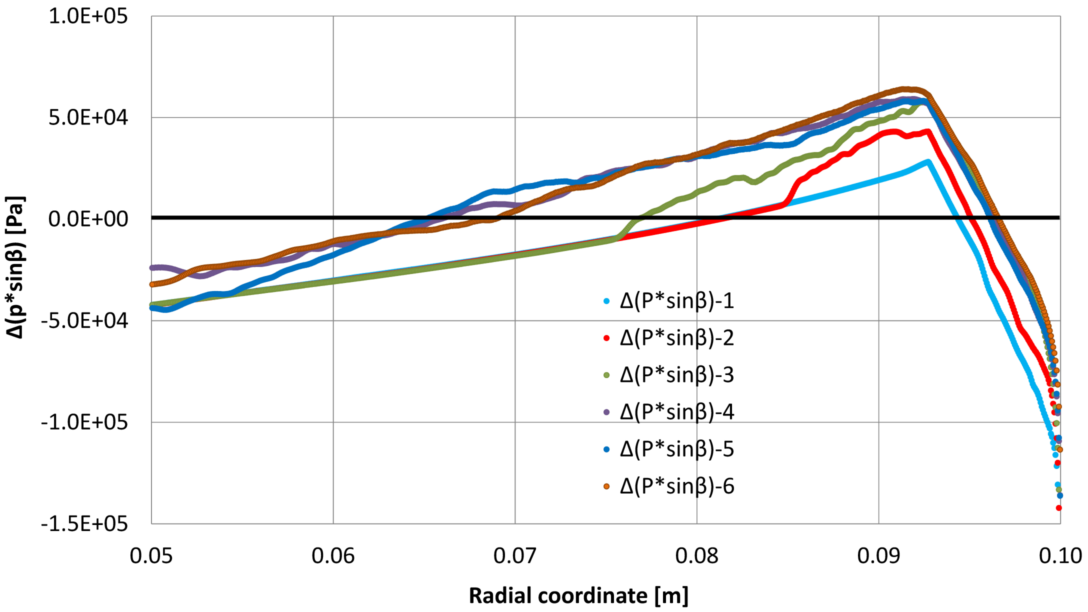

Figure 5-21: Δ(p*sinβ) at points 1, 2, 3, 4, 5 & 6 based on radial coordinates

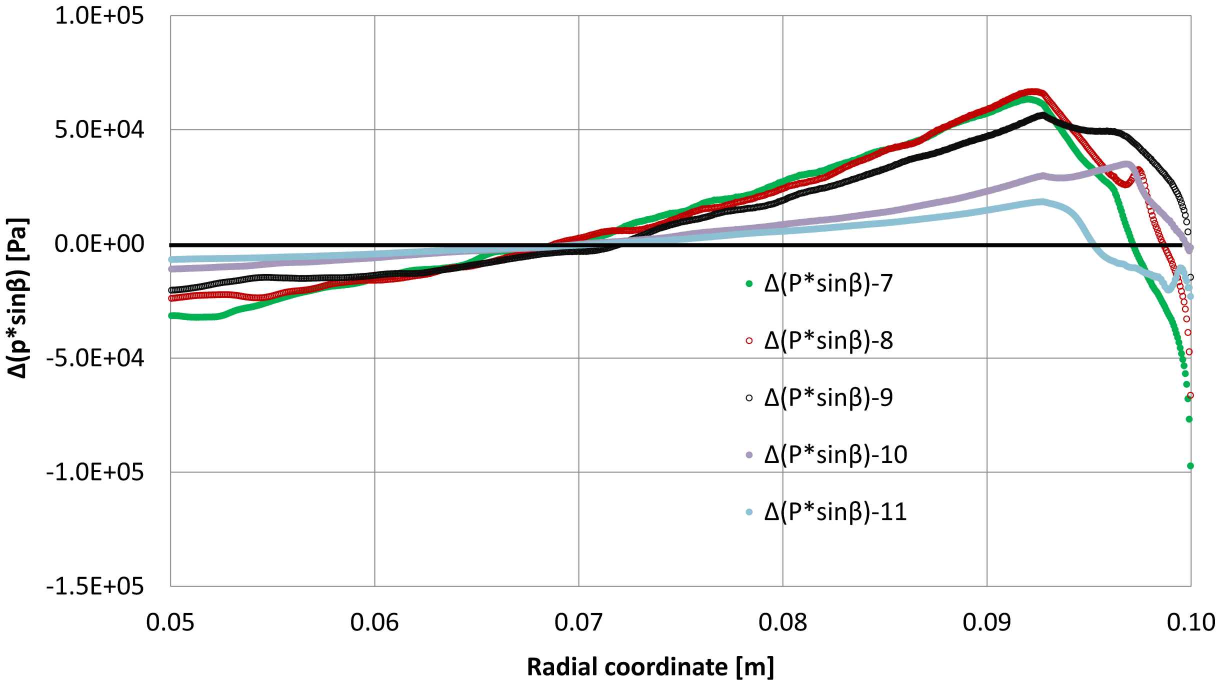

Figure 5-22: Δ(p*sinβ) at points 7, 8, 9, 10 & 11 based on radial coordinates.

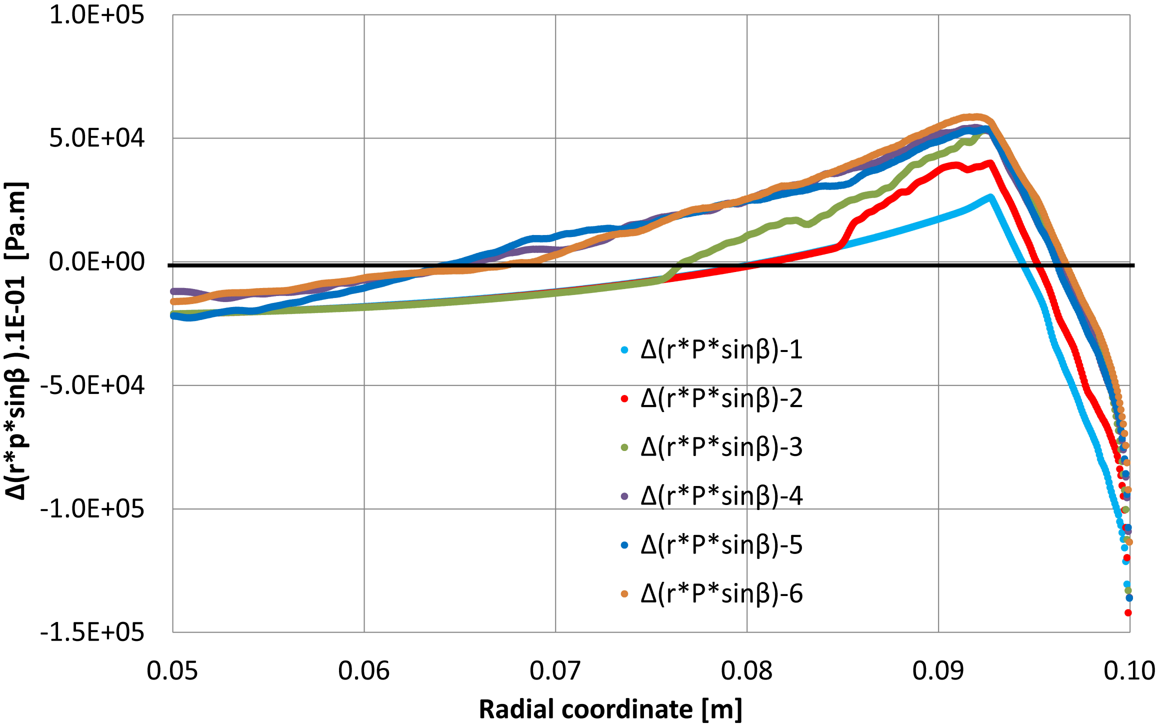

Figure 5-23: Δ(r*p*sinβ) at points 1, 2, 3, 4, 5 & 6 based on radial direction

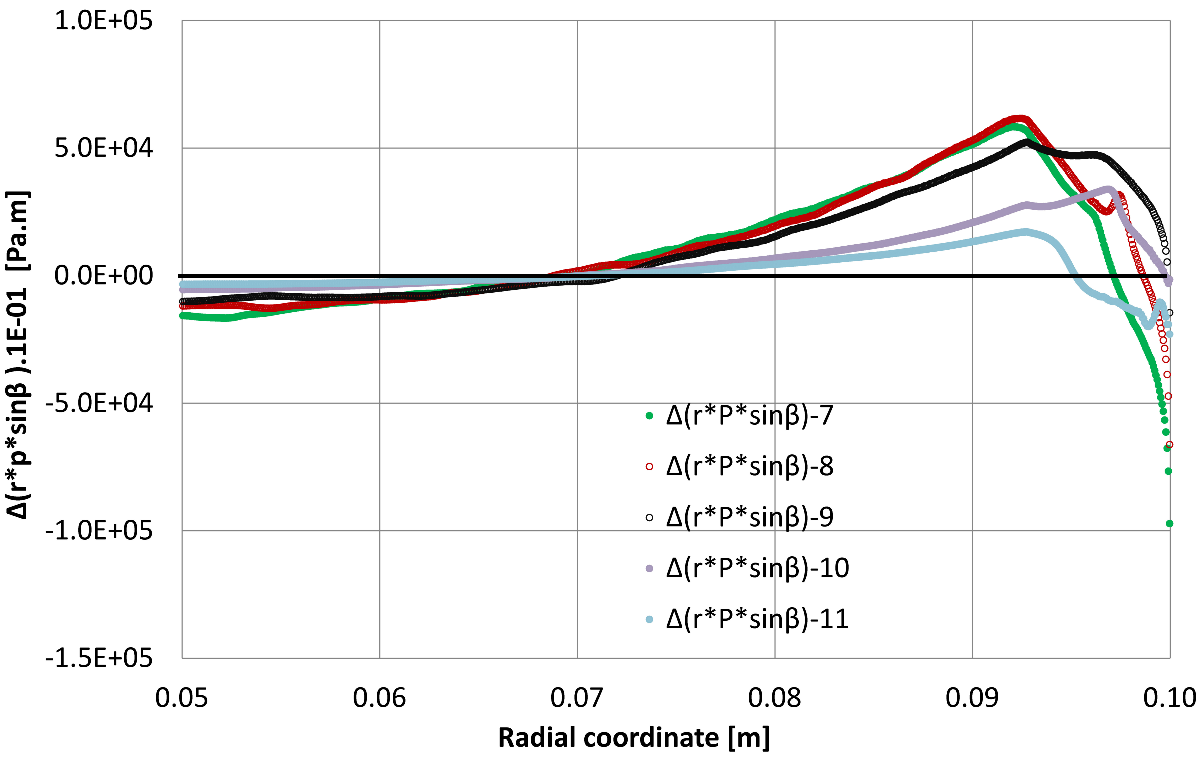

Figure 5-24: Δ(r*p*sinβ) at points 7, 8, 9, 10 & 11 based on radial direction

5.3. Impact on tangential force (torque generation) by changing θ parameter

The pressure and tangential forces (torque) applied to channel walls for a specific θ angle has been investigated. The θ angle was mentioned in Figure 2-2 (b) for constant cross-section channels made of two concentric circular arcs. In this section, the degree of impact on the tangential force (torque) is determined by varying the θ angle. The areas of influence (A_{PS} or A_{SS}) and the β angle (Figure 5-9), both along the pressure and suction walls, change by the alteration of θ angle.

When the head of the expansion wave propagates through the channel, isobaric line-contours appear from head to tail. The projection of each isobaric line-contour on pressure and suction walls creates different areas. These two areas are delimited by two concentric lines: r1 and r2 (Figure 5-25), and the projected areas are called “area of influence (AoI)”. The pressure on pressure side AoI is greater than the pressure on suction side AoI if the expansion wave is a left running wave. Thus, the isobaric line-contour produces a differential pressure between pressure and suction walls.

The differential force depends on six parameters: $p_{PS}, p_{SS}, A_{PS}, A_{SS}, \sin\beta_{PS}$ and $\sin\beta_{SS}$, according to Equation (5-9); the areas of influence and β angle will be the focus in this section.

To study the impact of the isobaric line-contour in the differential force, equation (5-9) will be utilized; this differential force is not confined to a specific radial location, but to an area location. Thus, the length-weighted average of sine of β will be considered in that equation instead of sin (β) only. The reason for this is β angle changes at each radial coordinate on the area of influence. The modified equation yields:

$$\Delta\vec{F}_{tan-p} = [p_{PS}A_{PS}\overline{\sin\beta_{PS}} - p_{SS}A_{SS}\overline{\sin\beta_{SS}}]\ \vec{e}_{\theta} \tag{5-15}$$

The length-weighted average of sin (β) is defined as:

$$\overline{\sin\beta} = \frac{\int \ \sin\beta dl}{L_{arc}} \tag{5-16}$$

Expressed as summation:

$$\overline{\sin\beta} = \frac{\sum_i^n \sin\beta_i . \Delta l_i}{L_{arc}} \tag{5-17}$$

Where:

L_{arc}: refers to the total arc length on the pressure or suction side of the area of influence

Δl_i: small length element

β_i: beta angle at the center of the small length element “i”

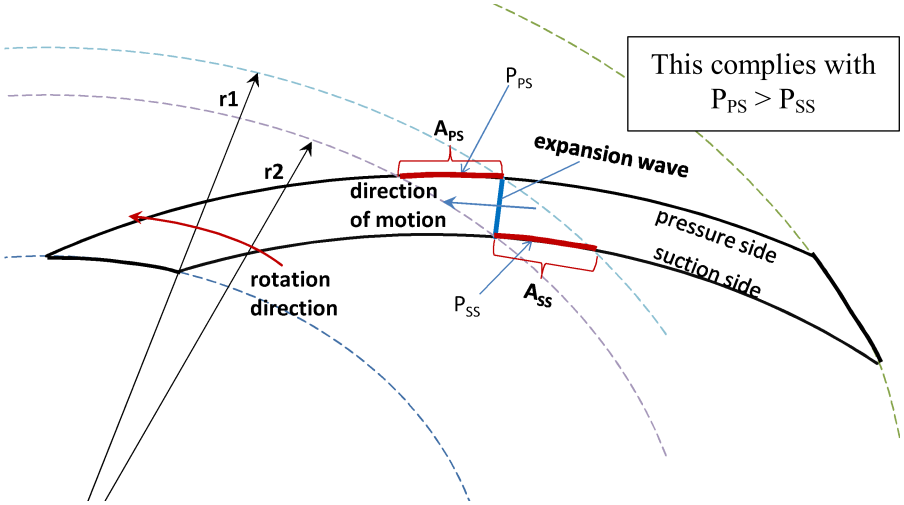

Figure 5-25: Area of influence projected by a single isobaric line-contour on pressure and suction walls

Results in Figure 5-26 correspond to channel geometry drawn by two concentric circle arcs to have a constant cross-section channel. The four graphs depict the variation of θ angle from 30 to 60 degrees, respectively, and as the θ angle is increased, the channel length increases also.

In Section 5.1.2, it is stated that beta angles near 90 degrees on the pressure wall or near 0 degrees on the suction wall benefits the generation of torque; this was concluded for a tangential force when applied at each radial coordinate. Here, the net tangential force is based on area of influence, and the orientation of line-contours causes this area to grow or shrink.

For the channel geometry described in Figure 5-26, β angle portrays a decreasing trend from leading to trailing edge. The opposite manner happens to the area of influence (A_{PS} or A_{SS}) of both pressure and suction sides. These results are used to calculate the terms of "$A_{PS}\overline{sin\beta_{PS}}$" and "$A_{SS}\overline{sin\beta_{SS}}$" from Equation (5-15), and the results are plotted in Figure 5-26. The intersection of the upper line-contour with the pressure side defines the radial coordinate used to plot these two terms. Radial coordinate of 60, 70, 80, 90 and 100 mm were used for each θ angle.

Figure 5-26 shows that both $A_{PS}\overline{sin\beta_{PS}}$ and $A_{SS}\overline{sin\beta_{SS}}$ resulted in similar values at each radial coordinate. Then, Equation (5-15) is re-written as:

$$\Delta\vec{F}_{tan-p} \approx A_{PS}\overline{sin\beta_{PS}}[p_{PS} - p_{SS}]\,\vec{e}_\theta \qquad (5\text{-}18)$$

Or

$$\Delta\vec{F}_{tan-p} \approx A_{SS}\overline{sin\beta_{SS}}[p_{PS} - p_{SS}]\,\vec{e}_\theta \qquad (5\text{-}19)$$

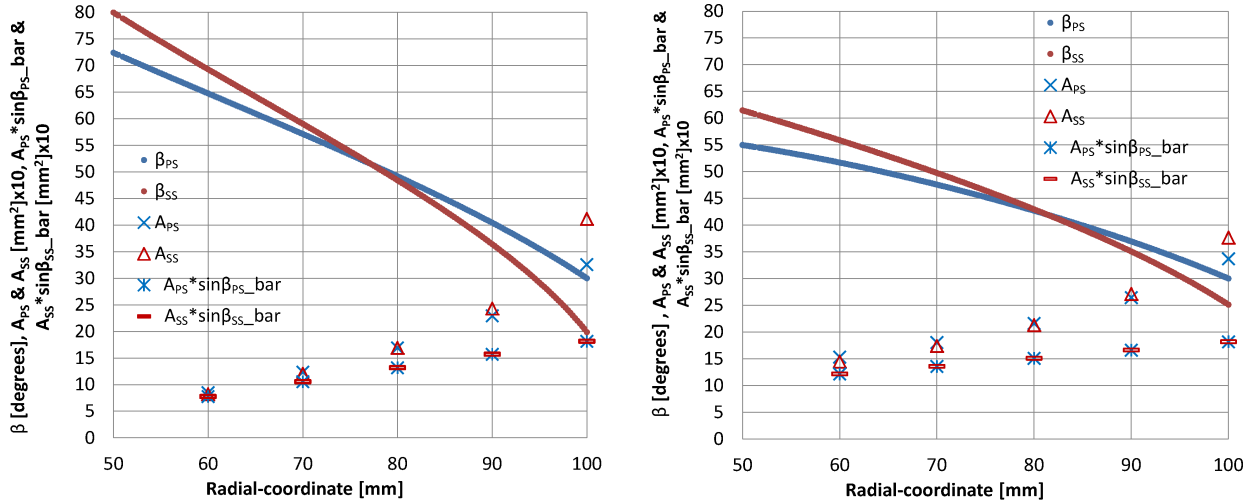

(a) θ=30 deg (a) θ=40 deg

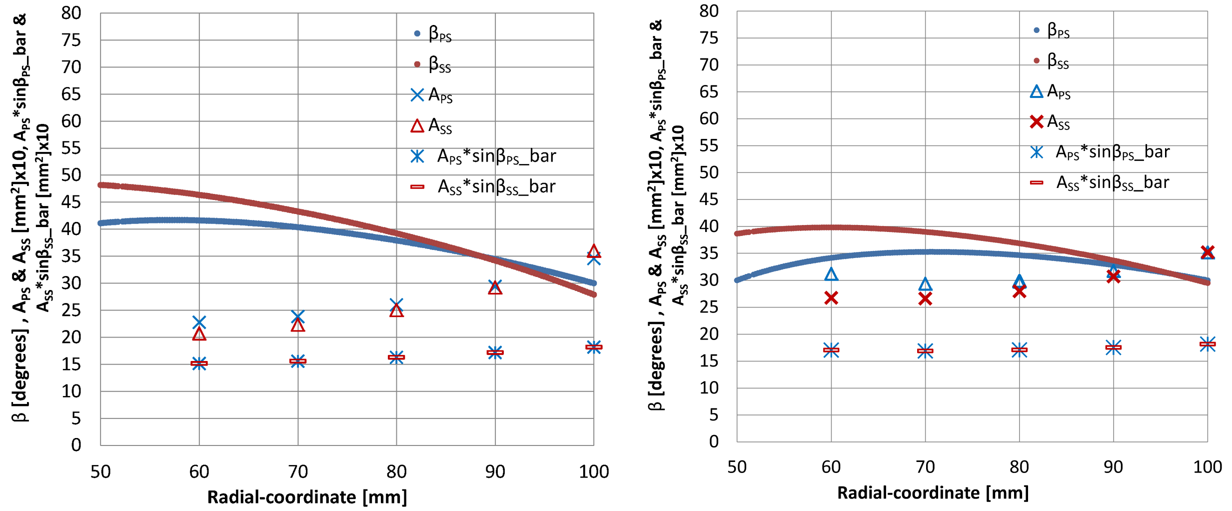

(a) θ=50 deg (a) θ=60 deg

Figure 5-26: β & area of influence (A_{PS} & A_{SS}) on pressure and suction walls created by line-contour when θ angle is changed

The amount of net tangential force over an area of influence depends on $A_{PS}\overline{sin\beta_{PS}}$ (or $A_{SS}\overline{sin\beta_{SS}}$) and pressure difference $(p_{PS} - p_{SS})$. The outcome of A$\overline{sin\beta}$ varies from lower values near channel inlet to greater toward outlet. Also, the trend is less steep as θ angle changes from 30 to 60. Thus, the net tangential force becomes greater in regions closer to the channel outlet. In addition, due to greater radius, greater torque values can be accomplished in that region.

CHAPTER 6. MOMENT OF MOMENTUM ANALYSIS

6.1. Moment of Momentum equation applied to a single channel of the WDE

The Equation (6-1) is a general formulation of the angular momentum principle for an inertial and non-deforming control volume [19] at any instant in time.

$$\vec{r}x\vec{F}_s + \iiint_{CV} \vec{r}x\vec{g}\rho d\forall + \vec{T}_{shaft} = \frac{\partial}{\partial t}\iiint_{CV} \vec{r}x\vec{V}\rho d\forall + \iint_{CS} \vec{r}x\vec{V}\rho\vec{V}.d\vec{A} \tag{6-1}$$

This investigation is focused on 2-dimensional models because all geometries investigated reflect that characteristic, and the initial concept of the WDE was to have a rotor with flat shroud and hub in the channels. Thus, the generation of torque is the result of the dynamic action of the fluid with the side walls. Figure 6-1 shows the control volume selected for the application of equation (6-1).

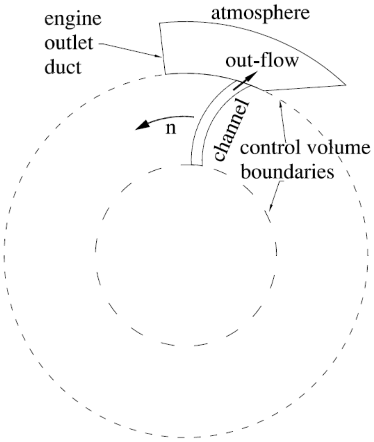

Figure 6-1: Control Volume selected for the Angular Momentum Equation Analysis

The three terms on the LHS of Equation (6-1) are described as follows:

$\vec{r}x\vec{F}_s$: represents the angular momentum of surface forces over the control volume (they can be due to pressure or friction). This term might be ignored due to the amount it represents when compared with the torque in the shaft.

$\iiint_{CV} \vec{r}x\vec{g}\rho d\forall$: refers to the torque generated by body forces. The direction of the torque generated is perpendicular to the rotation direction and therefore does not contribute to torque generation. Then, Equation (6-1) becomes:

$$\vec{T}_{shaft} = \frac{\partial}{\partial t}\iiint_{CV} \vec{r}x\vec{V}\rho d\forall + \iint_{CS} \vec{r}x\vec{V}\rho\vec{V}.d\vec{A}$$

During the unsteady expansion process, the fluid crosses the control surface through only one outlet, and the equation becomes:

$$\vec{T}_{shaft} = \frac{\partial}{\partial t}\iiint_{CV} \vec{r}x\vec{V}\rho d\forall + \iint_{outlet} \vec{r}x\vec{V}\rho\vec{V}.d\vec{A} \tag{6-2}$$

In Equation (6-2), the first term on the right hand side represents the rate of change of fluid's angular momentum within the control volume. The second term on the right hand side refers to the outflow rate of the angular momentum through the outlet area of the channel [19], [20]. The first and second terms hold the Joules units.

In a typical turbomachinery analysis, the first term of the RHS in Equation (6-1) vanishes due to steady state condition and becomes:

$$\vec{T}_{shaft} = \iint_{CS} \vec{r}x\vec{V}\rho\vec{V}.d\vec{A} = \iint_{outlet} rV_{\theta}\,(\rho V_r dA)\,\vec{k} - \iint_{inlet} rV_{\theta}\,(\rho V_r dA)\,\vec{k}$$

And considering uniform flow properties at the inlet and outlet:

$$\vec{T}_{shaft} = \dot{m}(r_{out}V_{\theta-out} - r_{in}V_{\theta-in})\vec{k}$$

This shows the extracted torque is based on the change of the fluid's angular momentum ($r\ \Delta V_{\theta}$), and this change is called turbomachinery principle. The fluid changes its angular momentum when going through a blade passage between inlet and outlet, and this change converts into torque.

For the unsteady expansion of the WDE, both RHS terms are kept and only one border crossing is considered (fluid outflow) in the second RHS term. Thus, the first RHS term refers to the turbomachinery principle in terms of the **rate** of "change of the angular momentum" **within the channel** to produce torque. The second RHS term indicates **the rate of flow of the angular momentum through outlet area** and suggests it is linked to mass flow rate (see Equation (6-18) for a 2-D case resulting from Equation (6-2)). Additional explanation of this last term is given in Section 6.2.2.

6.2. Analytical Analysis with respect to the Inertial Reference Frame

The present analysis is accomplished in cylindrical coordinates with the following conventions:

$$\vec{V} = \vec{V_r} + \vec{V_\theta} \qquad (6\text{-}3)$$

$$\vec{r} = r\vec{e}_r \qquad (6\text{-}4)$$

$$\vec{V_r} = V_r\vec{e}_r \qquad (6\text{-}5)$$

$$\vec{V_\theta} = V_\theta\vec{e}_\theta \qquad (6\text{-}6)$$

Orientation of the unit vectors is according to Figure 6-2.

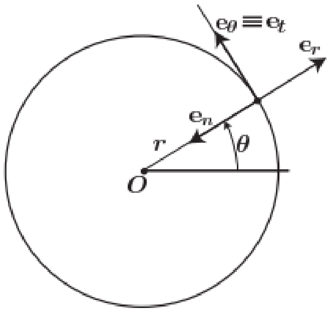

Figure 6-2: Orientation of radial and tangential unit vectors in cylindrical coordinates

The RHS terms of Equation (6-2) will be analyzed separately and in 2-D ($\vec{V_z} = 0$):

$$(\mathrm{I}) = \frac{\partial}{\partial t}\iiint_{CV}(\vec{r}\times\vec{V})\rho d\not{V} \tag{6-7}$$

$$(\mathrm{II}) = \iint_{outlet}(\vec{r}\times\vec{V})\rho\,\vec{V}\cdot d\vec{A} \tag{6-8}$$

6.2.1. The Rate of Change of the Angular Momentum in the Channel

Replacing (6-3) in (6-7):

$$\frac{\partial}{\partial t}\iiint_{CV}\left[\vec{r}\times\left(\vec{V}_r+\vec{V}_\theta\right)\right]\rho d\not{V} = \iiint_{CV}\frac{\partial\left(\left[\vec{r}\times\left(\vec{V}_r+\vec{V}_\theta\right)\right]\rho\right)}{\partial t}\,d\forall$$

$$= \iiint_{CV}\frac{\partial([\vec{r}\times\vec{V}_r+\vec{r}\times\vec{V}_\theta]\rho)}{\partial t}\,d\not{V}$$

$\vec{r}\times\vec{V}_r = 0$ does not produce rotation. Then:

$$\frac{\partial}{\partial t}\iiint_{CV}(\vec{r}\times\vec{V})\rho d\not{V} = \iiint_{CV}\frac{\partial[(\vec{r}\times\vec{V}_\theta)\rho]}{\partial t}\,d\not{V} \tag{6-9}$$

Working inside of the integral:

$$\frac{\partial\left[(\vec{r}\times\vec{V}_\theta)\rho\right]}{\partial t} = \frac{\partial\left[\vec{r}\rho\times\vec{V}_\theta\right]}{\partial t} = (\vec{r}\rho)\times\left[\frac{\partial\left(\vec{V}_\theta\right)}{\partial t}\right] - \vec{V}_\theta\times\frac{\partial(\vec{r}\rho)}{\partial t} =$$

$$= (\vec{r}\rho)\times\left[\frac{\partial\vec{V}_\theta}{\partial t}\right] - \vec{V}_\theta\times[\frac{\partial\vec{r}}{\partial t}\rho+\vec{r}\frac{\partial\rho}{\partial t}] =$$

$$= \left(\vec{r}\times\frac{\partial\vec{V}_\theta}{\partial t}\right)\rho - \left(\vec{V}_\theta\times\frac{\partial\vec{r}}{\partial t}\right)\rho - (\vec{V}_\theta\times\vec{r})\frac{\partial\rho}{\partial t} = \tag{6-10}$$

In the first term of expression (6-10), the partial derivative of the tangential velocity vector:

$$\frac{\partial\vec{V}_\theta}{\partial t} = \frac{\partial(V_\theta\vec{e}_\theta)}{\partial t} = V_\theta\frac{\partial\vec{e}_\theta}{\partial t} + \frac{\partial V_\theta}{\partial t}\vec{e}_\theta =$$

It is known that:

$$\frac{\partial\vec{e}_\theta}{\partial t} = -\dot{\theta}\vec{e}_r$$

Then:

$$\frac{\partial \vec{V}_\theta}{\partial t} = -V_\theta \dot{\theta} \vec{e}_r + \frac{\partial V_\theta}{\partial t} \vec{e}_\theta \tag{6-11}$$

In the third term for expression (6-10), the partial derivative of the radial vector:

$$\frac{\partial \vec{r}}{\partial t} = \frac{\partial (r\vec{e}_r)}{\partial t} = \frac{\partial r}{\partial t}\vec{e}_r + r\frac{\partial \vec{e}_r}{\partial t} = \frac{\partial r}{\partial t}\vec{e}_r + r\dot{\theta}\vec{e}_\theta = \frac{\partial r}{\partial t}\vec{e}_r + r\omega\vec{e}_\theta$$

Where $\dot{\theta} = \omega$

$$\frac{\partial \vec{r}}{\partial t} = \frac{\partial r}{\partial t}\vec{e}_r + r\omega\vec{e}_\theta \tag{6-12}$$

Replacing (6-11) and (6-12) in (6-10):

$$= \left(\vec{r} \times [-V_\theta\dot{\theta}\vec{e}_r + \frac{\partial V_\theta}{\partial t}\vec{e}_\theta]\right)\rho - \left(\vec{V}_\theta \times [\frac{\partial r}{\partial t}\vec{e}_r + r\omega\vec{e}_\theta]\right)\rho - (\vec{V}_\theta \times \vec{r})\frac{\partial \rho}{\partial t} =$$

Writing explicitly:

$$= \left((r\vec{e}_r) \times [-V_\theta\dot{\theta}\vec{e}_r + \frac{\partial V_\theta}{\partial t}\vec{e}_\theta]\right)\rho - \left((V_\theta\vec{e}_\theta) \times [\frac{\partial r}{\partial t}\vec{e}_r + r\omega\vec{e}_\theta]\right)\rho - ((V_\theta\vec{e}_\theta) \times (r\vec{e}_r))\frac{\partial \rho}{\partial t} =$$

$$= (0) + r\rho\frac{\partial V_\theta}{\partial t}\vec{e}_k + \rho V_\theta\frac{\partial r}{\partial t}\vec{e}_k - (0) + rV_\theta\frac{\partial \rho}{\partial t}\vec{e}_k =$$

$$= [r\rho\frac{\partial V_\theta}{\partial t} + \rho V_\theta\frac{\partial r}{\partial t} + rV_\theta\frac{\partial \rho}{\partial t}]\vec{e}_k \tag{6-13}$$

Replacing (6-13) in (6-9):

$$\frac{\partial}{\partial t}\iiint_{CV}(\vec{r} \times \vec{V})\rho d\cancel{V} = \iiint_{CV}\left[r\rho\frac{\partial V_\theta}{\partial t} + \rho V_\theta\frac{\partial r}{\partial t} + rV_\theta\frac{\partial \rho}{\partial t}\right]d\cancel{V}\ \vec{e}_k \tag{6-14}$$

Considering:

$V_r = \dot{r}$ and $V_\theta = r\dot{\theta}$, into (6-14):

$$\frac{\partial}{\partial t}\iiint_{CV}(\vec{r} \times \vec{V})\rho d\cancel{V} = \iiint_{CV}\left[r\rho\frac{\partial V_\theta}{\partial t} + \rho V_\theta V_r + rV_\theta\frac{\partial \rho}{\partial t}\right]d\cancel{V}\ \vec{e}_k \tag{6-15}$$

Analyzing every term in (6-15):

6.2.1.1. 1^{st} term

$$\begin{matrix} r & \rho & \frac{\partial V_\theta}{\partial t} \end{matrix}$$
$$[+][+][-/+] = [-/+]$$

The contribution would be according to the sign of the rate of change of the absolute tangential velocity and the direction of this velocity (positive if moving in the rotation direction of the channel and negative otherwise). Then:

If the fluid element moves in the rotation direction:

$$+\frac{\partial V_\theta}{\partial t}$$

The result is:

If accelerates: $+\frac{\partial V_\theta}{\partial t} = (+)(+) = (+)$

If decelerates: $+\frac{\partial V_\theta}{\partial t} = (+)(-) = (-)$

If the fluid element moves against the rotation direction:

$$-\frac{\partial V_\theta}{\partial t}$$

The result is:

If accelerates: $-\frac{\partial V_\theta}{\partial t} = (-)(+) = (-)$

If decelerates: $-\frac{\partial V_\theta}{\partial t} = (-)(-) = (+)$

The torque generation gain is when the local tangential velocity rate decreases and this velocity is in the same direction of the channel rotation. The second option for gain is when the local tangential velocity rate increases and this tangential velocity goes against the direction of the channel rotation.

The first statement for torque generation is explained graphically in Figure 6-3, where a small element in the channel (inertial frame of reference) experiences a local change in tangential velocity. This change is to a lower value after the head of the expansion wave passes that location. The gradient of the local tangential velocity at that location decreases but the local tangential velocity is still in the direction of the channel rotation. This effect produces a gain in the torque generation as stated above.

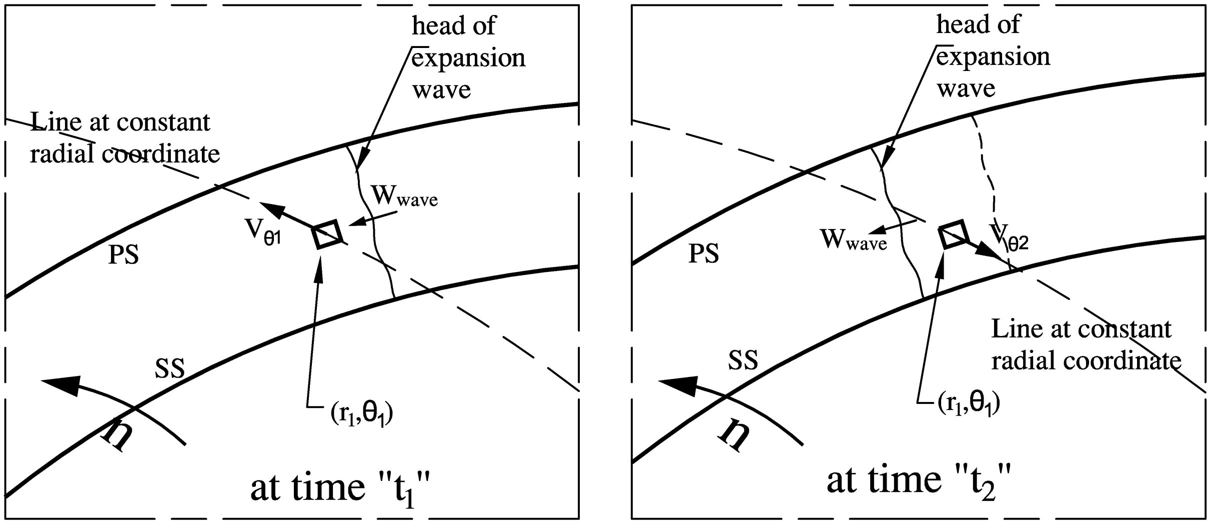

Figure 6-3: Changes in local tangential velocity after the head of the expansion wave passes (r_1, θ_1) position ($t_2 > t_1$).

6.2.1.2. 2nd term

$$\begin{array}{c} \rho \;\; V_\theta \; V_r \\ [+][?][+] = [?] \end{array}$$

The contribution is according to the sign of the Absolute Tangential Velocity.

If the fluid particle moves in the direction of the channel rotation:

$$\begin{array}{c} \rho \;\; V_\theta \; V_r \\ [+][+][+] = [+] \end{array}$$

If the fluid particle moves in the direction opposite the channel rotation:

$$\begin{gathered}\rho \;\; V_\theta \; V_r \\ [+][-][+] = [-]\end{gathered}$$

For the second term, the gain in torque generation happens when the direction of the local tangential velocity is against the direction of the channel rotation.

6.2.1.3. 3rd term

$$\begin{gathered}r \;\; V_\theta \;\; \frac{\partial \rho}{\partial t} \\ [+][?][?] = [?][?]\end{gathered}$$

The contribution is according to the sign of the Absolute Tangential Velocity and the rate of change of the density. Two cases are considered:

If the fluid particle moves in the direction of the channel rotation:

If there is an increase in the local density value

$$\begin{gathered}r \;\; V_\theta \;\; \frac{\partial \rho}{\partial t} \\ [+][+][+] = [+]\end{gathered}$$

If there is a decrease in the local density value

$$\begin{gathered}r \;\; V_\theta \;\; \frac{\partial \rho}{\partial t} \\ [+][+][-] = [-]\end{gathered}$$

If the fluid particle moves in the direction opposite the channel rotation:

If there is an increase in the local density value

$$\begin{gathered}r \;\; V_\theta \;\; \frac{\partial \rho}{\partial t} \\ [+][-][+] = [-]\end{gathered}$$

If there is a decrease in the local density value

$$\begin{gathered}r \;\; V_\theta \;\; \frac{\partial \rho}{\partial t} \\ [+][-][-] = [+]\end{gathered}$$

The gain in the torque generation is favored by two possibilities of the flow behavior. The first might be when the local tangential velocity is in the same direction of the channel rotation and the local density value decreases. The other possibility could be when the local tangential velocity goes against the direction of the channel rotation and the local density value increases.

There are two other parameters not mentioned in the discussion above: r and ρ. Having the highest values for those two parameters is desirable. In this case, "r" parameter holds highest values for local radial positions in the channel close to the outlet port. The "ρ" parameter has the highest values in the region before the head of the expansion wave; however it does not contribute to torque generation gain. The referred region is not favorable to produce torque due to the behavior of the fluid, reflected in the parameters of $V_\theta, \frac{\partial\, V_\theta}{\partial t}\ or\ \frac{\partial \rho}{\partial t}$.

6.2.2. The Net Rate of Flux of Angular Momentum at the Outlet cross section with Absolute Variables

Replacing (6-3) into (6-8):

$$(II) = \iint_{CS} (\vec{r} \times [\vec{V}_r + \vec{V}_\theta])\rho\left[\vec{V}_r + \vec{V}_\theta\right] \cdot d\vec{A}$$

Considering in cylindrical coordinates that:

$$d\vec{A} = dA\vec{e}_r$$

And relations in (6-4), (6-5) and (6-6) in cylindrical coordinates:

$$\iint_{CS} ((r\vec{e}_r) \times [V_r\vec{e}_r + V_\theta\vec{e}_\theta])\rho\,[V_r\vec{e}_r + V_\theta\vec{e}_\theta] \cdot (dA\vec{e}_r) =$$

$$\iint_{CS} (0 + rV_\theta\vec{e}_k])\rho\,[V_r dA + 0] = \iint_{CS} rV_\theta\rho\, V_r dA\, \vec{e}_k$$

$$(II) = \iint_{CS} (\vec{r} \times \vec{V})\rho \vec{V} \cdot d\vec{A} = \iint_{CS} rV_\theta V_r \rho dA\, \vec{e}_k \tag{6-16}$$

Analyzing the term in (6-16)**:**

$$\begin{array}{cccc} r & V_\theta & V_r & \rho \\ [+] & [+/-] & [+] & [+] \end{array} = [-/+]$$

At the outlet, the variable “r” becomes constant for every fluid element crossing the outlet boundary. The radial local velocity “V_r” keeps a positive value at the outlet while “V_θ” switches to (–) or (+).

For the second term in Equation (6-2), the gain in the torque generation happens when the direction of the local tangential velocity at the outlet is against the channel rotation direction in the integral. Likewise, torque benefits when the local radial velocity and the area swept by the integral retain higher values during the opening process. Mass flow rate is a variable inherently expressing the behavior of those two parameters (local radial velocity and area swept) as well as the fluid density.

The outer radius (r) does not change in the analysis; otherwise geometrical condition of the rotor had to be modified. In general, torque increases as this value becomes greater.
For the purpose of further analysis, this second RHS term is re-written as the second RHS in Equation (6-18):

$$RHS_{2nd} = \iint_{ch-outlet} rV_\theta V_r \rho dA = \iint_{ch-outlet} rV_\theta d\dot{m}$$

Overall values can be used as an approximation to analyze this second RHS in plots at every time step through expansion flow time. Then, area-weighted average value for V_θ and integral of mass flow rate ($\dot{m}$) can be utilized:

$$RHS_{2nd} = \dot{m} V_\theta r \tag{6-17}$$

Thus, the RHS_{2nd} will be mainly as a function of two parameters

6.3. Numerical analysis of the Integral Form of the Angular Momentum Equation

The Computational Fluid Dynamic Analysis is accomplished based on Equation (6-2) with cylindrical coordinate relations of (6-3) to (6-6). Then, it becomes:

$$\vec{T}_{shaft} = \frac{\partial}{\partial t}\iiint_{CV}(r\vec{e}_r)x(\vec{V}_r+\vec{V}_\theta)\rho d\forall + \iint_{ch-outlet}(r\vec{e}_r)x(\vec{V}_r+\vec{V}_\theta)\rho(\vec{V}_r+\vec{V}_\theta).d(A\vec{e}_r)$$

Considering that: $d(A\vec{e}_r) = dA\vec{e}_r$, because $\vec{e}_r$ does not change in this direction

The equation becomes:

$$= \frac{\partial}{\partial t}\iiint_{CV}([r\vec{e}_r x V_r\vec{e}_r] + [r\vec{e}_r x V_\theta\vec{e}_\theta])\,\rho d\forall$$

$$+ \iint_{ch-outlet}([r\vec{e}_r x V_r\vec{e}_r] + [r\vec{e}_r x V_\theta\vec{e}_\theta])\rho([V_r\vec{e}_r.dA\vec{e}_r] + [V_\theta\vec{e}_\theta.dA\vec{e}_r])$$

Also, taking into account that:

$r\vec{e}_r x V_r\vec{e}_r = rV_r(\vec{e}_r x\vec{e}_r) = 0$

$r\vec{e}_r x V_\theta\vec{e}_\theta = rV_\theta(\vec{e}_r x\vec{e}_\theta) = rV_\theta\vec{e}_k$

$V_r\vec{e}_r.dA\vec{e}_r = V_r dA\cos(0) = V_r dA\ (1) = V_r dA$

$V_\theta\vec{e}_\theta.dA\vec{e}_r = V_\theta dA\cos(90) = V_\theta dA(0) = 0$

The equation becomes:

$$= \tfrac{\partial}{\partial t}\iiint_{CV}([0] + [rV_\theta\vec{e}_k])\,\rho d\forall + \iint_{ch-outlet}([0] + [rV_\theta\vec{e}_k])\rho([V_r dA\ ] + [0]) =$$

$$= \tfrac{\partial}{\partial t}\iiint_{CV} rV_\theta\,\rho d\forall\vec{e}_k + \iint_{ch-outlet} rV_\theta\rho V_r dA\,\vec{e}_k = (\tfrac{\partial}{\partial t}\iiint_{CV} rV_\theta\,\rho d\forall + \iint_{ch-outlet} rV_\theta\rho V_r dA)\vec{e}_k$$

And finally, Equation (6-18) will be used for calculation of torque at each time step as well with the two terms in the scalar form.

$$\vec{T}_{shaft} = (\frac{\partial}{\partial t}\iiint_{CV} rV_\theta\, \rho d\cancel{V} + \iint_{ch-outlet} rV_\theta V_r \rho dA\,)\vec{e}_k \tag{6-18}$$

The sign convention in Equation (6-18) for the generation of torque will be negative and when any of the RHS terms have this sign they will be counted as a contribution for total torque production. A positive value would not be desirable, for it consumes the produced torque.

6.3.1. Unsteady Expansion with Constant Cross Section Channel

In Figure 6-16 is shown the torque history and the progress of the two RHS terms of Equation (6-18) along with the flow time. The rotational velocity is the changing variable while the channel geometry is kept same for all cases. In the same graph, dashed blue arrow indicates the time when the outlet port is fully open. This arrow moves to the left as the rotational velocity increases. This effect reflects the geometric and kinematic conditions of the channel (arc length and rotational velocity, respectively) and produces the maximum instantaneous torque as location shifts to the left.

The second dashed green arrow indicates the flow time when the head of the expansion wave reaches the inlet port wall; this position was found to be where a sudden increase happens in Δp_{in-i} plots. These values in plots were quantified by calculating the reduction of the area-weighted average value of static pressure at the wall during the current time with respect to a previous time step (Equation (6-19)). This is a graphical method in which the eye determines the position. This becomes an approximated value due to the area-weighted average value at the inlet wall and the graphical method. In Figure 6-4 is shown an example, the time when the expansion wave reaches the inlet wall. Plots for other cases can be found in Appendix A.

$$\Delta p_{in-i} = p_{in\_i} - p_{in\_i-1} \tag{6-19}$$

In Figure 6-5 was plotted all travel-times for the cases under study. Apparently, all cases portray the same travel-time for the head of the expansion wave to reach the inlet wall. However, there is a small deviation with respect to the GO10K case if considered as a reference case. This deviation increases as the rotational velocity increases, and the maximum deviation is 4.4% at GO@50K. This implies the head of the expansion wave takes more time to reach the inlet wall as the rotational velocity increases; this might be associated with centrifugal force effects on the fluid. Furthermore, in Figure 6-4, the area-weighted average value of static pressure at the inlet wall (P_{in}) decreases and Δp_{in-i} values oscillate periodically before the head of the expansion wave reaches its location. This effect appears to be linked to centrifugal force effects as well because this conduct is enlarged as the rotational velocity increases.

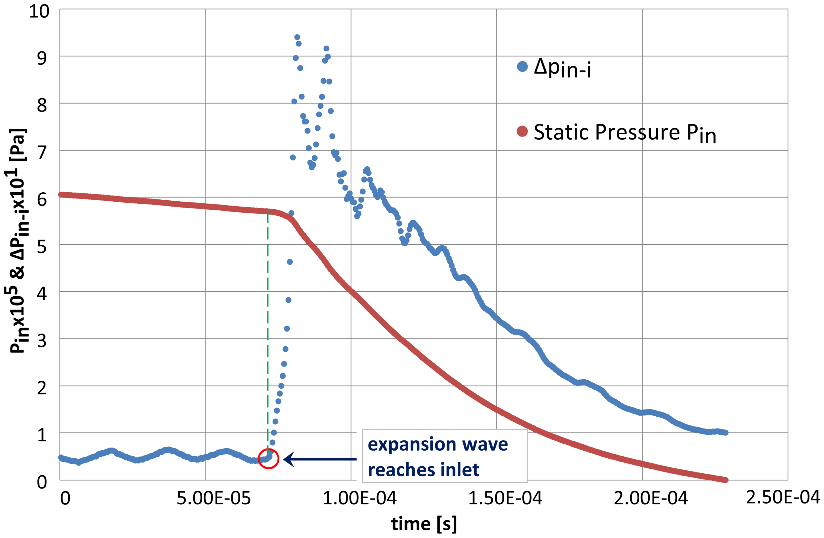

Figure 6-4: Graphical method to find the time when expansion wave reaches the inlet wall (GO@30,000 rpm)

All explanations have hitherto been concerned with time-locations of when channel outlet is fully open and the head of expansion wave impinges the channel inlet, and the following is the discussion of generated torque results. Figure 6-16 describes the progress of the torque generation (blue plot) at each time step. Also, there are two additional plots: the rate of change of the angular momentum (red plot) and the outflow rate of the angular momentum through channel outlet (green plot). Both graphs were plotted based on the two RHS terms of Equation (6-18), respectively, and the torque generation (blue plot) results when both plots are summed.

A comment for special recognition in Figure 6-16 is the sign of plots. According to previous Sections (6.2.1 and 6.2.2), a negative value means a gain in torque or torque generated during the expansion and a positive value is the opposite meaning, but for easy reading of graphs, the sign have been inverted.

The rate of outflow of the angular momentum -the green plot- is mainly shaped by $\dot{m}$ and V_θ since "r_{out}" coordinate is a constant value for all fluid particles at the channel outlet. All plots (green curves) start with a growing negative value, reaching a maximum and then decreasing until reaching a zero value, according to Figure 6-16. This zero value is correlated with zero tangential velocity (Figure 6-14 (c) and (d)). Thereafter, the rate of outflow of the angular momentum has positive values, but not fully for GO50Krpm case (Figure 6-16 (f)).

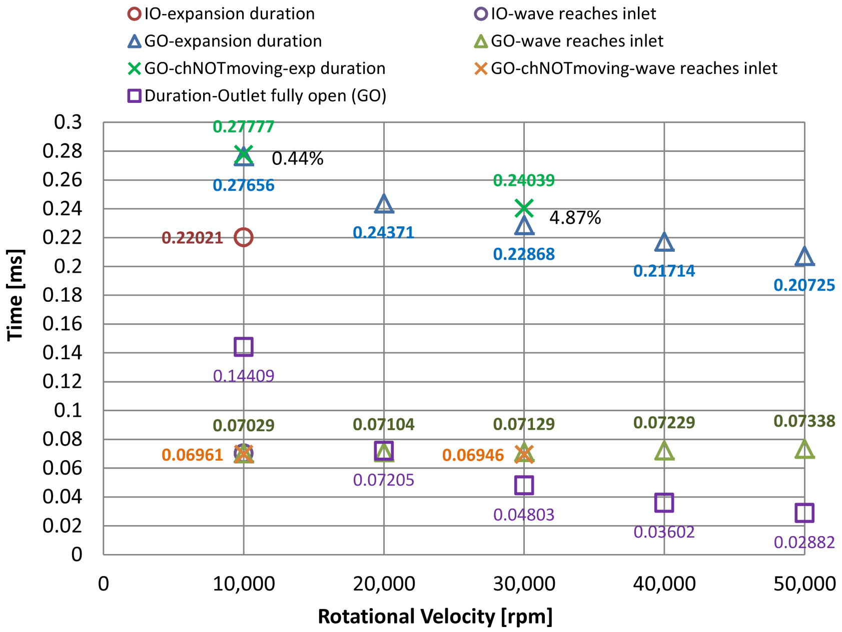

Figure 6-5: Expansion duration and expansion wave time to reach channel inlet

The $\dot{m}$ reaches a maximum value at the time the channel outlet is fully open and the full area of channel outlet favors this maximum, except for instant opening case (Figure 6-14 (a)). The channel rotational velocity increase causes earlier complete outlet opening, resulting in plots with its maximum $\dot{m}$ moving to the left.

The instant opening case has its maximum $\dot{m}$ at the beginning as the outlet is fully open. The starting point of maximum outflow rate of the angular momentum cannot be correlated since it is mostly influenced by the tangential velocity direction which adds or subtracts to the net of this outflow rate term. However, the time when $\dot{m}$ decreases is correlated with the decrease of the rate of outflow of the angular momentum, because the fluid is already following the channel shape, except for the GO50Krpm case.

The second agent taking an active role in the outflow rate of the angular momentum is the tangential velocity. The mass-weighted average of V_θ provides a glimpse of how it influences the rate of outflow of angular momentum. This second torque term becomes negative if V_θ direction is same as rotational channel velocity (Figure 6-7(a) and (b)). In all gradual opening cases, at the beginning of the process, $\dot{m}$ grows gradually as the channel outlet opens in the same manner. This fact with the quick increase of V_θ produces a rise in the negative second torque term. However, the following increase of $\dot{m}$ does not continue producing a rise in the negative second torque term because V_θ begins to decline until zero value.

In graphs that follow: Figure 6-7, Figure 6-8 and Figure 6-9, V_θ distributions at the channel outlet are plotted. The abscissa coordinates indicate the fractional opening of outlet area, measured in terms of angular units with respect to the pressure side.

The tangential velocity of the fluid particle at the outlet location is influenced by tip speed of the channel, pressure gradient in tangential direction, shape of pressure side, and opening speed of channel outlet. These factors act at each location of the outlet differently and because of that, three regions are considered: near pressure side (NPS), free stream (FS) and far from pressure side (FPS).

The direction change of absolute tangential velocity from positive to negative is depicted by the velocity diagram in Figure 6-6, this also shows the relationship with relative velocity and tip speed. This comparison is done for the same channel geometry and therefore β_{out} angle and tip speed (U_1) are the same values for both (a) and (b) diagrams.

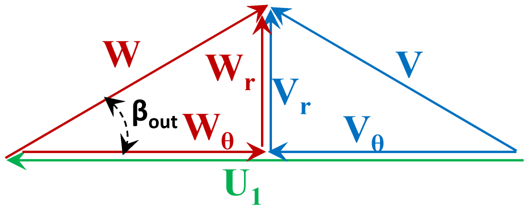

(a) Positive absolute tangential velocity (V_θ)

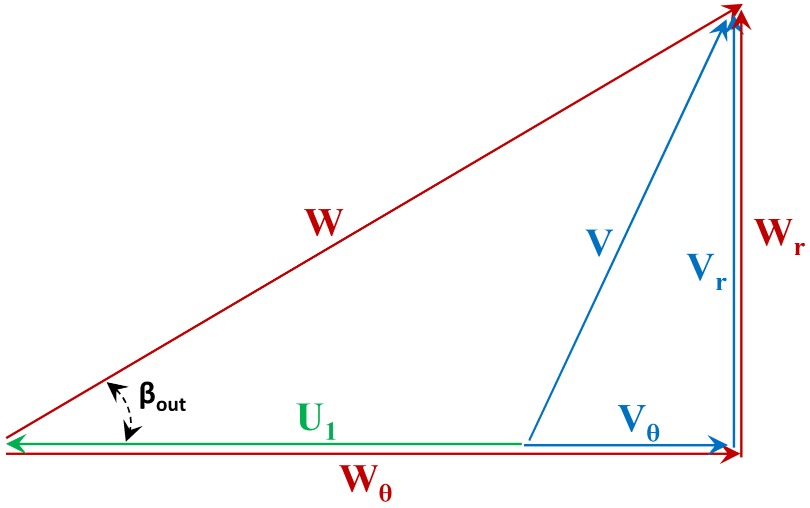

(b) Negative absolute tangential velocity (V_θ)

Figure 6-6: Triangle velocities for (a) positive tangential velocity and (b) negative tangential velocity in absolute and relative system at the channel outlet. The β_{out} angle and tip speed (U_1) are same for (a) and (b) velocity sketches.

Figure 6-7 shows V_θ distributions at the channel outlet at each selected point of Figure 5-16. This plot refers to the channel gradual opening case rotating at 10,000 rpm. At point-1, the fluid flow trajectory in the NPS region is constrained by the pressure side shape and thus, the fluid develops negative local tangential velocities which overcome the tip speed of the channel. The FS region appears to be not highly influenced by the pressure side shape and thus, the negative tangential velocity imposed by the wall shape is not enough to counteract the tip speed of the channel. On the other side of the opening, or FPS region, as the outlet opens more, the flow moves with a positive tangential velocity because it is not constrained to follow the channel shape. The pressure gradient in the tangential direction appears to contribute to this direction along with the tip speed of the channel.

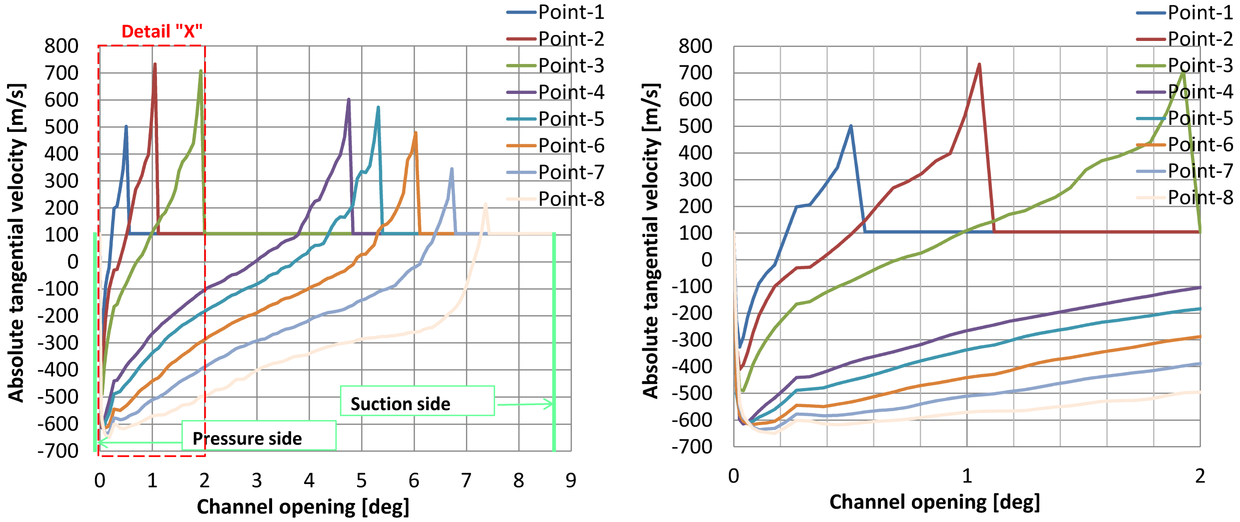

(a) (b)

Figure 6-7: (a) Absolute tangential velocities at the channel outlet with gradual opening rotating at 10,000 rpm, (b) Detail "X"

At point-2, both positive and negative tangential velocities continue increasing as the fluid flow accelerates. As the channel outlet opens more area, the effect of the pressure side shape spreads to zones near FS region and causes more portion of fluid to adjust its trajectory as parallel to the pressure side shape. Therefore, the positive absolute tangential flow velocity decreases and finally results in the negative tangential velocity which contributes to torque generation. In subsequent points (3 to 8), the fluid continues accelerating due to pressure gradients and keeps changing direction by the influence of the channel shape. Thus, greater regions of fluid move with absolute tangential velocity as more outlet area is opened.

At the channel rotational velocity of 50,000 rpm, the tip speed is higher than the previous case and to produce torque by negative tangential velocities the fluid must counteract this effect. The plot of V_θ distribution at the channel outlet is shown in Figure 6-8. The first four curves are of the period when the generated torque is negative (Figure 6-16 (f)). The effects of the pressure side shape and pressure gradient are not enough to produce higher velocities in the opposite direction of the rotation and overcome the tip speed. In addition, the fast opening effect of spreading parallel fluid trajectories to other regions do not influence sufficiently for negative tangential velocities.

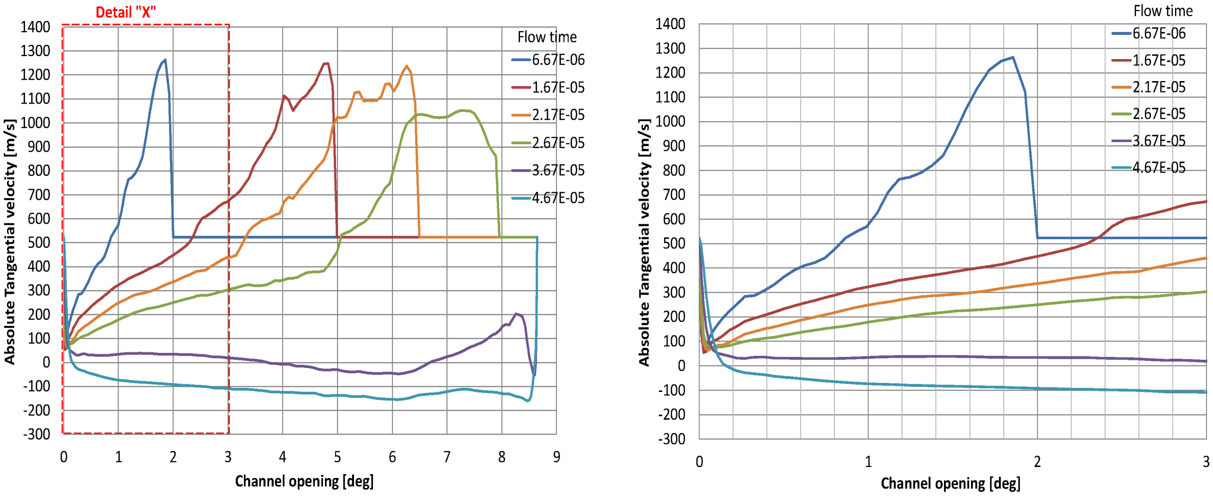

(a) (b)

Figure 6-8: (a) Absolute tangential velocities at the channel outlet with gradual opening rotating at 50,000 rpm, (b) Detail “X”

The plot in Figure 6-9 displays more regions of negative tangential velocities from the beginning of the expansion process at instant opening condition. During a short period of time, fluid flow with tangential velocities in the rotation direction occurs, which is why small negative torque is produced (Figure 6-16(a)). The first six curves belong to that time interval. The fluid flow develops negative tangential velocities in regions near the pressure and suction side.

The instant opening with respect to gradual opening presents better tangential velocity distribution at the channel outlet. The instant opening is an ideal condition to produce superior tangential velocity distributions, and the increase in rotational velocity can reproduce the quick opening at the outlet in the operation of a real engine. The benefit of fast opening by the rotational velocity increase is overshadowed by the tip speed effect which the fluid must overcome to achieve negative tangential velocities.

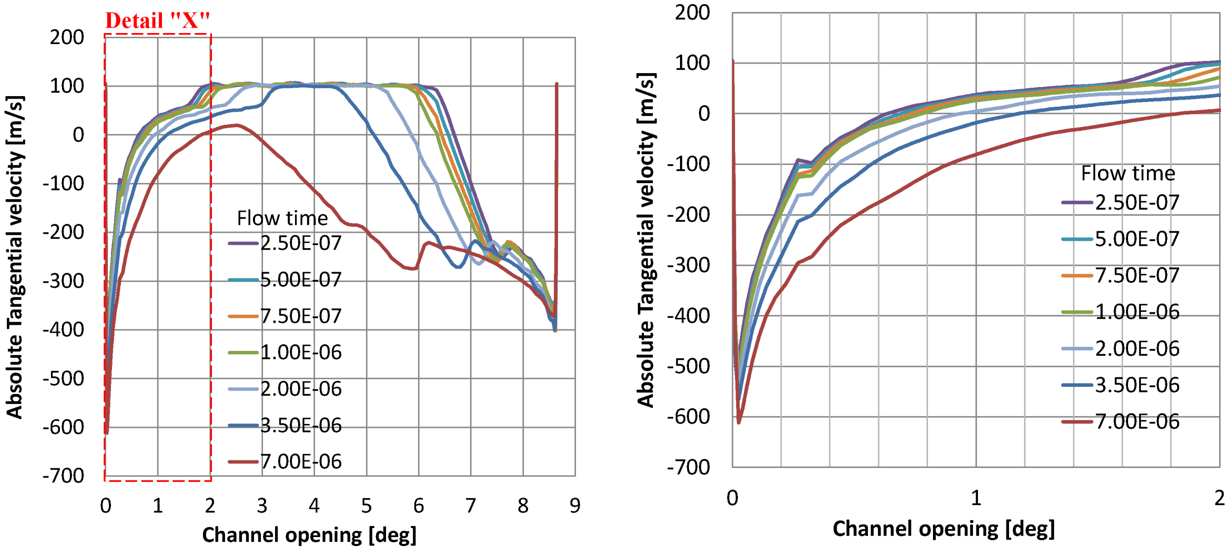

(a) (b)

Figure 6-9: (a) Absolute tangential velocities at the channel outlet with instant opening rotating at 10,000 rpm, (b) Detail “X”

Rate of Change of angular momentum is the other component contributing to the total generated torque by the unsteady expansion of a gas. This rate of change is composed of three terms according to Equation (6-15). Each term will be analyzed to determine the predominant factor in the rate of change. The first term to examine is $\rho V_\theta V_r$.

The history of the term $\rho V_\theta V_r$ during the unsteady expansion process is plotted in Figure 6-10 and shows a small contribution to the total value of the rate of change. With the increase of channel tip speed, term $\rho V_\theta V_r$ will decrease even more its contribution to torque generation. This decreasing contribution can be seen in Figure 6-10 (a) and (b) where the negative values become bigger and the positive values decrease as the rotational velocity speeds up from 20,000 to 40,000 rpm. The comparison with respect to the sum of $r\rho\frac{\partial V_\theta}{\partial t} + rV_\theta\frac{\partial \rho}{\partial t}$ indicates a significant part of the rate of change comes from the sum of these two terms aforementioned, and so the focus should be on them.

In Figure 6-11, 20 fixed points within the channel are selected to calculate the time rates of V_θ and ρ to determine which flow field variable produces the highest time rate. Results in Figure 6-12 show the time rate of V_θ is 1000 times bigger than the time rate of ρ and because of that $r\rho\frac{\partial V_\theta}{\partial t}$ is the main contributor to the rate of change. The plots in Appendix C show the contribution of each term: $r\rho\frac{\partial V_\theta}{\partial t}$, $\rho V_\theta V_r$, $rV_\theta\frac{\partial \rho}{\partial t}$ and indicates the small contribution of $\rho V_\theta V_r$ with respect to the other two. Also, these graphs support the conclusion of the term having $\frac{\partial V_\theta}{\partial t}$ with respect to the term having $\frac{\partial \rho}{\partial t}$, which contributes significantly to the rate of change. These results indicate the expansion wave create favorable conditions for the flow field variables expressed as a time rate of change.

Additionally, torque generation through the rate of change term benefits from the local deceleration or acceleration in the tangential direction, $(\frac{\partial V_\theta}{\partial t})$. Selected points 8 to 20 show local tangential velocities in the rotation direction of the channel decelerating. This result contributes to the gain in torque. Afterward, the fluid, with local tangential velocity opposite the channel rotation, accelerates at radial location between 97.5 to 100 mm.

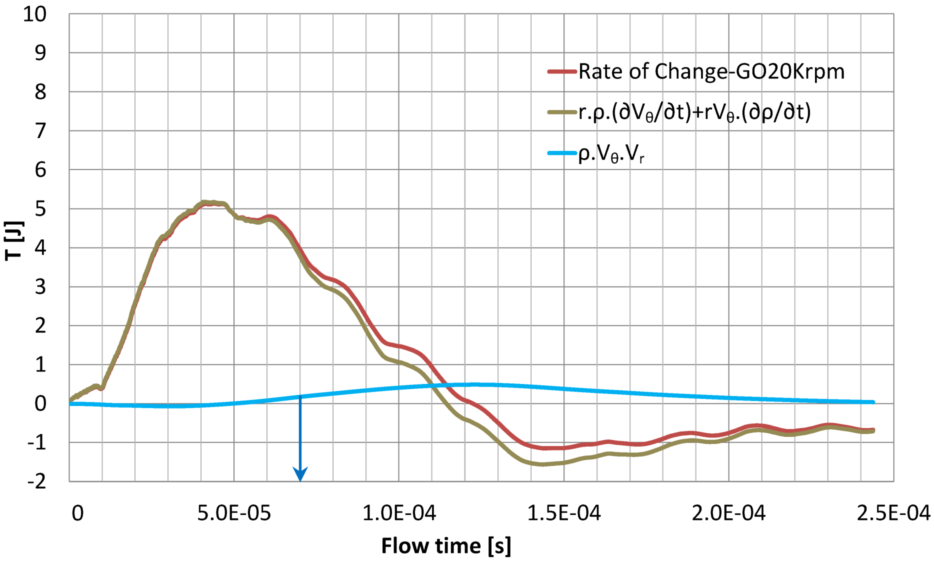

(a) Gradual opening at 20,000 rpm

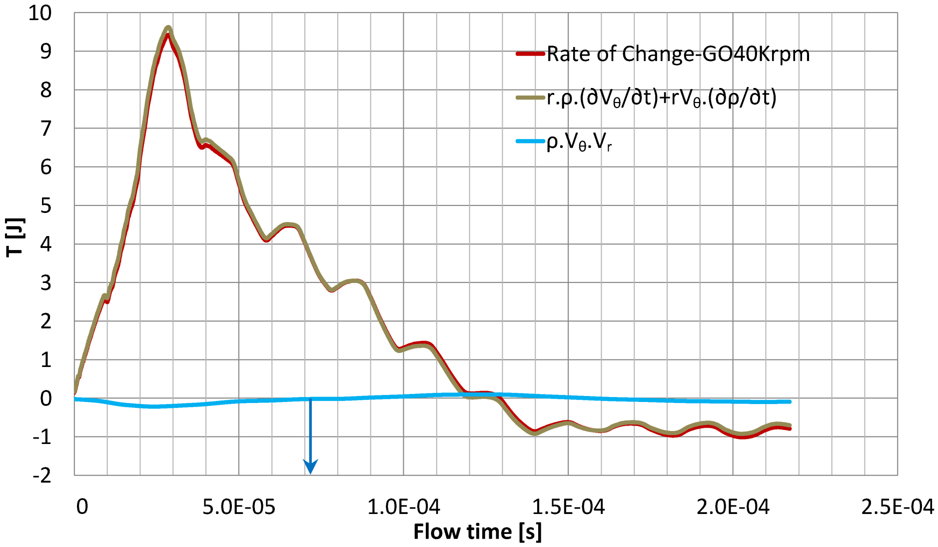

(b) Gradual opening at 40,000 rpm

Figure 6-10: Rate of Change of the Angular Momentum and components. Expansion wave impinges inlet wall "↓".

In addition, the $\frac{\partial V_\theta}{\partial t}$ benefits from the speed at which the outlet port opens. The faster the outlet opens, the greater is the time rate of local tangential velocity. The quicker opening of the channel outlet speeds up the process of decelerating and further accelerates the fluid element. Therefore, the rotational velocity increase raises the positive effect on torque generation and this can be corroborated in Figure 6-16 from (b) to (f), in which the crest of the rate of change moves to the left side and raises its tip value.

The $\frac{\partial V_{\theta}}{\partial t}$ is a predominant term among the other terms of the rate of change, contributing significantly to torque generation. In unsteady expansion processes, the second mechanism working for the generation of torque is the time rate of the tangential velocity.

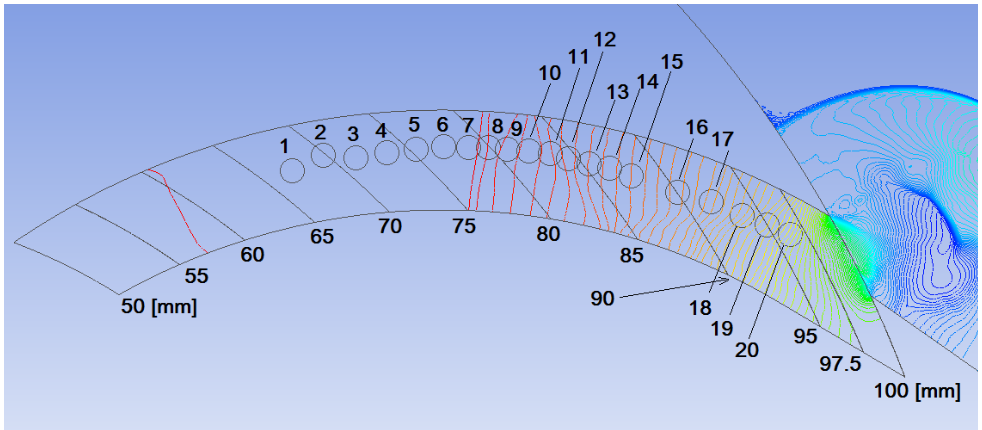

Figure 6-11: 20 fixed points selected within the channel of the GO20Krpm case

Centrifugal effect is another factor to be considered when the rotational velocity increases. In Figure 6-13 is compared the torque history produced by the gas expansion in both a stationary and rotating channel at 50,000 rpm. The channel outlet opens at the same speed in both cases. The rotating channel exhibits the history of higher torque values which demonstrates the effect of centrifugal forces acting on the fluid during the expansion process. Two other comparison cases are found in Appendix B for the channel rotating at 30,000 and 40,000 rpm.

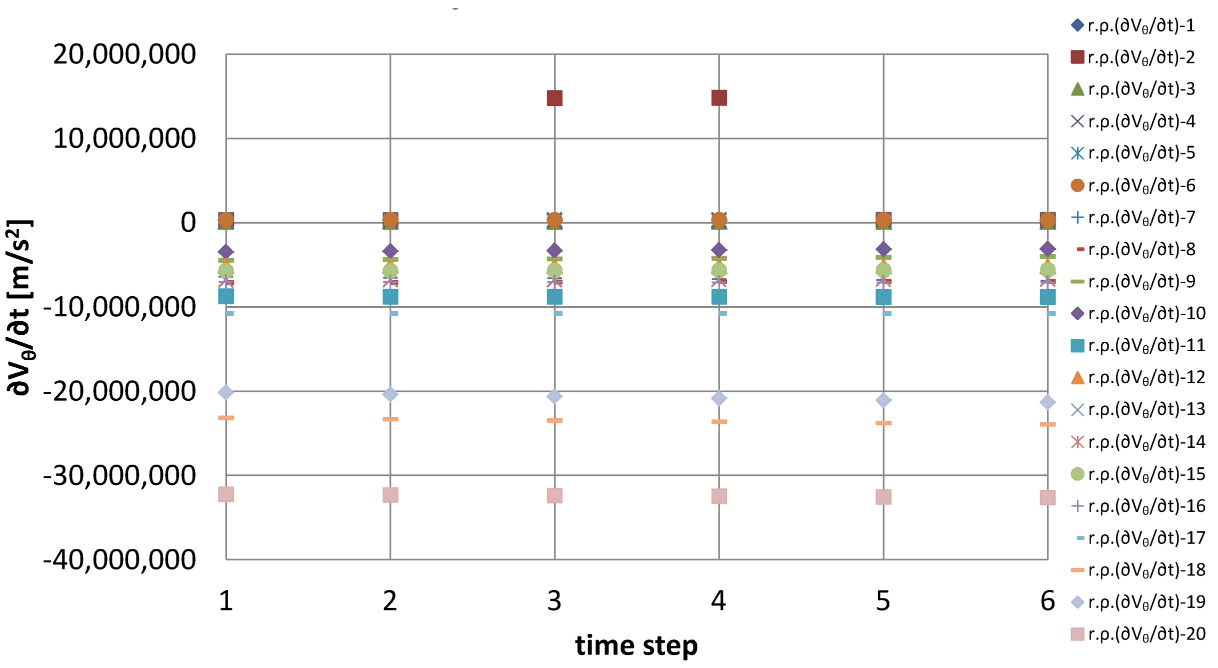

(a)

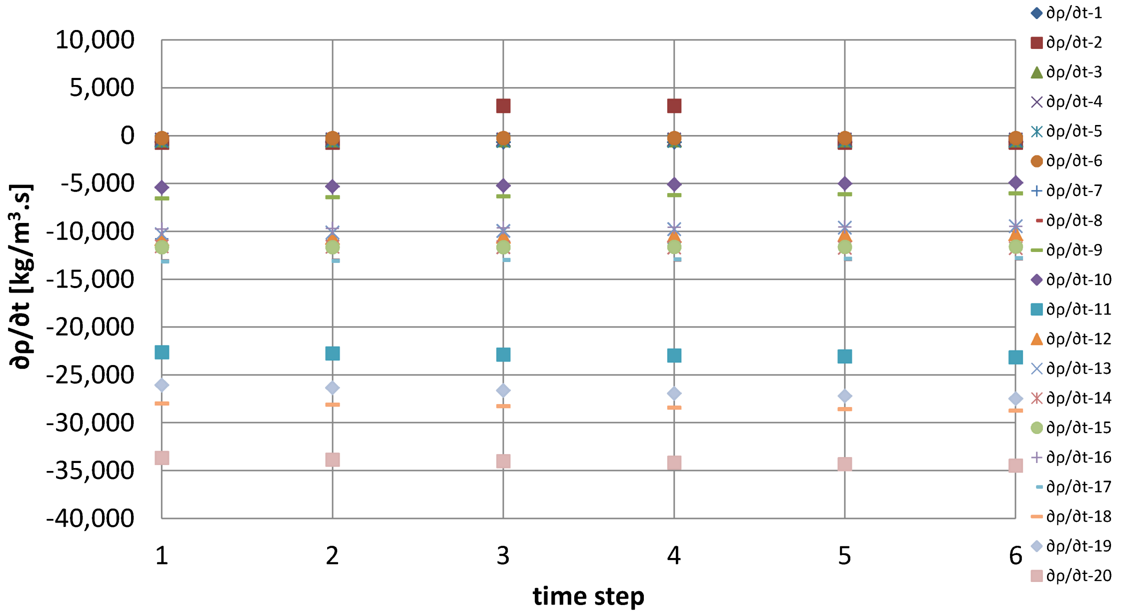

(b)

Figure 6-12: Time rate of local tangential velocity and density for Gradual Opening at 20,000 rpm

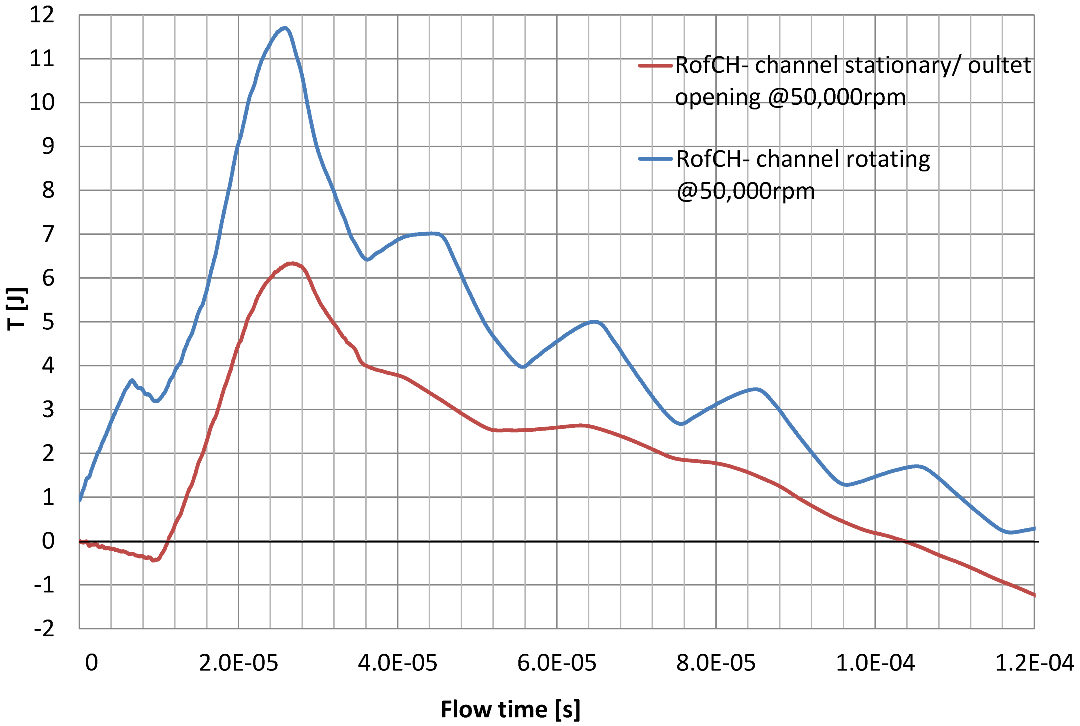

Figure 6-13: Rate of change of the angular momentum with rotating and stationary channel conditions at 50,000 rpm

Figure 6-16 displays all cases tested: Instant opening at 10,000 rpm and Gradual Opening at 10000, 20000, 30000, 40000 and 50000 rpm. The torque value posted on each graph was calculated based on the same exergy change in all cases.

The rate of change of angular momentum (RofCH) and the outflow rate of angular momentum (RofOF) exhibit opposite plot features in all cases. The RofCH works for the generation of torque from the start of the channel outlet opening to a specific time when RofOF starts to generate consistent torque and then the RofCH decreases. Both torque terms complement to continue torque generation until the end of the process. Concerning the comparison at 10,000 rpm for instant and gradual opening, the first case generates higher torque value of 52.7% with respect to gradual opening, which makes the instant opening against the gradual opening more desirable. Thus, the increase in rotational velocity was performed to reproduce the instant opening, but other effects were triggered by the increase.

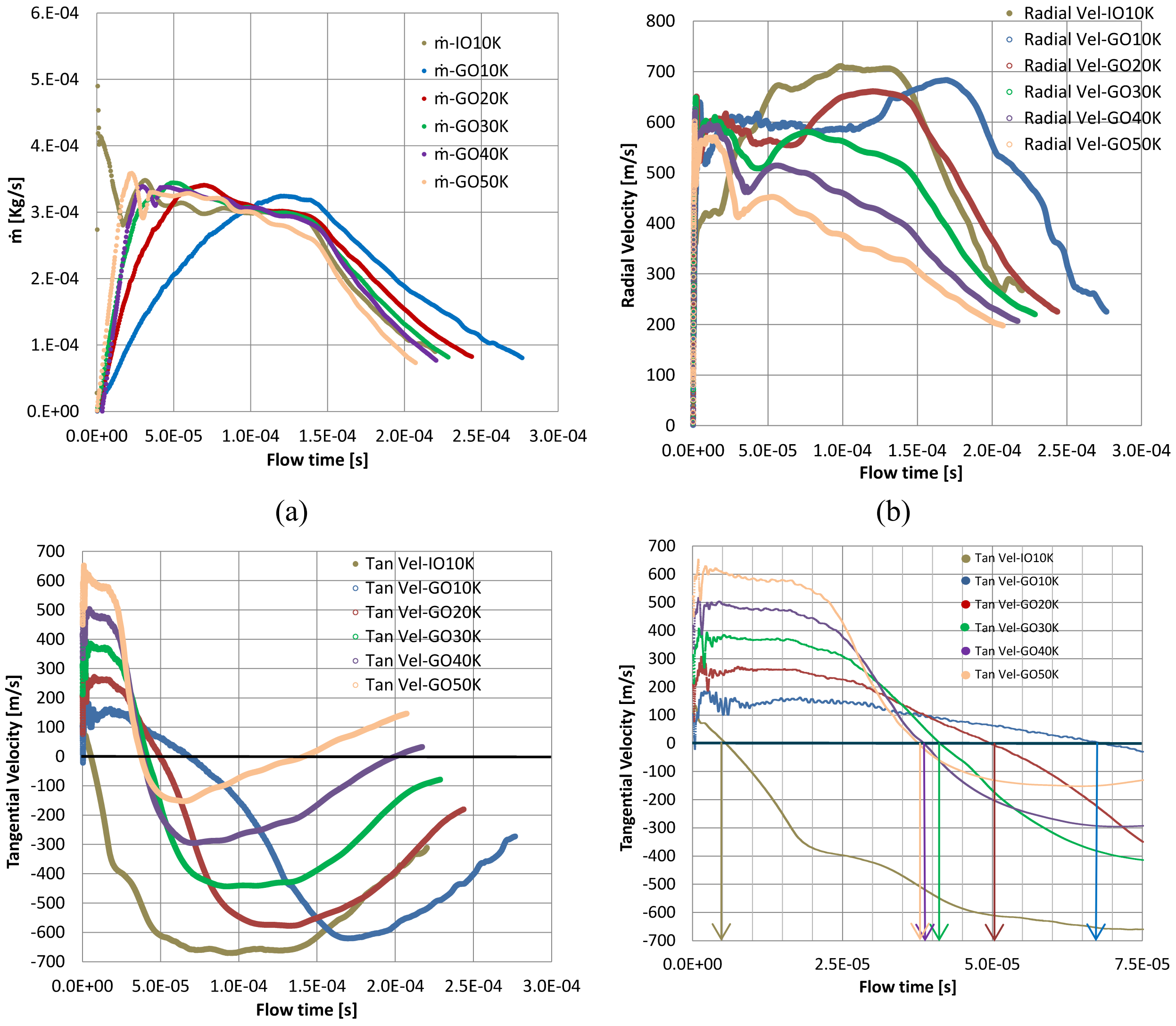

(a) (b)

(c) (d)

Figure 6-14: (a) ṁ and mass-weighted average values of (b) radial velocity & (c) tangential velocity at the channel outlet for several rotational velocity conditions, (d) Detail of Tangential Velocity

No correlation was found between the time when inlet is fully open or the expansion wave impinges the inlet wall with any maximum in RofCH or RofOF plots, which makes this unsteady expansion process a complex phenomenon.

The percentage of total values for RofCH and RofOF with respect to overall generated torque is presented in Figure 6-15. These percentages of RofCH and RofOF exhibit the same opposite characteristics as the plots in Figure 6-16. The rotational velocity increase favors RofCH within the channel but diminishes the RofOF at the channel outlet. Coincidentally, these two terms converge to a same overall percentage value at 30,000 rpm and then diverge.

Results in Figure 6-15 indicate the RofCH and RofOF are influenced by the outlet opening style but inversely proportional. Comparing instant and gradual opening at 10,000 rpm, the RofOF takes advantage of the quick opening effect to produce higher torque percentage with respect to the gradual opening case. The RofCH benefits from the gradual opening to generate higher torque percentage with respect to the instant opening case.

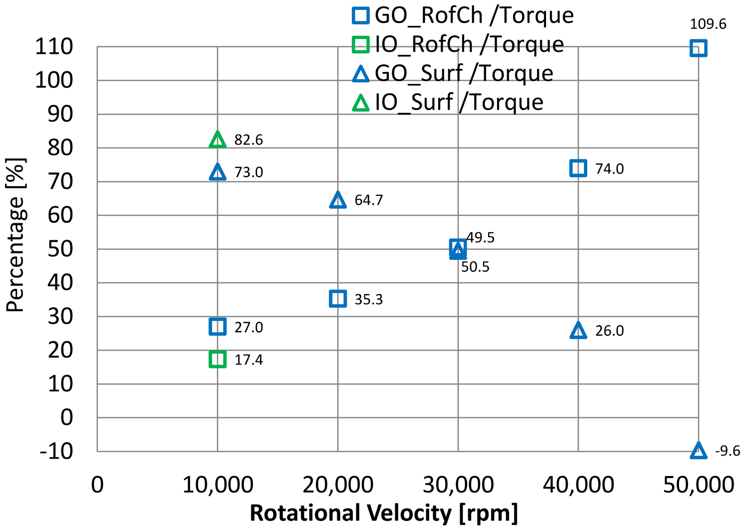

Figure 6-15: Area ratios of Rate of change/ Torque & Surface Outlet/Torque [%] for several rotational velocities (IO=Instant Opening & GO=Gradual Opening)

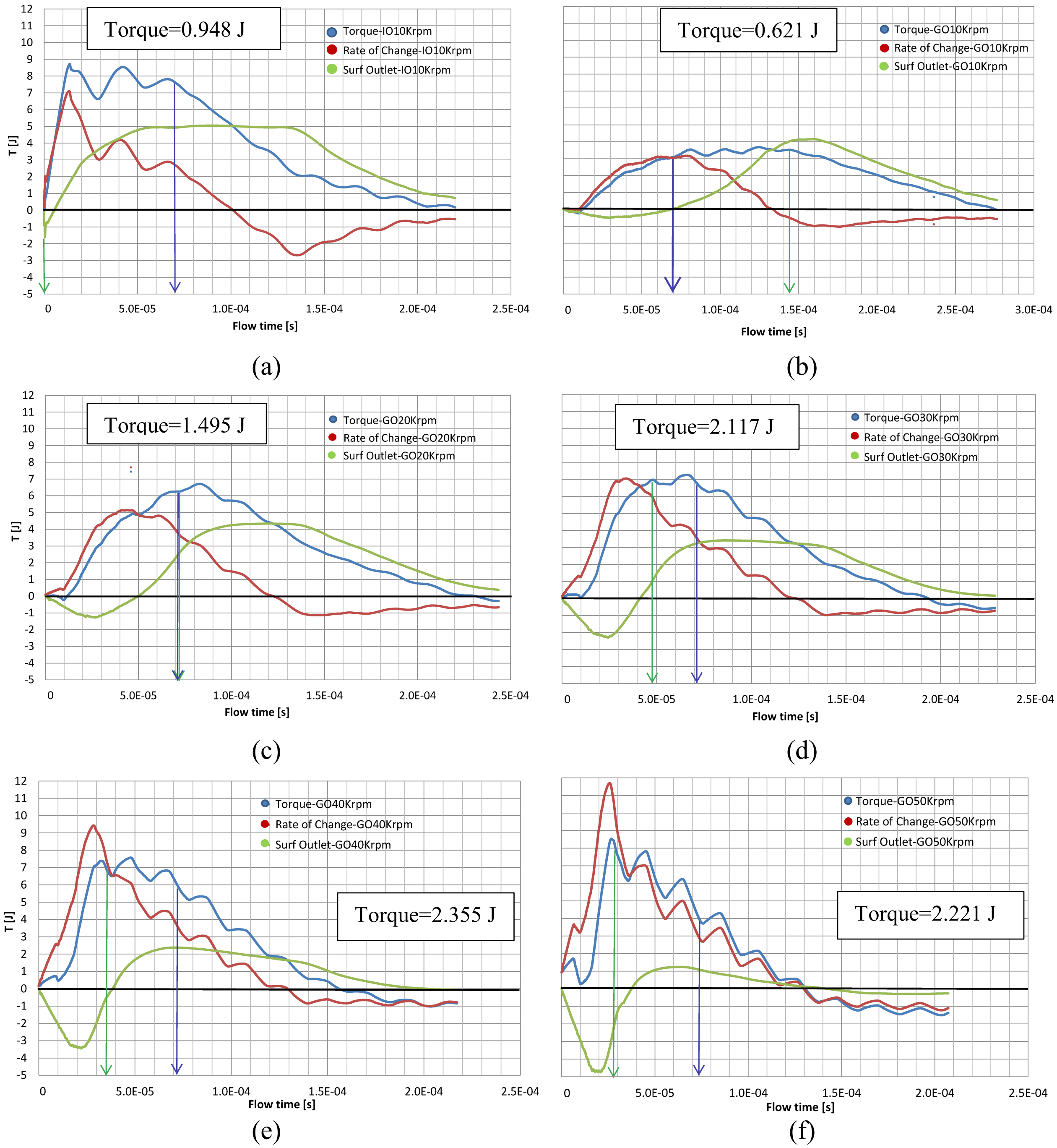

(a) (b) (c) (d) (e) (f)

Figure 6-16: History of torque extracted, time rate of change and the net rate of flux of the angular momentum during the expansion process (Gradual Opening at (b) 10000 rpm, (c) 20000 rpm, (d) 30000 rpm, (e) 40000 rpm & (f) 50000 rpm). “↓”, time when inlet is fully open. “↓”, time when Expansion Wave reaches the inlet port.

CHAPTER 7. CONCLUSIONS AND RECOMMENDATIONS

7.1. Conclusions

Factors positively influencing the generation of torque in radial rotor channels during the unsteady expansion process of the wave disc engine were determined.

In chapter 2, pressure side area and channel length were found to go hand-in-hand to improve generation of torque. The channel, in which the rise of pressure side area is a result of increasing height and channel length, showed the largest improvement in expansion efficiency when compared to channels in which height was reduced and length increased. The area increase produces more net force applied in the direction of the channel rotation and the increase in duration of the expansion process contributes to extend the application time of this force.

In chapter 3, exergy approach proves to be an appropriate method that evaluates objectively the performance of the unsteady expansion process. In exergetic efficiency, work extracted is compared with the sum of this work and destructed exergy; this term refers to the exergy no longer available because it was destroyed; flow exergy still can be used in subsequent expansion stages, however. The expansion efficiency values range between 37 to 67%. These results become 3 to 5% higher when the efficiency is calculated based on the extracted work over the internal energy added. In addition, flow exergy appears as potential exergy to use in further stages, ranging between 81 to 89% of fluid's exergy change within the channel.

In chapter 4, a zero dimensional macroscopic approximate balance equation was derived based on the first law of thermodynamics to calculate the unsteady generated work from the unsteady expansion process. Results show prolonging the duration of unsteady expansion process enhances the isentropic extracted work toward the maximum value. Longer duration times produce lower time rates of density change in the channel and channel outlet velocities.

Thus, the dynamic action time of the fluid with channel walls is extended. This result is consistent with the finding in Chapter 2; area is not regarded in this conclusion because the thermodynamic approach does not provide evidence of it, however. In addition, the gas expands more efficiently at lower pressure ratios. The pressure differential between the channel pressure and the surroundings becomes lower causing reduced time rate of density change and channel outlet velocities.

In chapter 5, the pressure and torque distribution on pressure and suction sides of the channel are analyzed. Two cases were considered: instant and gradual opening of the channel outlet. The instant opening causes pressure differentials which improve torque generation at the early stage of the unsteady expansion, but the gradual opening triggers adverse effects producing torque opposite the channel rotation direction. Furthermore, both cases indicate approximately 80% of channel length works to produce torque, and a significant fraction in the instant opening case is produced in the region near the channel outlet. The remaining length does not contribute actively on torque generation. The instant opening is an ideal case, exhibiting benefits at the early stage of the process, and the channel rotational velocity increase can reproduce this effect.

Furthermore, torque generation, composed of the action of two effects: the change of the fluid’s angular momentum within channel and the outflow rate of the angular momentum at the channel outlet, is investigated. These two components are referred as unsteady and steady effects, respectively, based on the mechanism to produce torque. Results show torque production benefits when the channel opens quickly. The increase of rotational velocity approximates the quick opening. Unsteady effects produce a significant part of the generated torque and the steady effect can be small at high speed.

7.2. Recommendations for future work

Fluctuations appear in the torque history as a consequence of the fluctuation in plots of the rate of change of angular momentum. These effects are the result of orientation change on the line-contours of pressure in the region near the channel outlet. Future work is recommended to determine the causes, as it influences the torque generation.

The channel outlet's instant opening is an ideal condition to generate torque, and the rotational velocity increase aims to reproduce this condition. An adverse effect appears in the outflow rate of angular momentum, and the investigation into reversing this effect is a recommended future work, a potential option for enhancing torque generation.

In the exergy section, available remaining exergy in terms of flow exergy is quantified resulting in high percentages. As a continuation, an investigation into improving torque generation by adding more rows of radial turbines can be done by applying the exergy approach to evaluate efficiency and exergy destruction.

In each CFD numerical simulation, the fluid working conditions at the beginning of the unsteady expansion process had a zero relative velocity with respect to the channel. The reason for that was to focus the investigation on mechanisms which generate torque without interference. Future work is to investigate this torque mechanism by adding a real complex condition inherited from the previous process: combustion.

APPENDICES

APPENDIX A: Incident expansion wave travel time

Figures present the time when the head of the expansion wave impinges the inlet wall.

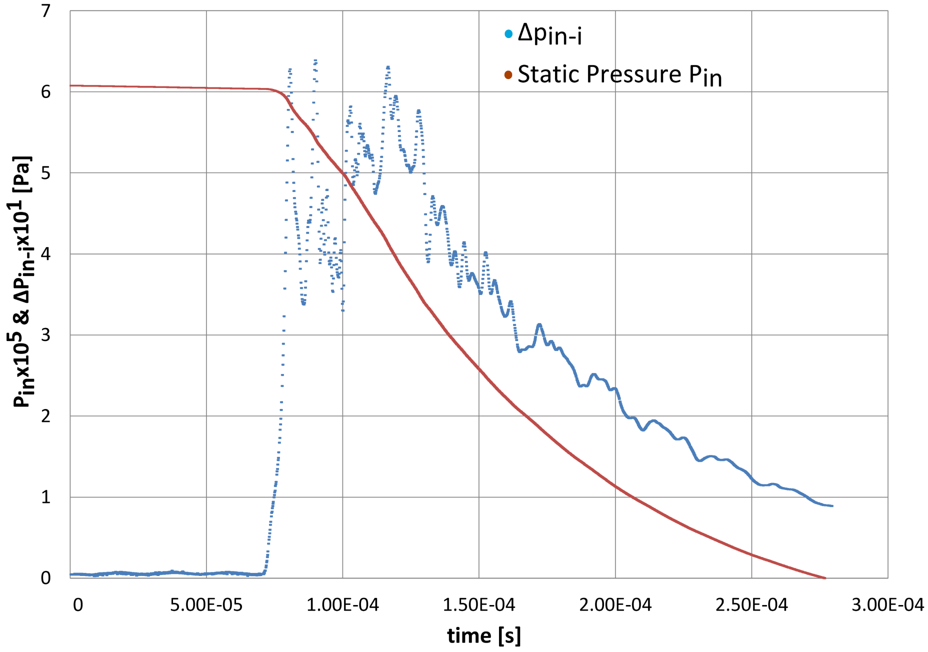

Figure 7-1: Incident expansion wave travel time at channel rotational velocity of 10,000 rpm

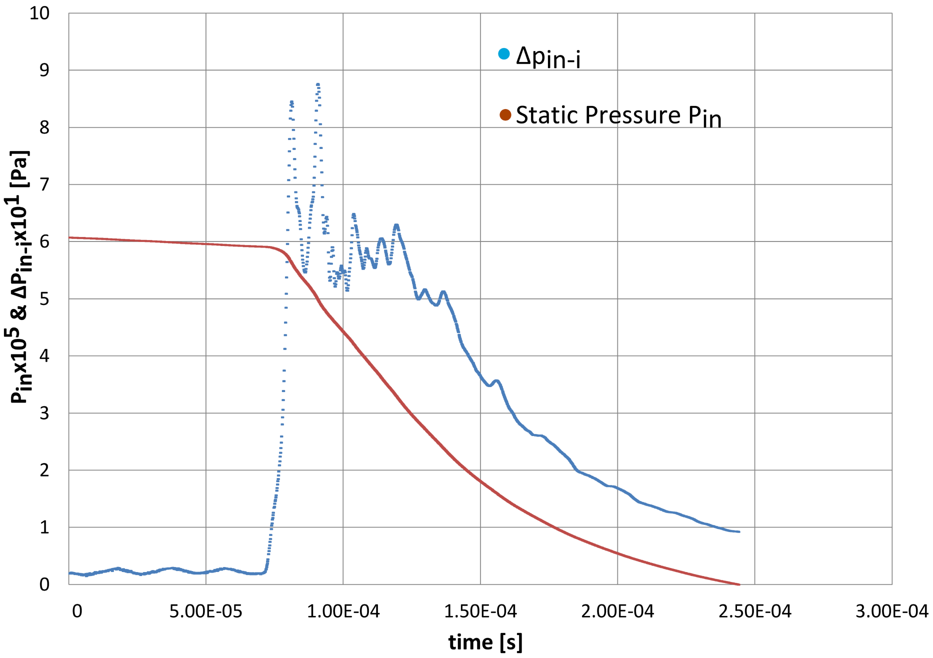

Figure 7-2: Incident expansion wave travel time at channel rotational velocity of 20,000 rpm

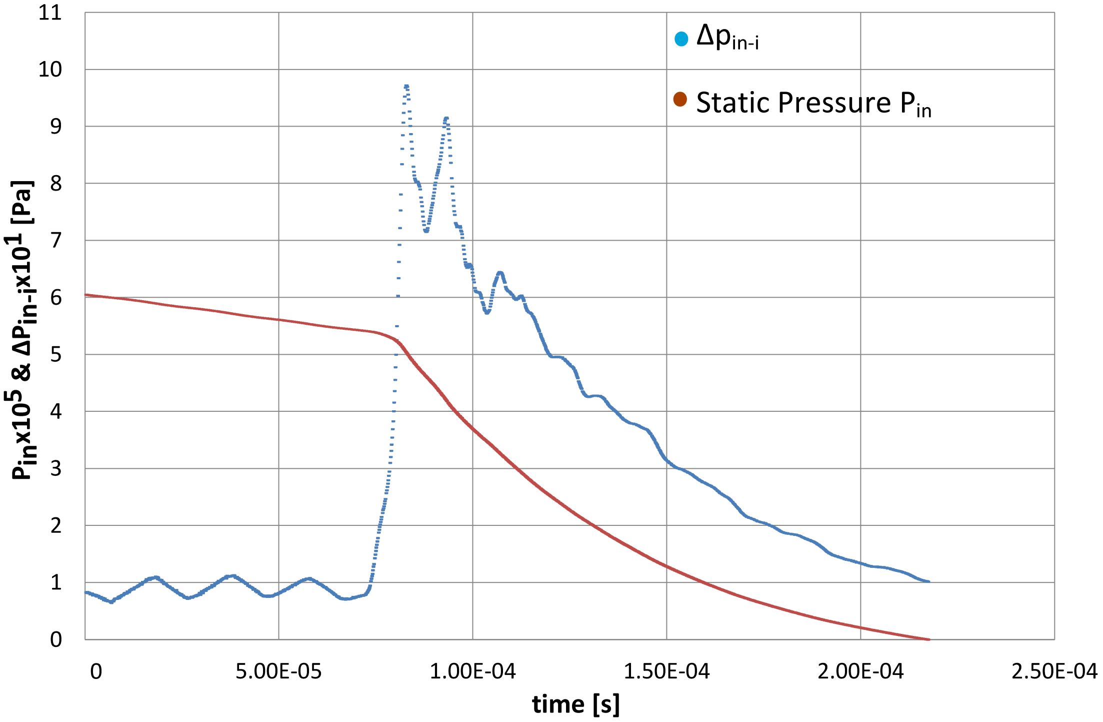

Figure 7-3: Incident expansion wave travel time at channel rotational velocity of 40,000 rpm

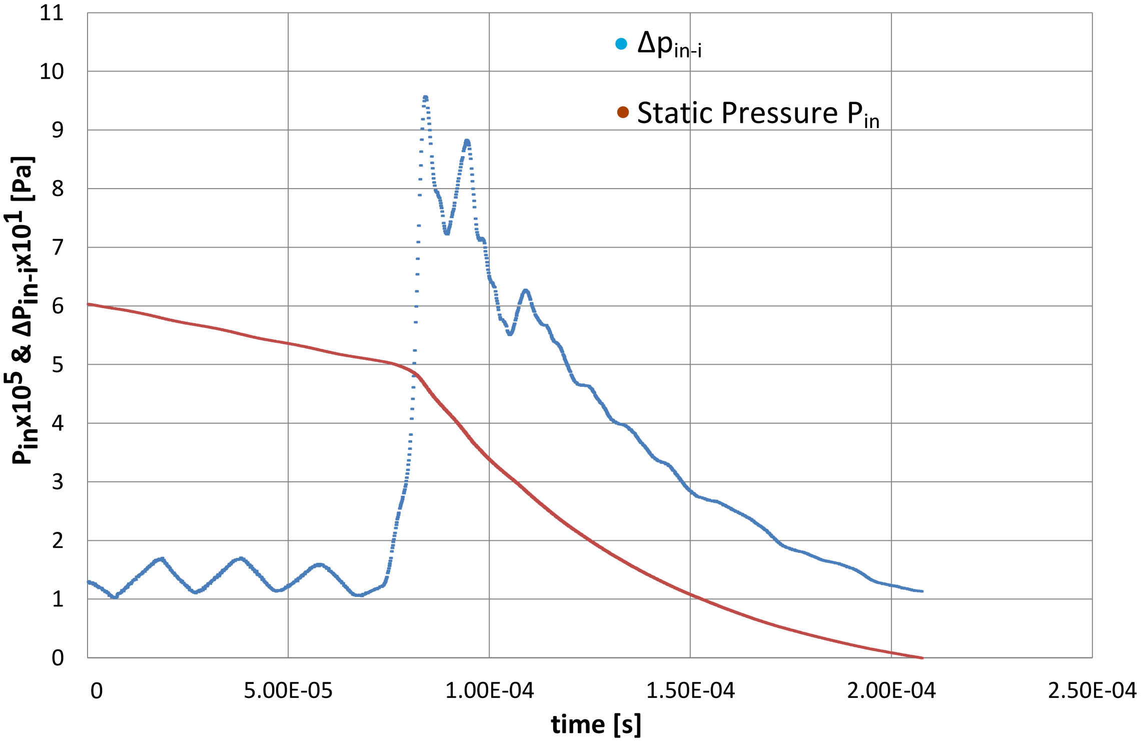

Figure 7-4: Incident expansion wave travel time at channel rotational velocity of 50,000 rpm

APPENDIX B: Centrifugal force effects

Figures depict the influence of centrifugal forces on the rate of change of angular momentum within the channel

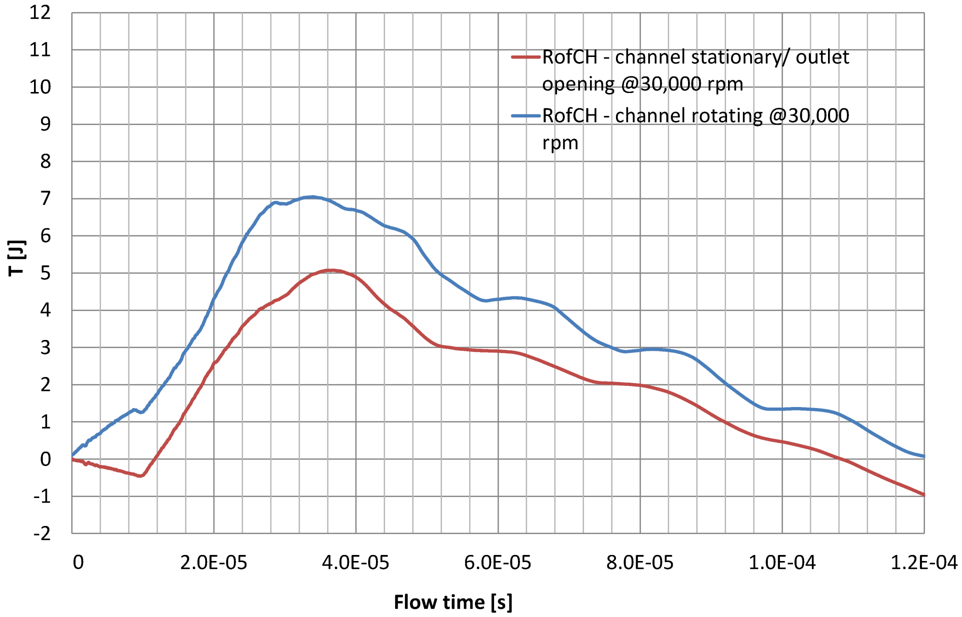

Figure 7-5: Centrifugal effects for channel rotating at 30,000 rpm

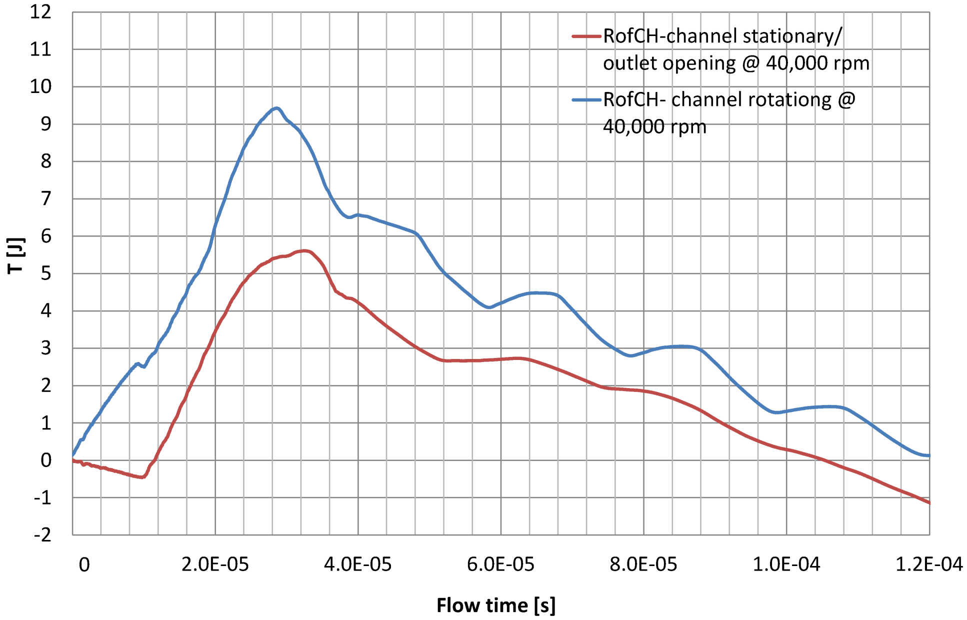

Figure 7-6: Centrifugal effects for channel rotating at 40,000 rpm

APPENDIX C: Components of rate of change of angular momentum

The following figures show plots of the three terms that constitute the rate of change of the angular momentum within the channel: $r\rho\frac{\partial V_\theta}{\partial t}$, $\rho V_\theta V_r$ and $rV_\theta\frac{\partial \rho}{\partial t}$.

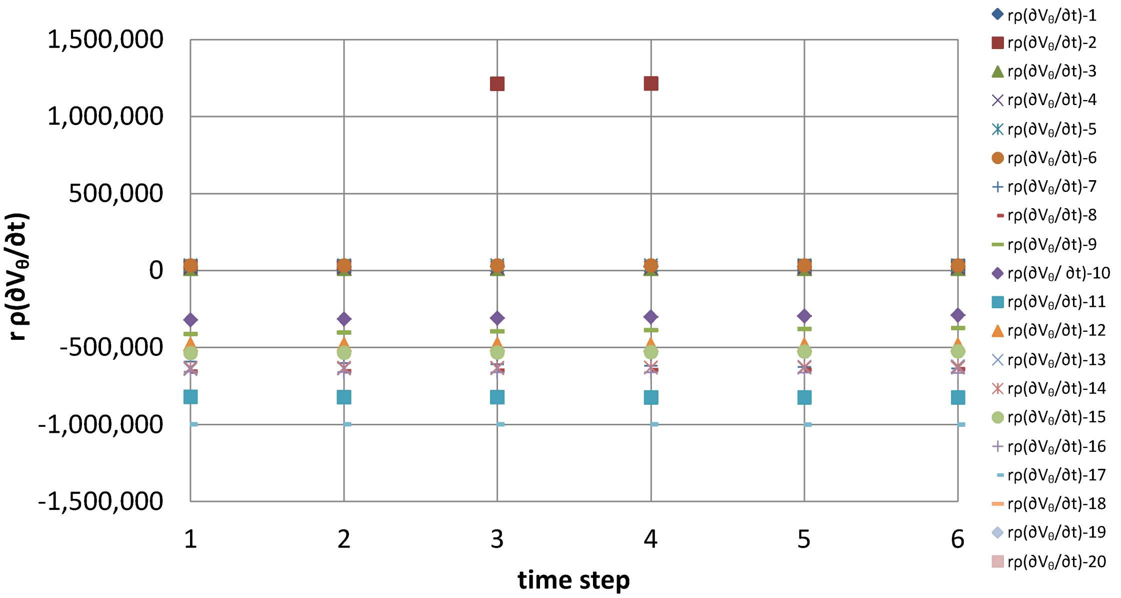

Figure 7-7: The term $r\rho(\partial V_\theta/\partial t)$ plotted for five time steps at every fixed point in the channel at GO20Krpm case

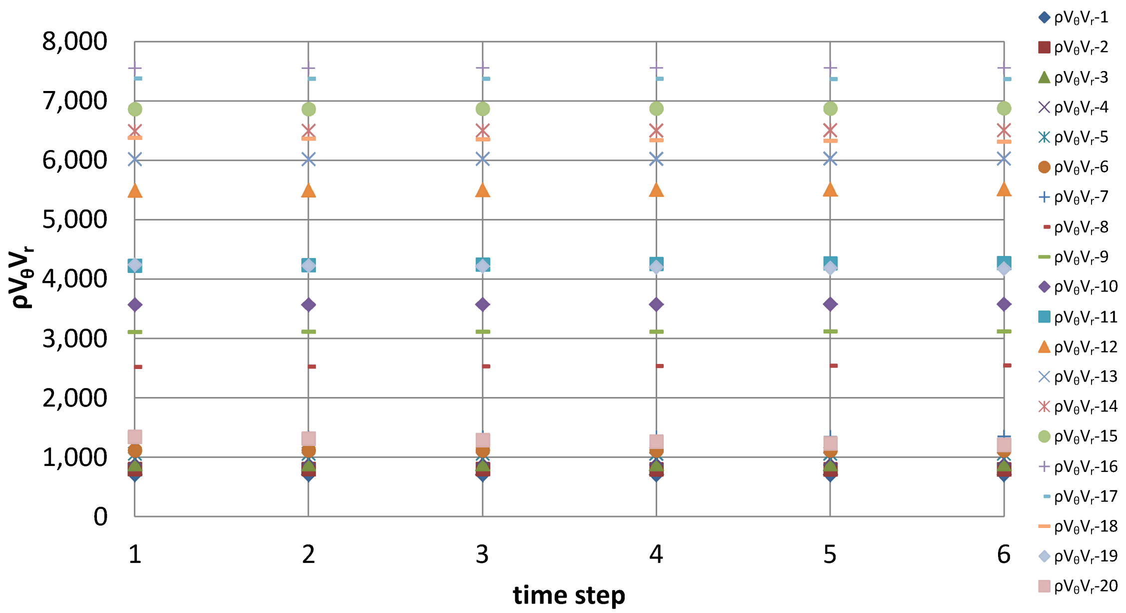

Figure 7-8: The term $\rho V_\theta V_r$ plotted for five time steps at every fixed point in the channel at GO20Krpm case.

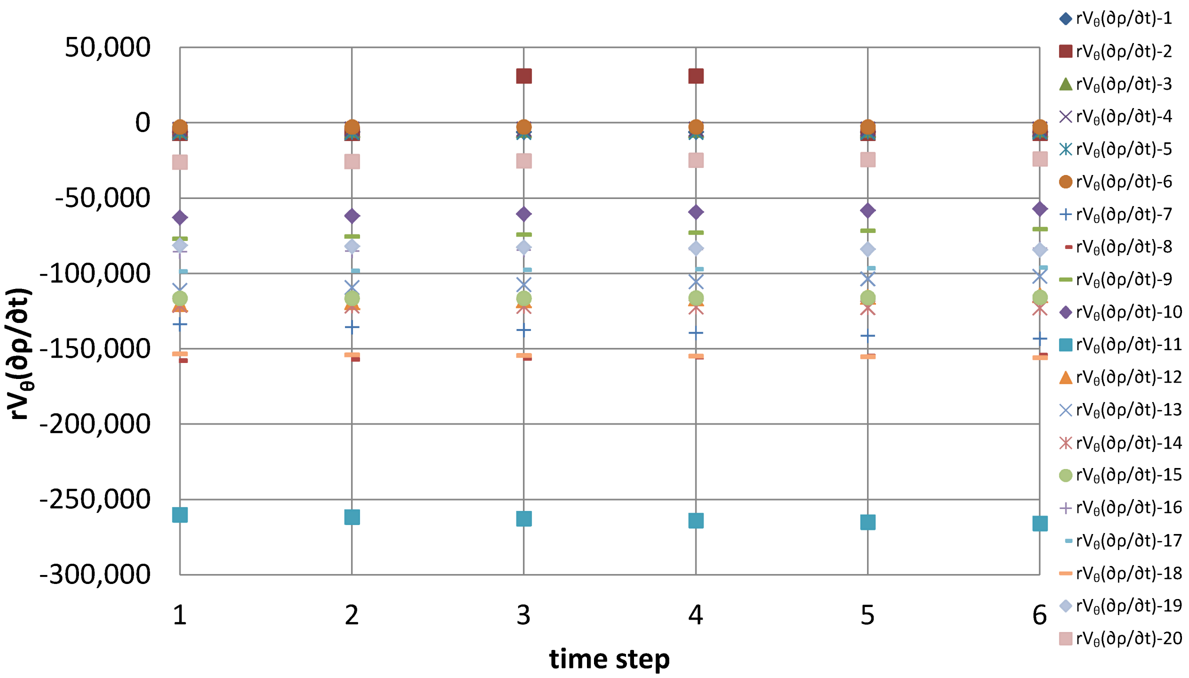

Figure 7-9: The term $rV_\theta(\partial\rho/\partial t)$ plotted for five time steps at every fixed point in the channel at GO20Krpm case.

APPENDIX D: Numerical simulation set-up

Geometry

2-dimensional

Solver

Type	Density-Based
Time	Transient

Viscous Model

Model	Reynolds Stress

Fluid

Type	Air
Density	Ideal gas
Specific heat	Piecewise-polynomial
Viscosity	Sutherland law

Time-step Size

1.00E-08	[s]

Figure 7-10: Numerical simulation set-up for 2-dimensional cad models

Geometry

3-dimensional

Solver

Type	Pressure-Based
Time	Transient

Viscous Model

Model	Large Eddy Simulation
Subgrid-Scale Model	Smagorinsky-Lilly
LES Model Options	Dynamic Stress

Fluid

Type	Air
Density	Ideal gas
Specific heat	Piecewise-polynomial
Viscosity	Sutherland law

Time-step Size

1.00E-08	[s]

Figure 7-11: Numerical simulation set-up for 3-dimensional cad model

REFERENCES

REFERENCES

[1] MSU, *Contract signed msu&Arpa-e,* East Lansing, 2010.

[2] P. H. Azoury, Engineering Applications of Unsteady Fluid Flow, John Wiley & Sons Ltd, 1992.

[3] J. Piechna, N. Mueller, P. Akbari and F. Iancu, "Radial-flow wave rotor concepts, unconventional designs and applications," in *2004 International Mechanical Engineering Congress*, USA, 2004.

[4] R. Nalim, "Preliminary Assesment of Combustion Modes for Internal Combustion Wave Rotors," in *31st Joint Propulsion Conference and Exhibit*, San Diego, 1995.

[5] M. R. Nalim and D. E. Paxson, "A Numerical Investigation of Premixed Combustion in Wave Rotors," *ASME Journal of Engineering for Gas Turbine and Power,* vol. 119, no. ASME paper 96-GT-116, pp. 668-675, 1997.

[6] G. Sun, P. Akbari, B. Gower and N. Mueller, "Thermodynamics of the Wave Disk Engine," in *AIAA paper 2012-3704*, 2012.

[7] G. Sun, "Numerical study of the aerodynamic characteristics of a wave disc engine," PhD Dissertation, Department of Mechanical Engineering, Michigan State University, East Lansing, 2012.

[8] K. Rohitashwa, "Numerical Simulations for Performance Enhancement of a Radial Pressure Wave Driven, Internal Combustion Engine," PhD Dissertation, Department of Mechanical Engineering, Michigan State University, East Lansing, 2013.

[9] J. Piechna and D. Dyntar, "Hybrid Wave Engine concept and Numerical Simulation of Engine Operation," *The Archive of Mechanical Engineering,* vol. 57, no. 1, pp. 65-95, 2010.

[10] S. L. Dixon and C. A. Hall, Fluid mechanics and thermodynamics of turbo-machinery, 6th ed., Burlington, MA: Butterworth-Heinemann/Elsevier, 2010, p. 477.

[11] I. Dincer and M. A. Rosen, Exergy: Energy, Enviroment and Sustainable Development, 2nd ed., Oxford: Elsevier Science, 2013.

[12] M. A. Rosen and J. Etele, "Aerospace systems and exergy analysis: applications and methodology development needs," *International Journal of Exergy,* vol. 1, no. 4, pp. 411-425, 2004.

[13] M. J. Moran, H. N. Shapiro, D. D. Boettner and M. B. Bailey, Fundamentals of Engineering

Thermodynamics, 8th ed., New York: John Wiley & Sons Inc, 2014, p. 1056.

[14] A. Bejan, "Fundamentals of exergy analysis, entropy generation minimization, and the generation of flow architecture," *International Journal of Energy Research,* vol. 26, no. 7, pp. 545-565, 2002.

[15] A. Bejan, Entropy Generation Minimization: The Method of Thermodynamic Optimization of Finite-Size Systems and Finite-Time Processes, Boca Raton, New York: CRC Press, 1995, p. 400.

[16] Y. Cengel and M. Boles, Thermodynamics: An Engineering Approach, 7th ed., New York: McGrawHill, 2011.

[17] ANSYS, ANSYS Fluent Theory Guide, 16.2 ed., Canonsburg: ANSYS, 2015, p. 814.

[18] J. A. Kentfield, Nonsteady, One-Dimensional, Internal, Compressible Flows: Theory and Applications, Oxford Science Publications.

[19] R. W. Fox, P. J. Pritchard and A. T. McDonald, Fox and McDonald's Introduction to Fluid Mechanics, 8th ed., Hoboken, New Jersey: John Wiley & Sons, Inc, 2011, p. 896.

[20] B. R. Munson, D. F. Young, T. H. Okiishi and W. W. Huebsch, Fundamentals of Fluid Mechanics, 6th ed., Hoboken, NJ: J. Wiley & Sons, 2006, p. 783.

[21] M. J. Moran, H. N. Shapiro, D. D. Boettner and M. B. Bailey, Fundamentals of Engineering Thermodynamics, 7th ed., John Wiley & Sons, Inc, 2011.

[22] P. Akbari, A. Kharazi and N. Mueller, "Utilizing Wave Rotor Technology to Enhance the Turbo Compression in Power and Refrigeration Cycles," in *2003 International Mechanical Engineering Conference*, 2003.

[23] P. Akbari, R. Nalim and N. Mueller, "A review of Wave Rotor Technology and its applications," *Journal of Engineering for Gas Turbines and Power,* vol. 128, p. 19, October 2006.

[24] J. J. Anderson, Computational Fluid Dynamics: The basics with applications, McGraw-Hill International Editions, 1995, p. 547.

[25] K. Kurec, J. Piechna and N. Mueller, "Numerical Investigation of the radial Disk internal Combustion Engine," in *PowerMEMS 2009*, Washintong DC, 2009.

[26] J. R. Piechna, "Micro Ring-Engine Numerical Fluid Dynamics Analysis," in *Proceedings of PowerMEMS+microEMS2008*, Sendai, Japan, 2008.

[27] H. E. Weber, Shock Wave Engine Design, John Wiley & Sons, Inc, 1994.

[28] R. E. Sonntag, C. Borgnakke and G. Van Wylen, Fundamentals of Thermodynamics, 6th ed., New York: Wiley, 1998.

[29] P. Parraga-Ramirez, "Practical Power and Combustion Investigation on First Wave Disk Engine Prototypes," PhD Dissertations, Department of Mechanical Engineering, Michigan State University, East lansing, 2013.

[30] J. Piechna and D. Dyntar, "Numerical investigation of the Wave Disk Micro-Engine concept," *International Journal of Gas Turbine, Propulsion and Power Systems,* vol. 2, no. 1, pp. 1-8, December 2008.

[31] T. Cao, T. Xu, M. Yang and R. Martinez-Botas, "Radial Turbine Rotor Response to Pulsating Inlet Flows," *Journal of Turbomachinery,* vol. 136, no. 071003, p. 10, July 2014.

[32] D. Lapinski and J. Piechna, "Improvement in the turbo-engine by replacement of conventional combustion chamber by a pulse combustion chamber," *Archive of Mechanical Engineering,* vol. 60, no. 4, p. 14, 2013.

[33] P. Akbari, "Performance Prediction and Preliminary Design of Wave Rotors Enhancing Gas Turbines Cycles," PhD Dissertation, Department of Mechanical Engineering, East Lansing, 2004.

[34] P. A. House, "Analysis of a Radial-Outflow reaction turbine concept for geothermal application," Lawrence Livermore Laboratory, Livermore, 1978.

[35] R. L. Turner and L. G. Desmon, "Performance of Blowdown Turbine Driven By Exhaust Gas of Nine-Cylinder Radial Engine," National Advisory Committee for Aeronautics, Washington, D C, 1944.